

**NOVEL RESIST MATERIALS FOR
NEXT GENERATION LITHOGRAPHY**

by

Jedsada Manyam

A thesis submitted to
The University of Birmingham
for the degree of
DOCTOR OF PHILOSOPHY

Nanoscale Physics Research Laboratory
School of Physics & Astronomy
The University of Birmingham
October 2010

UNIVERSITY OF
BIRMINGHAM

University of Birmingham Research Archive

e-theses repository

This unpublished thesis/dissertation is copyright of the author and/or third parties. The intellectual property rights of the author or third parties in respect of this work are as defined by The Copyright Designs and Patents Act 1988 or as modified by any successor legislation.

Any use made of information contained in this thesis/dissertation must be in accordance with that legislation and must be properly acknowledged. Further distribution or reproduction in any format is prohibited without the permission of the copyright holder.

Abstract

The demand for a reduction in the minimum feature size printed by microlithography technologies has continued. Recently, next generation lithography (NGL) technologies utilising shorter wavelengths of light or a charge particle beam have been the subject of research to meet the resolution requirements of the semiconductor industry roadmap. In conjunction with advances in the lithography tools, a development of a novel resist material is necessary as the resolution capability of conventional polymeric resists will reach its limit by the time of the 22 nm technology node in 2016, when the lithographic feature roughness requirements become smaller than the size of polymer molecule. In addition to the capability for high resolution, a new resist must also have sufficiently high sensitivity to give a reasonable manufacturing throughput and has high etch resistance to be able to fabricate structures at a useful aspect ratio in subsequent pattern transfer processes. Molecular resists, such as oligomers, molecular glasses, discotic liquid crystals and inorganic materials, have become increasingly attractive as they have the potential to reduce feature roughness due to the smaller size of their molecules in comparison to polymers.

Fullerene derivatives, fragmented by high doses of electron irradiation, have been demonstrated as negative tone resists for electron beam lithography with impressive capability for high resolution and high plasma etching resistance, due to their carbon-rich nature. Their primary drawback, extremely poor sensitivity, has been addressed by implementation of chemical amplification. A three-component chemically amplified negative tone resist has been developed via the addition of a photoacid generator and a crosslinker to a fullerene derivative. Two orders of magnitude enhancement of the resist sensitivity has recently been demonstrated with an epoxy crosslinker whilst high resolution and etch durability were maintained.

This thesis work presents a significant extension of the previous work. The resists have undergone comprehensive optimisation, and systematic characterisation of electron beam lithography behaviours. In the first part, a systematic study into chemical amplification of negative tone fullerene resists through variation of resist composition, additive, and resist processing in order to optimise sensitivity, resolution, line width roughness and etch resistance is presented. Sensitivity of sub 10 $\mu\text{C}/\text{cm}^2$ at 20 keV, half pitch resolution of 20 nm, a minimum sparse feature line width of 12 nm, line width roughness of sub 5 nm, and high etch resistance comparable with a commercial novolac resist have been demonstrated. Utilisation of the resist as a mask material in a high resolution pattern transfer process using dry plasma etching is also introduced. The second part presents the development of a chemically amplified positive tone fullerene based resists with the advantage of aqueous base solution development. Their lithographic capability is evaluated and discussed.

Acknowledgments

I would like to express my gratitude to my supervisors Dr. Alex P. G. Robinson and Professor Richard E. Palmer for giving me the opportunity to study in the Nanoscale Physics Research Laboratory (NPRL) and for introducing me to the novel lithographic material project. Your invaluable supervision and constant supports throughout the course of the study helped me to overcome difficulties and achieve the goals in my research works. Importantly, studying in your high quality and good environmental research group gives me a good opportunity to a professional career in the field of nanotechnology.

I would like to thank Professor Jon A. Preece and his group in the School of Chemistry at University of Birmingham for supporting the knowledge of fullerene chemistry which is one of the essential part of the research. I especially would like to thank Dr. Mayandithevar Manickam for synthesis of the variety of fullerene derivatives. I would like to acknowledge the Innovative electronics Manufacturing Research Centre (IeMRC) for financial support of this research. I also would like to acknowledge the Royal Thai Government for a financial support for my study program.

I am so grateful to my colleagues who shared experiences in the cleanroom, Dr. Francis Gibbons, Dr. Mi Yeon Song, and Dr. Andreas Frommhold. I learned a lot from all of you to become a master of microfabrication. I would like to thank technical staffs for the support on laboratory maintenance, helping me to carry on the experiments smoothly. I would like to thank my friends at the NPRL for their friendship and contribution of a good atmosphere to our research group.

Finally, I would like to thank my parents for their tireless support and encouragement from the beginning until the completion of my PhD programme.

Publications

Gibbons, F. P., Manyam, J., Diegoli, S., Manickam, M., Preece J. A., Palmer R. E., Robinson, A. P. G., Chemically amplified molecular resists for e-beam lithography, *Microelectron. Eng.* 85 (5-6), 764-767 (2008).

Manyam, J., Gibbons, F. P., Diegoli, S., Manickam, M., Preece, J. A., Palmer, R. E., Robinson, A. P. G., Chemically amplified fullerene resists for e-beam lithography, *Proc. SPIE*, 6923, 69230M (2008).

Manyam, J., Manickam, M., Preece J. A., Palmer R. E., Robinson, A. P. G., Low activation energy fullerene molecular resist, *Proc. SPIE*, 7273, 72733D (2009).

Manyam, J., Manickam, M., Preece J. A., Palmer R. E., Robinson, A. P. G., Characterization of the effects of base additives on a fullerene chemically amplified resist, *Proc. SPIE*, 7639, 76391N (2010).

Contents

Abstract	ii
Acknowledgments	iii
Publications	iv
Contents	v

Chapter 1

Background	1
1.1 Introduction.....	1
1.2 Microlithography.....	2
1.2.1 Photolithography.....	3
1.2.2 Immersion lithography.....	5
1.2.3 International Technology Roadmap for Semiconductors.....	6
1.3 Next generation lithography.....	7
1.3.1 Double patterning lithography.....	8
1.3.2 Extreme ultra violet lithography.....	9
1.3.3 Nanoimprint lithography.....	10
1.3.4 Electron beam lithography.....	11
1.3.4.1 Electron beam direct-write lithography.....	11
1.3.4.2 Electron–solid interactions.....	12
1.3.4.3 Multiple electron beam direct-write lithography.....	13
1.4 Resist materials.....	16
1.4.1 Resist characteristics.....	16
1.4.1.1 Sensitivity and contrast.....	17
1.4.1.2 Resolution.....	18
1.4.1.3 Line edge roughness; Line width roughness.....	18
1.4.1.4 Etch resistance.....	19
1.4.2 Resist roadmap.....	20
1.5 Chemically amplified resists.....	21
1.5.1 Principle of chemical amplification.....	21
1.5.2 Fundamental limit.....	24
1.6 Electron beam resists.....	25
1.6.1 Polymer resists.....	25
1.6.1.1 Poly(methyl methacrylate).....	25
1.6.1.2 Shipley Advanced Lithography resists.....	26
1.6.2 Molecular resists.....	26
1.6.2.1 Calixarene derivatives.....	26
1.6.2.3 Triphenylene Derivatives.....	27
1.6.2.4 Fullerene Derivatives.....	28
1.7 Thesis structure.....	29

Chapter 2

Experimental Techniques	31
2.1 Equipment.....	31
2.1.1 Scanning electron microscope (SEM).....	31
2.1.2 Electron beam lithography system.....	33
2.1.3 Plasma etcher and asher.....	34
2.1.4 Surface profiler.....	37
2.2 Resist processing.....	37

2.2.1 Substrate preparation	38
2.2.2 Resist preparation and processing	39
2.3 Resist characterisation.....	40
2.3.1 Sensitivity and contrast	40
2.3.2 Resolution	41
2.3.3 Line width roughness analysis	42
2.3.4 Etch resistance	43
Chapter 3	
Negative Tone Chemically Amplified Fullerene Based Molecular Resists.....	45
3.1 Resist preparation.....	45
3.2 Sensitivity	47
3.2.1 Composition ratios.....	48
3.2.2 Post application bake and post exposure bake.....	50
3.3 Resolution.....	52
3.3.1 pure MF07-01	52
3.3.2 Composition ratios.....	53
3.3.3 Post exposure latitude.....	58
3.3.4 Dose latitude	61
3.3.5 Casting solvent.....	63
3.3.6 Developer.....	65
3.4 Line width roughness	67
3.5 Etch resistance.....	68
3.6 Post exposure delay.....	70
3.7 Aging effects	72
3.8 Conclusions	74
Chapter 4	
Effects of Base Quenchers.....	76
4.1 Sample preparation.....	76
4.2 Sensitivity.....	77
4.3 Resolution.....	79
Chapter 5	
Line Width Roughness Analysis	85
5.1 Effects of resist formulation	85
5.1.1 Crosslinkers ..	85
5.1.2 Acid levels	86
5.1.3 Base quencher levels	88
5.1.4 Casting solvent.....	89
5.2 Effects of resist processing	90
5.2.1 Post application bake.....	90
5.2.2 Post exposure bake	91
5.2.3 Development.....	91
5.3 Film thickness.....	92
5.4 Pitch size.....	94
5.5 Conclusions	94
Chapter 6	
Plasma Etching for High Resolution Pattern Transfer.....	96
6.1 Experimental setup.....	96
6.2 Effects of etching gas flow rate	97

6.3 Effects of gas pressure	98
6.4 Effects of ICP power.....	100
Chapter 7	
Positive Tone Chemically Amplified Fullerene Based Molecular Resists	104
7.1 Resist Preparation.....	104
7.2 MF-THP-based resists.....	106
7.3 MF- <i>t</i> BAC-based resists.....	106
7.3.1 Sensitivity	107
7.3.1.1 CA MF- <i>t</i> BAC(1) resists.....	107
7.3.1.2 CA MF- <i>t</i> BAC(2) resists.....	108
7.3.1.3 CA MF- <i>t</i> BAC(6) resists.....	110
7.3.2 Resolution	112
7.3.2.1 CA MF- <i>t</i> BAC(2) resists.....	113
7.3.2.2 CA MF- <i>t</i> BAC(6) resists.....	116
7.3.3 Dissolution characteristics.....	118
7.3.3.1 Unexposed resist films.....	118
7.3.3.2 Exposed resist films	119
7.3.4 Etch resistance	121
7.4 Conclusions	122
Chapter 8	
Conclusions and Future Outlooks ..	125
8.1 Conclusions	125
8.2 Suggested future work	127
References	129

Chapter 1

Background

1.1 Introduction

The demonstration of the first point contact semiconductor transistor in 1947 by Bardeen, Brattain, and Shockley [1] was a milestone in the field of electronics. Due to its small size and efficiency, the transistor promised to replace the bulky vacuum tube which dominated the electronics industry at that time. Manufacture of commercially available transistors began in the early 1950s, giving rise to the semiconductor industry. A variety of transistors such as the point contact transistor and the junction transistor were supplied to markets, initially the defence industry and eventually the mass consumer market. The next great leap of semiconductor technology came with the invention of the integrated circuit (IC) in 1959 by Jack Kilby [2,3] and shortly afterward by Robert Noyce [4]. The IC concept allows an entire electronic circuit composed of transistors, passive components, and interconnection wiring to be integrated onto a single semiconductor chip by utilising planar fabrication technology. Soon after ICs were commercialised in the 1960s, transistor based devices rapidly replaced vacuum tubes in almost every application with the advantages of reduction in size, energy consumption, and reliability. It also led to a range of new applications such as space electronics and microelectronics.

Modern technologies have increasingly demanded more complex circuits in smaller devices. In other words, ICs have tended to have a higher number of transistors and electronics components in smaller chips, resulting in a faster and more powerful devices as well as a reduced production cost. The trend of increasing the number of transistors in microelectronic devices for a given cost was first observed by Gordon Moore in 1965 [5]. He gave a prediction, the so-called Moore's Law, based on data over a few generations of ICs, that the number of transistors in integrated circuits doubles about every two years. The law had been used as a roadmap for the semiconductor industry to develop and

release succeeding generations of IC devices to the market. Driven by Moore's Law, which has continued to be realised for over four decades up to today, the most advanced IC devices now contain billions of transistors in a single chip [6].

From a manufacturing point of view, increasing the number of transistors is accomplished by making the transistors smaller so that more can be packed together on the same chip. Advancement in lithographic technology has played a major role in the incredible shrinkage of semiconductor devices. Lithography processes not only enabled the fabrication of ICs from the beginning but also determined the feature size of its components. The development of lithography tools and the photoresist materials used in lithography processes has been an active research area for the past 40 years. It aims to provide the advanced manufacturing techniques and materials needed to decrease the minimum feature size of devices with reasonable cost. It is expected that the current lithographic technology will no longer serve industry requirements in the near future. In exposure technology, the transition of the operating exposure wavelength in the conventional lithography tool from 193 nm to 157 nm has encountered material difficulties [7]. Moreover, in resist technology, the minimum feature requirement is approaching molecular size in photoresists, the intrinsic resolution limit of the material [8]. A lot of investment and effort has been made recently to pursue an alternative technology, called next generation lithography, in order to support the advance of semiconductor technology and bring more comfort to our everyday life.

1.2 Microlithography

Microlithography refers to the process of printing a microscopic pattern onto a substrate. Specifically, in semiconductor manufacturing, lithography is the process of producing a patterned mask on a semiconductor. This mask allows the selection of parts of a substrate to be treated in subsequent processes such as etching, doping, or metal deposition whilst other areas are protected from the processing. Lithography is an essential part of IC fabrication as it determines the density of devices in the chip, and is thus the workhorse behind the miniaturization of ICs. The most common technique

used for microlithography is photolithography which has been utilised since the beginning of the IC industry.

1.2.1 Photolithography

Photolithography uses a light source projected through a patterned reticle and onto a substrate. The basic steps of the photolithographic process are schematically illustrated in Figure 1.1.

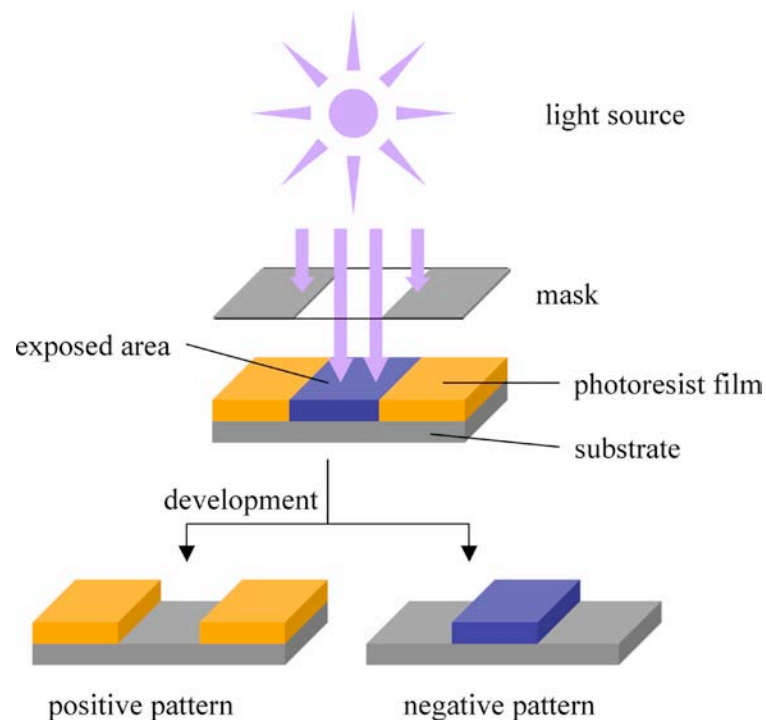


Figure 1.1 Schematic diagram of a photolithography process to transfer a positive or negative image onto a substrate.

First, a substrate is coated with a thin film of photosensitive material called a photoresist. Second, a pattern of light is projected onto the resist film by shining light through a mask on which the required pattern has previously been fabricated, leaving the mask transparent in some areas and opaque in others. The solubility of a photoresist in a particular developer solvent is altered by exposure to radiation, typically light in the ultraviolet (UV) region for photolithography. Therefore an exposed/unexposed area of a resist film can be removed leaving a positive/negative tone resist pattern on the substrate after the development process. The resist pattern acts as a temporary mask in the

subsequent fabrication process and can be removed after being used. Since the 1970s, a system of projection lenses has been integrated into the photolithography tool to make use of reduction optics in which an image of the pattern on a mask is demagnified typically four or five times before projection onto the resist film.

Resolution capability is an important factor to determine the performance of a lithography tool. The resolution is the smallest feature of the image that can be printed onto a sample. In an optical exposure system, resolution is limited by the diffraction phenomenon of light. The resolution, R , of an optical projection system is derived from the Rayleigh criterion, as expressed as [9]

$$R = k_1 \frac{\lambda}{NA}, \quad (1.1)$$

where k_1 is the factor attributed by resist processing and other process factors, λ is the wavelength of the radiation source, and NA is the numerical aperture of the lens. The numerical aperture of a lens is defined as

$$NA = n \sin \theta, \quad (1.2)$$

where θ is the half-angle of the maximum light cone which can enter or exit the lens, and n is the refractive index of the surrounding medium. Another important quantity to describe the capability of the optical system is the depth of focus, DOF . It is the range over which an optical image is clear and considered to be in focus. The DOF limits the thickness of the resist film to be exposed and the tolerance in positioning the sample to maintain an image in focus. The general form of DOF is also derived from the Rayleigh criterion and expressed as [10]

$$DOF = k_2 \frac{\lambda}{NA^2}, \quad (1.3)$$

where k_2 is a constant found by experiment. It is clearly seen from Equations (1.1) and (1.3) that the resolution and focus capabilities of an exposure tool depend only on wavelength, numerical aperture, and constants. These parameters guide how to approach a higher resolution lithography system. The traditional approach is to shorten the radiation wavelength, which is the trend that has been seen for five decades. The mercury g-line at 436 nm was the first light source used in photolithography for

micrometre-scale resolution. It was succeeded by the mercury i-line at 365 nm and krypton fluoride (KrF) excimer laser at 245 nm, successively. Currently, the most advanced system operating at 193 nm has been used [11]. However, in order to reach a high feature resolution with 193 nm light, it has been necessary to significantly improve NA , and reduce the k factor. The numerical aperture of the exposure system has increased from 0.28 to 0.93 with dry and 1.35 with water immersion. The k factors can be reduced either by using a variety of resolution enhancement technologies such as optical proximity correction (OPC), off-axis illumination (OAI), and a phase-shifting mask (PSM) [12] or by improving the properties of resist material and resist processing.

1.2.2 Immersion lithography

Immersion has been a common technique used to enhance the resolving power of optical microscopes since the 1880s [13]. The operating principle is to replace the air between the final lens and the sample with a high refractive index liquid to increase NA . In modern photolithography, the immersion technique provides an improvement of both resolution and DOF , by enabling the system to operate with NA greater than one [14]. The maximum value of NA of conventional photolithography is limited to less than one due to the refractive index of the air gap, of about 1.0, between the final lens and the photoresist. In an immersion system, the air gap is filled with higher refractive index liquid, for example purified water with a refractive index of about 1.44, during the exposure process. Light travels with a shorter wavelength in the liquid than in air, giving an image with better definition. At a given incident angle in an objective lens, θ_1 , the refraction angle at the lens/air interface, θ_2 , is greater than the angle at the lens/liquid interface, θ_3 , as shown in Figure 1.2. In other words, immersion reduces the refractive angle and thus increases DOF at a given NA value. Introducing water does not directly increase NA , but it allows one to design a high NA exposure system in which light travelling from a large incident angle can refract onto a resist film. Immersion lithography systems, using a 193 nm optical scanner with water as an immersion liquid, are already in production.

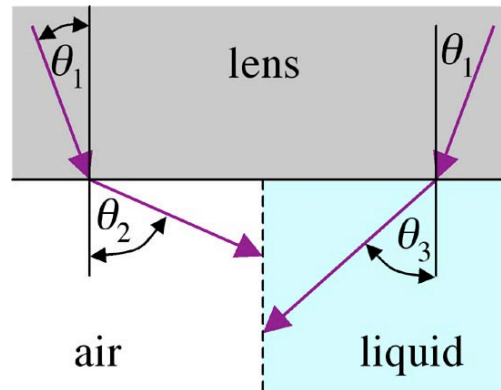


Figure 1.2 Schematic representations of optical paths between dry and immersion systems, assuming that $n_{\text{lens}} > n_{\text{liquid}} > n_{\text{air}}$.

However, there are several problems associated with immersion lithography such as incompatibility between the immersion liquid and the resist material and defects due to bubbles forming and particles getting trapped at the immersion liquid/resist interface [14-16]. These challenges add difficulty to designing tools and relevant materials and introduce process complexity. Performance of immersion tools can be further improved using a combination of high index materials for the immersion liquid, the objective lens, and the photoresist [14,17].

1.2.3 International Technology Roadmap for Semiconductors

The International Technology Roadmap for Semiconductors (ITRS) details the requirements and technological challenges which must be addressed in the near and longer term to sustain progress in semiconductor manufacturing [18]. It is a cooperative work of international organisations including industry manufacturers, companies, government organisations, and universities, aiming to provide a direction for research and development and to sustain growth within the semiconductor industry. Table 1.1 shows the resolution requirements for lithographic technology and the expected technological solution according to the year of production. The smallest feature size, called half pitch, in a new generation dynamic random access memory (DRAM) to be released in the year of production is often used to mark the resolution capability of lithographic technology. It is expected that 193 nm

immersion lithography will be used until 2012 and the first next generation lithography (NGL) is predicted to be ready for beta testing in high volume production in 2011.

Table 1.1 The lithographic technology requirements and solutions by the year of production.

Year of Production	2009	2010	2011	2012	2013	2014	2015	2016
DRAM Metal Half Pitch (nm)	52	45	40	36	32	28	25	23
Exposure Tool Potential solution	193i	193i	193i/ NGL	193i/ NGL	NGL	NGL	NGL	NGL

1.3 Next generation lithography

The minimum feature size achievable by photolithography is already smaller than the radiation wavelength, and the cost of improving its resolution is increasing exponentially, meaning that it is rapidly becoming economically unviable [19]. However, the demand for critical feature size reduction continues, and current technology cannot support it. In order to continue miniaturization, a number of alternative technologies called next generation lithography (NGL) are currently being developed. Some emerging NGL technologies have been included in the ITRS 2009 edition. There are 193 nm immersion with multiple patterning lithography, extreme ultraviolet (EUV) lithography, imprint lithography, and maskless lithography.

The most realizable approach to NGL is to extend the resolution capability of photolithography. The extension can avoid costs and complexity in the establishment of a new technology and also save time to ensure readiness of the technology according to a timeline. A couple of technologies to be combined with the 193 nm photolithography for the next technology node are immersion and double patterning lithography.

1.3.1 Double patterning lithography

Double patterning (DP) lithography is one of the simplest emerging NGL to implement because it is based on lithographic technology that already exists. The double patterning technique splits the required pattern into two steps, in such a way as to separate adjacent features onto separate masks. As sparse feature resolution is generally higher than dense feature resolution this allows higher resolution. A 32 nm half-pitch resolution pattern has been demonstrated using DP and 193 nm dry lithography [20]. An even higher resolution of 22 nm half-pitch has been patterned using a combination of DP and 193 nm immersion lithography [21]. A variety of DP techniques have been presented. The most common is called the litho-etch, litho-etch (LELE) method and uses two steps of lithography and etching successively [20,22,23] as shown schematically in Figure 1.3 (a). The first litho-etch step transfers half of the pattern onto a hard mask layer. The second litho-etch step transfers the other half of the pattern onto the hard mask and then the whole pattern is transferred to the substrate through an etching process. A second DP technique is called self-aligned double patterning (SADP) [21,24] and uses a lithographic pattern itself to position a higher density pattern without the need for advance mask overlaying. The basic SADP process is illustrated in Figure 1.3 (b). The resist layer is patterned first, followed by deposition of spacer material. The coating layer is then etched to remove the spacer material on top and also the resist leaving just the sidewalls spacer forming a masking pattern. The spacer pattern is finally transferred onto a hard mask layer underneath. SADP can be extended to give multiple patterning by repeating the deposition of space material and etching steps [25]. The resolution achievable using the DP technique is promising for the next technology node, but implementation of DP also doubles the difficulties and manufacturing costs associated with lithography processes. Furthermore as feature sizes continue to diminish it will be necessary to move to quadruple and so on, leading to an exponential cost increase.

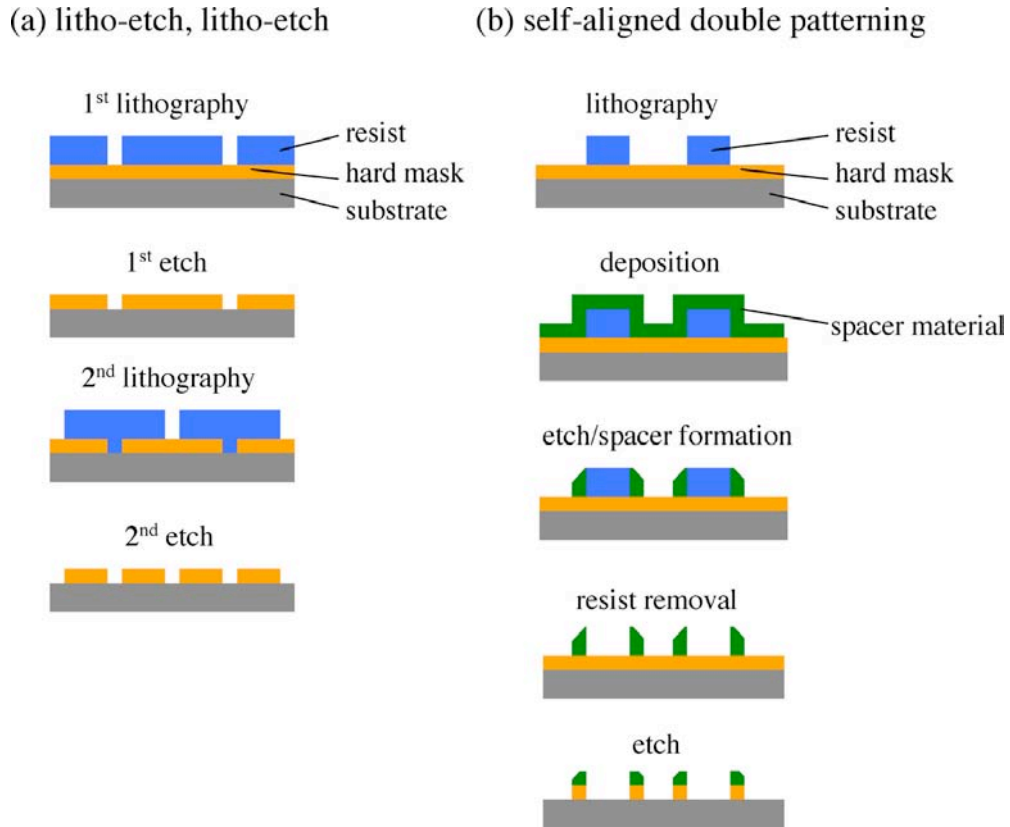


Figure 1.3 Schematic representations of (a) LELE process and (b) SADP process.

1.3.2 Extreme ultra violet lithography

Extreme ultra violet lithography (EUVL) is considered by ITRS as the leading candidate among several NGL technologies. The first commercially available prototype EUVL exposure system has been introduced at the resolution of 32 nm to demonstrate its cost effectiveness [26]. Development of a full commercial EUVL system is underway, and EUVL is expected to be ready for high-volume manufacturing by 2013 [27, 28]. EUV lithography employs a short wavelength source in the soft x-ray region between 11 nm and 14 nm. EUV light can be produced from a synchrotron accelerator, but in commercially designed systems a laser-produced plasma (LPP) source or a discharge-produced plasma (DPP) source are used. Because EUV lights are strongly absorbed in most materials, EUVL works by means of reflection optics using a set of high-reflective mirrors and operates in a vacuum environment. The EUV reflective mirror is made of multilayer of absorber and spacer materials coating in periodicity with thickness that the maximum reflectivity is achieved under the Bragg's

condition. The multilayer coating system of molybdenum and silicon (Mo/Si) is one of the candidate materials providing high reflectivity of 65% to EUV lights and typically used for EUV light at wavelength of 13.5 nm [29]. In the EUV exposure system, EUV light generated from a source is focused onto a reflecting mask using condenser and positioning mirrors. An image of two dimensional patterns on the mask is reflected with a series of reduction mirrors for demagnification, and finally projected onto a wafer to expose a resist film. A schematic representation of the optics system in EUVL is shown in Figure 1.4. Although EUVL demonstrates promising resolution capability, it requires operation in a vacuum chamber, limiting production throughput. In addition, there are several challenges regarding the implementation of EUVL in high-volume manufacturing. The critical requirements for EUVL include a high power and long life source, a defect-free mask, a defect inspection method, and a novel resist material [27, 28].

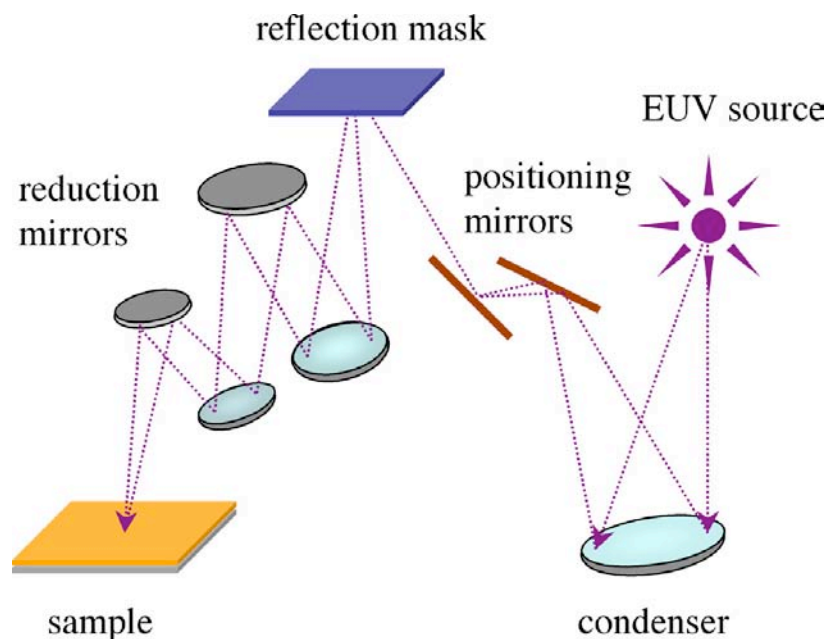


Figure 1.4 Schematic representation of EUVL optics.

1.3.3 Nanoimprint lithography

Nanoimprint lithography is a relatively new technique and is increasingly drawing attention as an NGL due to its potential to pattern high resolution features with low cost and high throughput. In the

nanoimprint technique, a high resolution three-dimensional pattern on a replica mould surface is simply transferred into a resist film at 1:1 scale by means of mechanical contact. The resist layer is shaped under compression pressure with the assistance of thermal [30] or UV curing [31]. After imprinting, the resist pattern may be treated by oxygen plasma etching to remove any thin residual layer left in the areas that should be cleared. A number of variants of the technique have been developed and several commercial tools are now available [32]. The nanoimprint technique is widely applied in micro- and nano-technology research; however, it is not ready for high-volume application in the IC industry. Its speed and reliability need to improve to allow it to compete with other NGL technologies.

1.3.4 Electron beam lithography

1.3.4.1 Electron beam direct-write lithography

Electron beam lithography (EBL) has been used in the IC industry since the 1960s. However, because of its very low throughput, its application is limited to small volume production such as in fabrication of photo masks to be used for photolithography and in device prototyping [33]. The first electron beam lithography tool was a modified scanning electron microscope (SEM). In an EBL tool, the electron beam is accelerated and focused onto a sample under a vacuum environment. While an SEM rasters the beam across a sample to image it, an EBL tool directs the finely focused electron beam to any position of a sample for a particular duration and draws a shape by controlling the position, and on/off status of the beam. Patterning requires a deflection and a blanking system which uses electrostatic or electromagnetic lenses to control the beam position, as shown schematically in Figure 1.5. As an EBL tool can draw an arbitrary pattern without using a mask, it is categorised as a maskless lithography.

An EBL is the most promising lithographic technique among lithographic technologies in terms of resolution capability. The resolution of EBL is not limited by the diffraction phenomenon as a wavelength of an electron at usable accelerating voltage, 1–100 kV, is only a fraction of a nanometre,

but only by the beam spot size and electron-solid scattering as described in the next section. EBL also has a very large *DOF*, typically several micrometres - a strong advantage over photolithography.

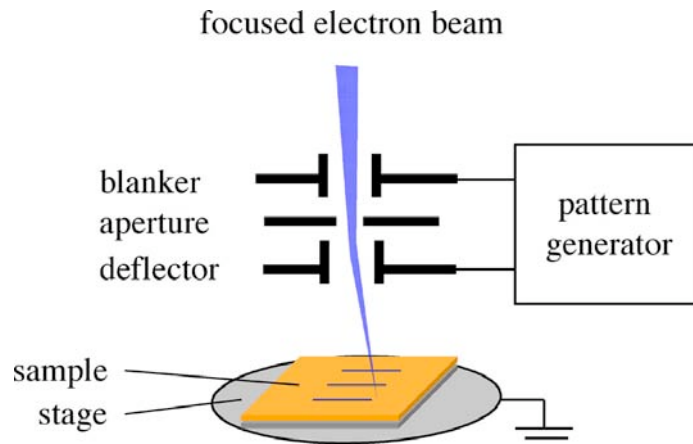


Figure 1.5 Schematic representation of beam control elements in electron beam direct writing lithography.

1.3.4.2 Electron–solid interactions

Although the electron beam in EBL tools can be tightly focussed to have an extremely small beam diameter of a few nanometre [34], it is unusual to achieve a nanometre size feature in a resist film. Electron–solid interactions cause electron scattering within the resist which limit the final resolution. As primary electrons strike the resist, they experience two types of scattering events, forward scattering and backscattering, as shown in Figure 1.6.

Forward scattering causes incident electrons to change their direction by a small angle, broadening the beam diameter as electrons penetrate toward the bottom of the resist film. Backscattering is a large angle scattering event. Backscattering usually happens when primary electrons collide with a heavy ion core. Some backscattered electrons travel back through the resist at a range as far as micrometres away from the incident beam. These backscattered electrons are responsible for the proximity effect in which scattered electrons deposit energy into unexposed areas of a resist film. The range of backscattered electrons depends on the energy of the primary electron. A primary electron with higher energy allows the backscattered electron to go a longer distance.

Primary or backscattered electrons can experience inelastic scattering events in the resist film and dissipate their energy to form secondary electrons. The energy dissipation continues and generates a number of secondary electrons along the pathway of the primary electron until the primary electron loses all of its energy, initially between 5 and 50 keV in EBL. Secondary electrons with energies in a range of 2 to 50 eV are responsible for the majority of resist exposure process. They are considered to cause additional beam diameter widening as they can travel a short distance, on the order of nanometres, in the resist before reacting with a resist molecule.

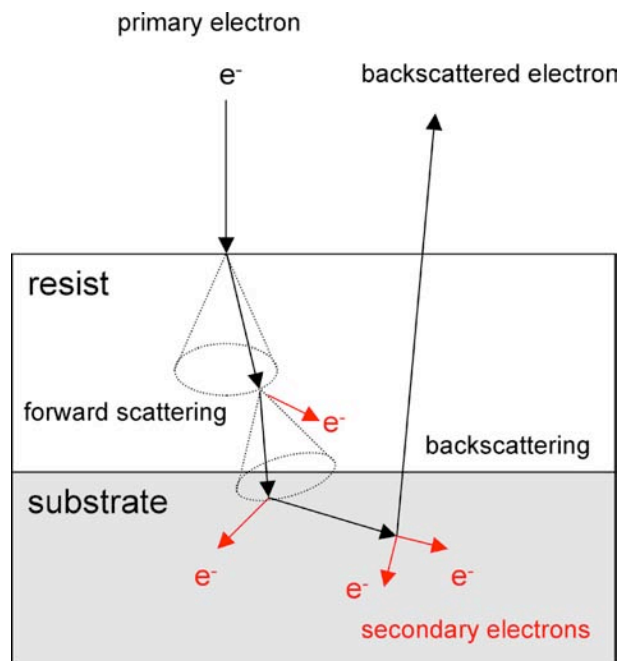


Figure 1.6 Schematic representation of electron–solid interactions within a resist/substrate specimen.

1.3.4.3 Multiple electron beam direct-write lithography

The major disadvantage of direct-write EBL is the low throughput. An electron beam writes the pattern in a serial manner, and thus extremely slow, achieving less than one wafer per hour in contrast to the 50-100 wafers per hour which can be patterned by photolithography. To overcome the throughput limitation of direct-write EBL, a variety of approaches are under consideration for NGL. An example of next generation EBL currently active is maskless lithography (ML2) based on

multibeam technology [35], including multiple aperture pixel by pixel enhancement of resolution (MAPPER) and projection maskless lithography (PML2).

MAPPER technology is a maskless, direct writing, electron beam technique developed by MAPPER lithography. The MAPPER concept is based on massively parallel direct writing electron beams, each of which is programmed to operate independently with the assistance of high speed optical data transfer [36]. MAPPER's current design aims to exploiting 13,000 parallel beams to pattern at a high resolution of 45 nm with throughput of 10–20 wafers (300 mm) per hour [36]. To achieve that speed and avoid overlay problems due to wafer heating, a low electron energy of 5 kV is used [37]. Recently, patterning of 45 nm half-pitch resolution in HSQ resist film has been demonstrated using the MAPPER tool with 110 electron beams [38]. A schematic of the MAPPER system is illustrated in Figure 1.7.

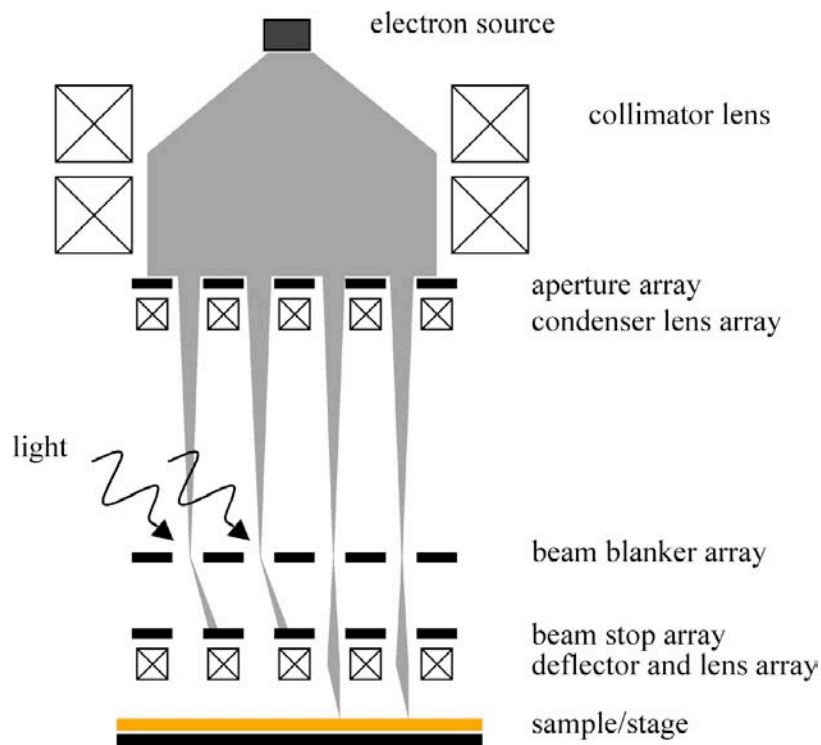


Figure 1.7 Schematic representation of MAPPER system.

In the MAPPER system, electrons are generated from a high brightness electron source and they are collimated to cover the aperture plate using a collimator lens. A single collimated beam is split up into 13,000 electron beams at the aperture array. Each beam is focused by the condenser lens array, having the focus plane at the photo-activated beam blanker array, which can deflect an individual beam away from its optical axis and intercept the beam at the beam stopper array. The beams passing through the beam stopper are deflected to perform scanning by the deflector lens array underneath. The beams are finally focused by the projection lens array onto the wafer on the moving stage. In this setup, the data system takes control of beam writing through switching of 13,000 light beams, one for each beam blanker, so that each electron beam has its own blanking system, allowing thousands of electron beams to work independently.

PML2 is another maskless multibeam technology being developed by IMS Nanofabrication. It uses hundreds of thousands of parallel beams, which are individually controllable, to make patterns simultaneously [39]. An outline of the PML2 system is illustrated in Figure 1.8. Like MAPPER, the PML2 tool uses a single electron source to produce a large area collimated electron beam. In contrast, the collimated beam of 5 kV energy is split into thousands beamlets at the programmable aperture plate system (APS) found only in PML2 technology. The electron beamlets are then accelerated to energies of up to 50 keV, before being demagnified 200 times by condenser lenses. These beamlets are finally projected through the aperture at the beam cross-over plane onto a wafer to perform spot exposure while the wafer stage is still or moving. The APS consists of an aperture array at the top plate and deflection arrays at the bottom plate. An electron beamlet is produced at the aperture plate, and is blanked if required by the blanking plate below. Electrodes in the blanking plate deflect the beam so that it does not pass through the aperture at the beam cross-over, instead hitting the beam stop plate. The PML2 proof-of-concept tool has demonstrated 16 nm resolution patterning in Hydrogen silsesquioxane (HSQ) resist using a 15 keV electron beam [40]. The current PML2 tool employs 2,300 beams, leaving the challenge of scaling it up in the future to reach the goal of 290,000 beams. The critical technology behind the success of both aforementioned lithography systems is micro-electro-

mechanical-systems (MEMS), where thousands of microscopic elements such as aperture and deflection electrodes need to be made as identical as possible for every single electron beamlet.

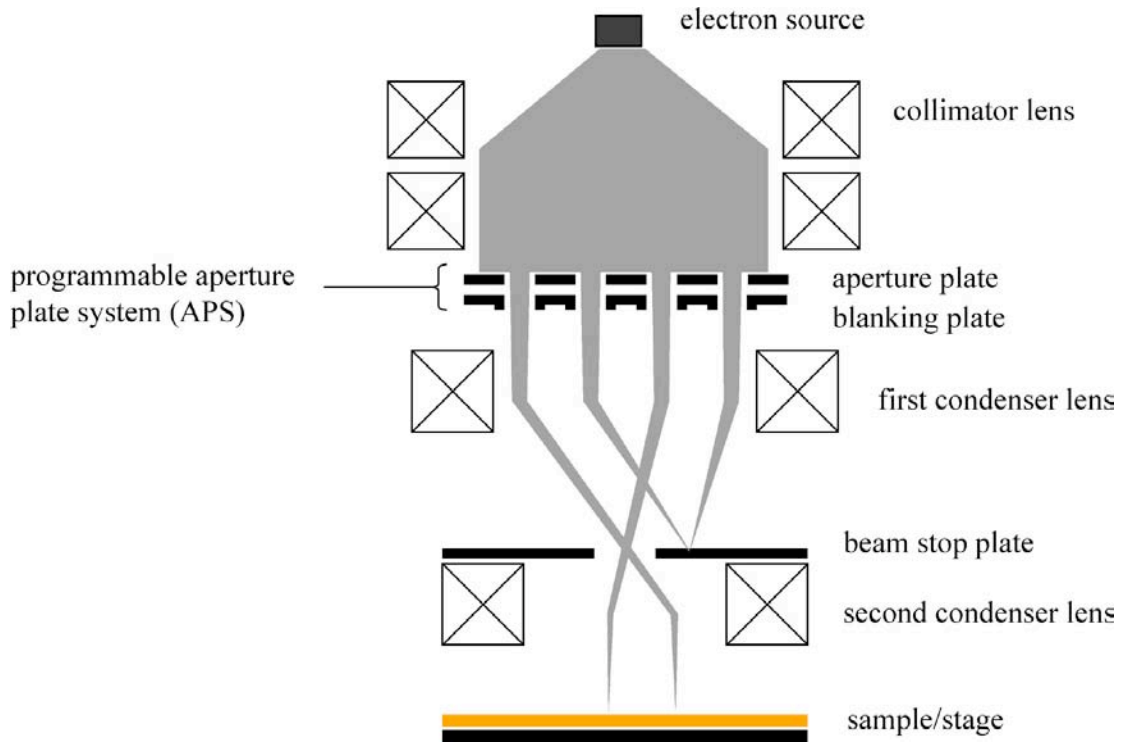


Figure 1.8 Schematic representation of PML2 system.

1.4 Resist materials

1.4.1 Resist characteristics

The word 'resist' refers to a material, typically a polymer, which is able to coat and protect an underlying substrate from etching, diffusion, deposition, or implantation in device manufacturing processes. They can form a thin film on the substrate by means of the spin coating technique. Resists are irradiation sensitive materials. Exposure of the resist to a specific radiation source causes a change in its solubility in a suitable developer. Thus the resist is able to capture an image produced by a lithography tool and form a physical mask with the appropriate pattern, after a development process. Resist materials are typically classified into positive tone or negative tone types, according to their response to irradiation. In a positive tone resist, an exposed area becomes more soluble in the

developer. In contrast, an exposed area of a negative tone resist becomes less soluble in the developer. Resist performance can be defined using a set of resist characteristics including sensitivity, contrast, line edge roughness, and etch resistance, which are described in the following sections.

1.4.1.1 Sensitivity and contrast

Sensitivity and contrast are intrinsic properties of a resist material, depending on wavelength or energy of the radiation source as well as process conditions such as baking and development. The sensitivity of a resist is the minimum dose of radiation required to transform it, where dose is an amount of energy deposited onto a resist per unit area, usually expressed in mJ/cm^2 in photolithography. For electron beam lithography, dose is an amount of electric charge or the number of electrons per unit area, expressed as $\mu\text{C}/\text{cm}^2$. An area dose, D , is expressed by an equation

$$D = \frac{It}{A}, \quad (1.4)$$

where I is the light intensity or electron beam current, t is the exposure time and A is the exposure area. The contrast quantifies the rate change of resist transformation with respect to an increment of exposure dose.

Both sensitivity and contrast of the resist can be determined from a response curve, a relation produced by plotting the remaining thickness of the resist after development against the exposure dose, as shown in Figures 1.9 (a) and (b) for a positive tone resist and negative tone resist, respectively. Film thickness in a positive tone resist begins to drop at a threshold dose and drops with a finite slope as exposure dose increases. Sensitivity is defined as the dose at which all resist is removed, D_2 [41]. In the case of a negative tone resist, film thickness rises with an increase in exposure dose, and the sensitivity is the dose at which 50 % of the thickness is retained, D_3 . Contrast, γ , is defined as the slope of a linear portion of the curve expressed by [42]

$$\gamma = \left| \log_{10} \left(\frac{D_2}{D_1} \right) \right|^{-1}. \quad (1.5)$$

An ideal resist should have high sensitivity and contrast. The highly sensitive resist requires a low dose and hence little time to process, giving a high manufacturing throughput. A higher contrast resist is preferable because it changes in a smaller range of doses around the critical dose and it is able to provide more vertical sidewall profiles.

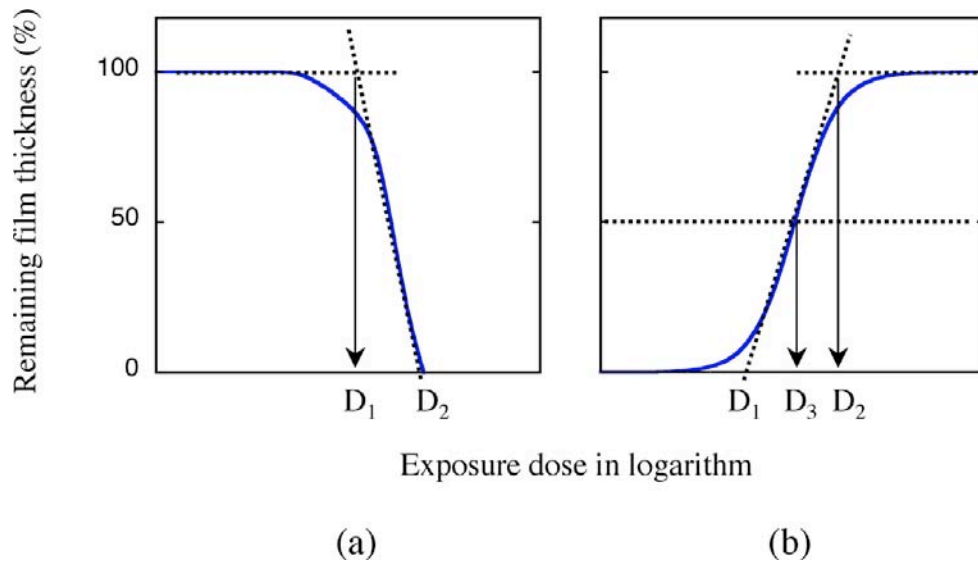


Figure 1.9 Response curve of (a) a positive tone resist and (b) a negative tone resist.

1.4.1.2 Resolution

Although resolution depends on both the capability of the exposure tool and that of the resist material, it is defined as the minimum feature size one can print in a resist film. In practice, the feature size printed in the resist can differ from the nominal size due to process conditions such as exposure dose and development as well as intrinsic properties of the resist. The resolution should be presented with specifications of the lithography tool and notes on resist processing. Pitch and line width are terms usually used to define dense and sparse resolutions. Pitch is the distance covering a line and a space in a dense (1:1) periodic pattern. Line width is the width of an isolated line in a sparse pattern.

1.4.1.3 Line edge roughness; Line width roughness

Line edge roughness (LER) is a random fluctuation at the edge of a resist feature that changes the feature size adversely, whilst line width roughness (LWR) describes the deviation of both sides of the

feature from the target dimension. A relation between LER and LWR can be given in the case of uncorrelated edges as [43]

$$\text{LWR} \approx \sqrt{2}\text{LER}. \quad (1.6)$$

Control of LWR is important in fabrication of ICs as a small variation in the feature size of electronic components can affect a performance of the circuit drastically. It has been reported that LWRs of transistor logic gate lengths of larger than 10 % of the nominal length causes significant variance in electrical characteristics of the devices [44-46]. A number of factors have been studied to investigate the causes of the feature roughness. LER has been attributed to a number of material factors such as the molecular weight of resist component [47,48-50], molecular weight distribution [51], molecular structure [52,53], and distribution of resist components [54,55]. It has been suggested that reduction of LER can be achieved by using resists with low molecular weight or with low polydispersity. A contribution from the lithography processes to LER is also observed. The presence of mask defects [56], a poor aerial image contrast [57,58], shot noise effects (random fluctuation in exposure dose due to the low number of irradiation events required in modern resists) [48,59,60], and unsuitable development processes [61-63] can lead to an increase in feature roughness. Studies of chemical reactions and transport effects in a resist film, especially in the case of chemically amplified resists as described in section 1.5, revealed that the random walk nature of acid diffusion and increase of LER are closely related [48,49,64].

1.4.1.4 Etch resistance

Dry plasma etching is one of the most common pattern transfer techniques used in IC industry. A patterned resist layer acts as a mask for an underlying substrate such as silicon during the etching process. Although the etch rate of a resist depends on etching gases and process conditions, a resist should have a good resistance to the plasma etching in comparison to that of a substrate. Specifically, the resist should be etched at slower rate than the substrate material so as to product an etched structure with a sufficient aspect ratio. Etch resistance is generally represented as an etch selectivity

between the underlying material and the resist - the ratio of the etch rate of the material to be etched to that of the resist.

1.4.2 Resist roadmap

The ITRS details the requirements for a resist in the near-term years as shown in Table 1.2 [18]. Dense and sparse resolutions are required as the pitch size in DRAM and gate length of microprocessor unit (MPU) require dense and sparse features, respectively. Critical dimension control is the variation in size among features printed. LWR is measured at low spatial frequency from $0.5 \mu\text{m}^{-1}$ to MPU pitch⁻¹. The requirement for the resist sensitivity is specified with respect to the lithographic technology as shown in Table 1.3.

Table 1.2 ITRS resist requirements by the year of production.

<i>Year of Production</i>	<i>2009</i>	<i>2010</i>	<i>2011</i>	<i>2012</i>	<i>2013</i>	<i>2014</i>	<i>2015</i>	<i>2016</i>
<i>DRAM 1/2 Pitch (nm)</i>	52	45	40	36	32	28	25	23
<i>MPU gate in resist length (nm)</i>	47	41	35	31	28	25	22	20
<i>CD control (nm, 3σ)</i>	3	2.8	2.5	2.3	2.1	1.9	1.7	1.6
<i>LWR (nm, 3σ)</i>	3.7	3.2	2.8	2.5	2.2	2.0	1.8	1.6

Table 1.3 ITRS requirements for resist sensitivity.

Radiation source	Sensitivity
193 nm photolithography	20-50 mJ/cm ²
EUV (13.5 nm) lithography	5-20 mJ/cm ²
High voltage e-beam (50-100 kV)	5-30 μC/cm ²
Low voltage e-beam (1-5 kV)	0.2-1.0 μC/cm ²

1.5 Chemically amplified resists

1.5.1 Principle of chemical amplification

The concept of chemical amplification of resists was proposed by Ito, Willson, and Frechet in the early 1980s to address the issue of the poor photosensitivity of resists for DUV lithography [65, 66]. In a chemical amplified resist (CAR) system, a single photo event produces a catalyst by photoreaction of a photoactive compound upon irradiation, which then induces a cascade of chemical reactions. Therefore a single irradiation event can lead to multiple resist exposure events, increasing the photosensitivity. This is a significant advantage over using irradiating energy to directly alter solubility in conventional resists. As the CAR concept is simple and effective, it has been widely accepted and has become a mainstream subject of research for modern resist materials. Various chemical amplification schemes have been designed and studied, originally including depolymerisation for positive tone images, deprotection for dual-tone images, and polymerisation for negative tone images [67]. Some of those mechanisms are described below.

In the original concept [66], a CAR was designed to work on acid-catalysed deprotection mechanism. The CAR was a two-component system consisting of a polymer resin protected with an acid labile functional group and a photo acid generator (PAG), which is a photoactive compound used to initiate acid catalysis. The mechanism of CAR can be explained in two steps: acid generation and deprotection. In the first step, an acid is generated from a photoreaction in which PAG is decomposed upon irradiation, producing a strong acid. In the second step, the acid starts catalysis in which an acid labile group is cleaved off a polymer chain and the acid is regenerated to carry out subsequent catalytic reactions. The cleavage of the protecting group changes the polarity of the polymer. With an adequate number of polarity switches, the solubility of the exposed polymers changes. The catalytic deprotection reaction typically requires thermal energy to activate. Therefore, a post exposure bake (PEB) at an elevated temperature is applied to the resist after the exposure process, to promote acid catalysis.

The first CAR introduced into the DRAM manufacturing process with 248 nm Deep UV lithography was IBM's *t*BOC resist [68]. The *t*BOC resist was composed of a polymer resin poly(4-*tert*-butoxycarbonyloxystyrene) (PBOCST) blended with 4.75 wt% of triphenylsulfonium hexafluoroantimonate (TPS-SbF₆) PAG. The PBOCST resin basically is a hydrophilic poly(4-hydroxystyrene) (PHOST) with the phenolic sub-units protected using a lipophilic *tert*-butoxycarbonyl (*t*BOC) functional group. The protecting group makes the PBOCST insoluble in polar solvents. The CA mechanism of the *t*BOC resist is shown in Figure 1.10.

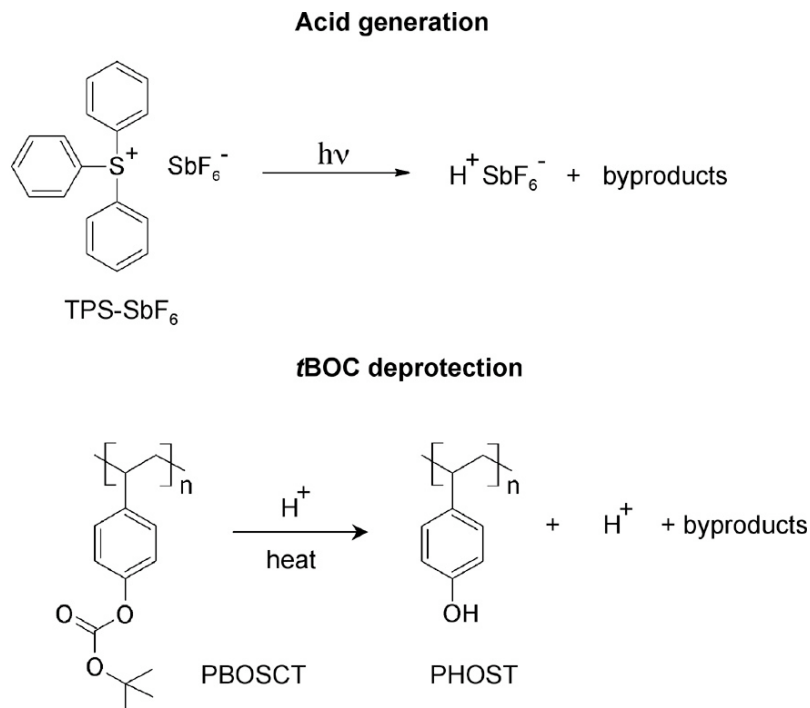


Figure 1.10 Acid-catalysed deprotection of the *t*BOC resist.

The PAG produces a strong acid upon exposure to Deep UV radiation. Upon the PEB at about 100 °C, acid catalysis cleaves the acid labile *t*BOC group, releases by-products, and produces another acid. Acid-catalysed cleavage of a *t*BOC group converts PBOCST back to hydrophilic PHOST. The resist can be exploited as either a positive tone or a negative tone resist, depending on the development process. A positive tone image is achieved when developed in polar solvent or aqueous base solution in which hydrophilic PHOST, in an exposed area, is readily dissolved in the developer solvent and

washed away. A typical aqueous base, widely used in manufacturing processes, is tetramethylammonium hydroxide (TMAH) at 0.26 N concentration. In contrast, a negative tone image is generated when developed in a non-polar organic solvent such as anisole in which unexposed lipophilic PBOCST is removed leaving a pattern of remaining PHOST. The catalytic chain length of the *t*BOC resist was estimated to be 1000 under normal processing conditions [69], resulting in a huge enhancement in resist sensitivity.

Polymerisation is another chemical amplification scheme devoted to negative tone resist formation. For instance epoxy crosslinking via an acid-catalysed ring-opening of an epoxide functional group was proposed for use in a negative tone CAR [65]. The resist was a blend of a resin with a pendant epoxide group and a PAG. An onium salt photoinitiator, developed for epoxy curing [70,71], was used as a PAG in this resist system. The photo-generated acid reacts and causes an epoxide ring to open, producing a highly reactive site enabling to crosslink with another molecule. As a result, the three-dimensional crosslinked network forms in the exposed area and becomes insoluble in an organic developer. The crosslinking of an epoxy resin is illustrated in Figure 1.11. An example of a commercially available resist based on epoxy crosslinking is SU-8 (MicroChem). It is very often used for transferring pattern into a silicon substrate in a range of applications [72]. A primary difficulty in implementing a crosslinking negative tone resist for high resolution patterning is feature swelling, which results during development process, as the organic solvent penetrates into the crosslinked network and distorts the pattern. The swelling problem was suppressed in aqueous base soluble epoxy resists. This resist is formulated by blending PHOST with PAG and an appropriate amount of epoxy novolac resin [73,74].

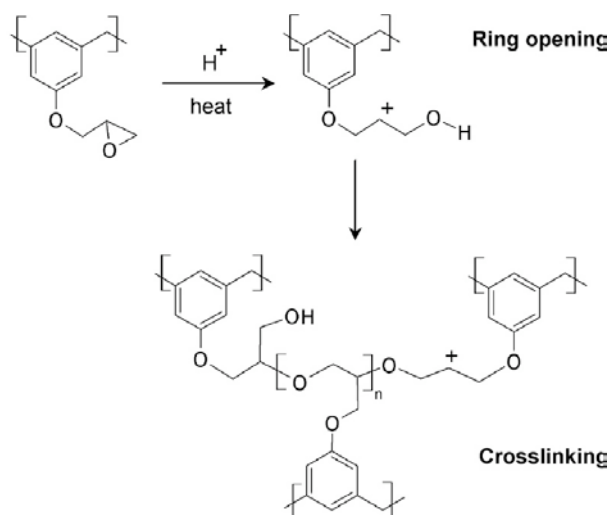


Figure 1.11 Crosslinking of an epoxy resin via acid-catalysed ring opening.

1.5.2 Fundamental limit

In a chemically amplified resist system the catalytic reaction of an acid is utilised to increase the resist sensitivity. An acid generated by irradiation can diffuse from its original position and catalyse deprotection or crosslinking, driven by a baking process. Acid diffusion helps to smoothen feature roughness attributed to statistical fluctuations in the exposure energy, but it can also cause image blur when an acid diffuses across the boundary defined by an aerial image and reacts with molecules in unexposed areas. In contrast, limitation of acid diffusion can limit the number of deprotection or crosslinking events, resulting in poor resist sensitivity and feature roughness at a molecular scale. Moreover, in a highly sensitive resist, an image can suffer from feature roughness due to the shot noise effect [59,75] when exposure with a very low dose is used. This shows an example of the trade-off relation between sensitivity, resolution, and LWR, known as the RLS trade-off [76,77] in which one parameter can be optimised but at the cost of degradation of other parameters according to the relation

$$\sigma_{LER}^2 \times dose \times blur \approx \text{constant}, \quad (1.7)$$

where σ_{LER}^2 , *dose*, and *blur* are the factors representing the root mean square roughness, the exposure dose, and the resist diffusion blur, respectively. The trade-off gives a fundamental limit to the best performance from a particular chemically amplified resist. In order to minimise the trade-off

effect, the development of a new resist material, enabling high sensitivity, high resolution, and low LWR simultaneously, is critical.

1.6 Electron beam resists

1.6.1 Polymer resists

Conventional resists for e-beam lithography are polymers. Polymers are versatile and easy to process. They are able to form a smooth film on a variety of substrates by the spin coating technique. Examples of common polymeric e-beam resists are Poly(methyl methacrylate) and Shipley's SAL601.

1.6.1.1 Poly(methyl methacrylate)

Poly(methyl methacrylate) (PMMA) was one of the first polymers developed for electron beam lithography [78]. PMMA is typically used as a positive tone resist, although it acts as a negative tone resist at very high dose, about two orders of magnitude greater than that used for the positive tone behaviour. Upon e-beam irradiation, the polymer can undergo either bond breaking (chain scission) or radiation-induced bonding (crosslinking) simultaneously. Chain scission dominates in the positive tone mode of PMMA, leading to a reduction in the molecular weight of the polymer, and thus enhancing solubility in particular developers. Crosslinking events forming a higher molecular weight polymer, which becomes insoluble, dominate in the negative tone mode of PMMA. PMMA has a capability for high resolution and is considered as the standard high resolution resist. Lines with a width resolution below 5 nm were demonstrated in positive tone PMMA using a molecular weight of 100K [79]. A 12 nm wide isolated line was also achieved in negative tone PMMA [80]. Its disadvantages are poor sensitivity and poor etch resistance to plasma etching. A sensitivity of about $350 \mu\text{C}/\text{cm}^2$ was reported for a positive PMMA using 50 keV and a mixture of methyl isobutyl ketone: isopropyl alcohol (1:3) as a developer [78].

1.6.1.2 Shipley Advanced Lithography resists

Shipley advanced lithography (SAL) is a family of chemically amplified resists supplied by Rohm and Hass Electronics Materials. SAL601, the first SAL resist, is a three-component negative-tone e-beam resist composed of a base polymer, an acid generator and a crosslinking agent. As with typical chemically amplified resists, a baking process after exposure is required and the baking conditions are critical to control acid diffusion and thus lithographic feature size. An isolated line with feature size as small as 20 nm was achieved in 20 nm thick SAL601 film using 5 keV beam [81]. SAL601 has a very high sensitivity; however, under practical processing conditions the resolution is about 50 nm. Its sensitivity was 7-9 $\mu\text{C}/\text{cm}^2$ at 20-40 kV [82]. SAL601 has high etch resistance comparable to the novolac base polymer.

1.6.2 Molecular resists

It is predicted that the conventional polymeric resists will reach their resolution limit by the time of the DRAM resolution of 22 nm in 2016, when the lithographic feature roughness requirements become smaller than the size of polymer molecules. The concept of molecular resists has been proposed to meet requirements of high resolution and low LER by utilising a small molecule material rather than a polymer. A range of molecular materials are currently subject of resist research.

1.6.2.1 Calixarene derivatives

Calixarene is a cyclic oligomer containing repeating units of phenolic hydroxyl groups linked with methylene bridges as shown in Figure 1.12. Various calix[n]arene derivatives have been studied as the negative tone resists for e-beam lithography [83-85]. With molecular size of about 1 nm, the material has the potential for high resolution lithography. Sub 10 nm feature resolution was achieved in a film of p-methyl-acetoxycalix[6]arene. However, its sensitivity was of the order of mC/cm^2 . Chemical amplification of a calix[4]arene derivative using a cationic polymerisation scheme has been demonstrated [86]. A sensitivity of 15 $\mu\text{C}/\text{cm}^2$ at 25 keV was achieved in the two-component

calix[4]arene derivative:PAG resist, whilst features with a resolution of 30 nm were patterned using 30 keV.

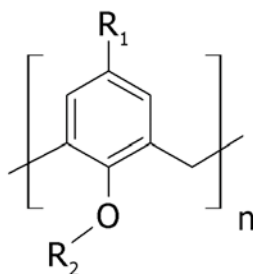


Figure 1.12 Schematic diagram of calixa[n]rene with functional groups R_1 and R_2 .

1.6.2.3 Triphenylene Derivatives

A triphenylene, $C_{18}H_{12}$, is a discotic liquid crystal molecule consisting of four benzene rings bound together. Its polysubstituted derivatives, as shown in Figure 1.13, were demonstrated as negative tone e-beam resists [87-89]. The derivatives were dissolved in chloroform and were able to spin coat a silicon chip. They have sensitivity between 1.5 and 6.5 mC/cm^2 at 20 keV. The derivative C5/C5 ($R_1=R_2=C_5H_{11}O$) showed positive tone behaviour at relatively low doses. A high resolution of 14 nm was achieved in the same derivative using 30 keV beam and development in monochlorobenzene. The etch resistance of the triphenylene derivatives was about 2 times that of a common novolac resist. Chemical amplification of the triphenylene derivatives has been demonstrated [90-92]. A sensitivity enhancement to 7 $\mu C/cm^2$ at 20 keV was achieved with a blend of the derivative C5/epoxide ($R_1=C_5H_{11}O$, $R_2=epoxy$), the derivative C5/C0 ($R_1=C_5H_{11}O$, $R_2=OH$), and an onium salt PAG. Features with a resolution of 40 nm was achieved in the same resist.

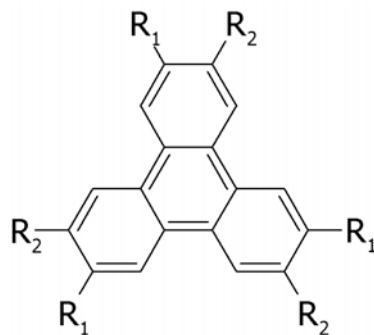


Figure 1.13 Schematic diagram of a triphenylene derivative with functional groups R_1 and R_2 .

1.6.2.4 Fullerene Derivatives

The fullerene C_{60} is a closed cage structure molecule consisting of sixty carbon atoms [93], Figure 1.14 (a). The small molecular size of 0.7 nm in diameter makes C_{60} the potential material for high resolution lithography. It has been demonstrated by Tada et al. that C_{60} acts as a negative tone resist for e-beam lithography [94]. The C_{60} resist reduces its dissolution rate in a developer due to fragmentation of the C_{60} molecule upon irradiation of e-beam [95]. Because of the low viscosity of the C_{60} solution, the C_{60} film was prepared by deposition using vacuum sublimation. The electron sensitivity of the C_{60} resist was in the order of 10 mC/cm^2 at 20 keV. Its high etch durability allowed silicon pillar structures with a resolution of 20 nm to be fabricated. The resist properties was improved using chemical modification of the fullerene [96-98] in which side chains of a functional group are add to the C_{60} cage via a methano bridge as shown in Figure 1.14 (b). The maximum of six methano bridges can be incorporated into the C_{60} molecule. It was found that the chemically modified fullerene resist can enhance the solubility in an organic solvent, as a result the resist film can be prepared by spin coating. In addition, some fullerene derivatives showed an improvement of sensitivity, one order of magnitude higher than that of the C_{60} resist, whilst maintaining capability for high resolution and high dry etch durability. A further improvement of the resist sensitivity has been achieved using two different approaches, low-voltage electron beam lithography and chemical amplification. Using low-voltage electron beam exposure at 1 kV, the resist sensitivity can be enhanced to about $20 \text{ } \mu\text{C/cm}^2$ [99]. Using the chemical amplification principle, a three-component, negative tone, chemically amplified, fullerene resist system, in which the fullerene resist is blended with an onium salt PAG and

an epoxy novolac crosslinker, has been presented [90,100,101]. The resist sensitivity as low as $6 \mu\text{C}/\text{cm}^2$ at 20 keV has recently been demonstrated. A feature size of 15 nm with LWR(3α) of sub 5 nm can also be routinely achieved. The etch resistance to SF_6 plasma etching was comparable with that of SAL601 at the same etching conditions.

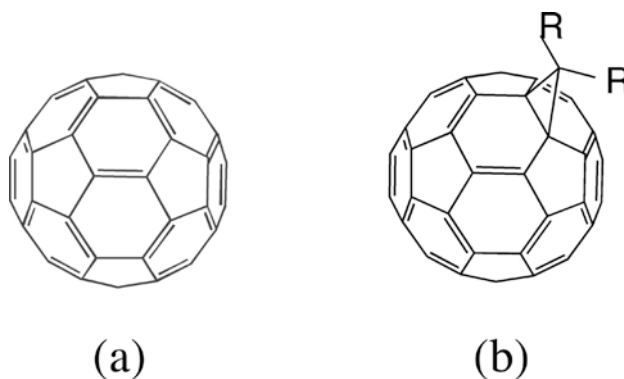


Figure 1.14 Schematic diagram of (a) fullerene C_{60} and (b) C_{60} with a methano bridge.

1.7 Thesis structure

This thesis presents work concerning the development and characterisation of novel resist materials for next generation lithography, primarily focussing on the electron beam writing technique. The resist materials were developed through the molecular concept and chemical amplification schemes. They are aimed at meeting the requirements of a resist material for lithography in the next technology node and beyond. In this chapter I give an introduction to microlithography and an overview of lithographic technologies and resist materials, covering current technologies and trends into the future. In chapter 2, I give detailed descriptions of the electron beam lithography tool, analytical equipment, and experimental techniques used for the preparation and characterisation of resist materials. Chapter 3 presents the results of chemical amplification of negative tone fullerene molecular resists, detailing their formulation, characterisation, and process optimisation, whilst chapter 4 covers a study of effects of base quenchers to characteristics of the same resist system. Chapter 5 presents a line width roughness (LWR) analysis of the negative tone chemically amplified fullerene resists, detailing the effects of resist processing on the LWR of lithographic features. Chapter 6 looks at the demonstration

of high-resolution resist pattern transfer using the plasma anisotropic etching technique. Chapter 7 presents the results of the formulation and characterisation of positive tone chemically amplified fullerene molecular resists. Chapter 8 summarises the results and gives recommendations for future work.

Chapter 2

Experimental Techniques

In this chapter the experimental techniques used are described, summarising the principles behind and basic operation of the main items of equipment. These include a scanning electron microscope coupled with a pattern generator which was used as a lithographic and analytical tool, plasma etchers used for resist pattern transfer or resist stripping and a contact surface profiler which was used for step height measurement of a thin film. Methods applied in the preparation and processing of chemically amplified resists are then detailed. Finally, the characterisation of a resist sample is described by providing definitions of resist characteristics and details of evaluation techniques. Those resist properties evaluated include sensitivity and contrast, resolution, line width roughness and etch resistance.

2.1 Equipment

2.1.1 Scanning electron microscope (SEM)

An XL30 SFEG SEM (FEI) was used throughout this study to visualise micro- and nano-scale features of the resist sample. The SEM used a focused electron beam as a probe to scan the surface of a sample. It is able to magnify the sample surface detail at very high spatial resolutions of approximately 5 nm to 10 nm, depending on beam spot size. The SEM technique was considered suitable for measurement of resist feature size in this study, as patterns of critical size smaller than 100 nm were fabricated. A schematic diagram of the SEM is shown in Figure 2.1. The main components of the SEM are an electron gun, collimating aperture, condenser lens, blanking aperture, deflection coils, objective lens and an electron detector. The electron beam is generated in an ultra high vacuum chamber, $\sim 10^{-10}$ mBar, by the Schottky field emission gun (SFEG) from which electrons are drawn and

accelerated toward a positively biased anode. The accelerated beam is collimated and de-magnified while travelling along the optical axis through a series of apertures and electromagnetic lenses. The beam can be turned on and off by a beam blanker which either allows the beam on or sweeps the beam off the optical axis. Deflection coils are used to deflect the electron beam to any position on, or perform a raster scan across, a sample's surface. The finely collimated beam is finally focused onto the sample by an objective lens, with the final spot size potentially as small as a few nanometres. Another important component is the stigmator, a lens used to minimise astigmatism aberration in which electron beams have different focus points in different perpendicular planes.

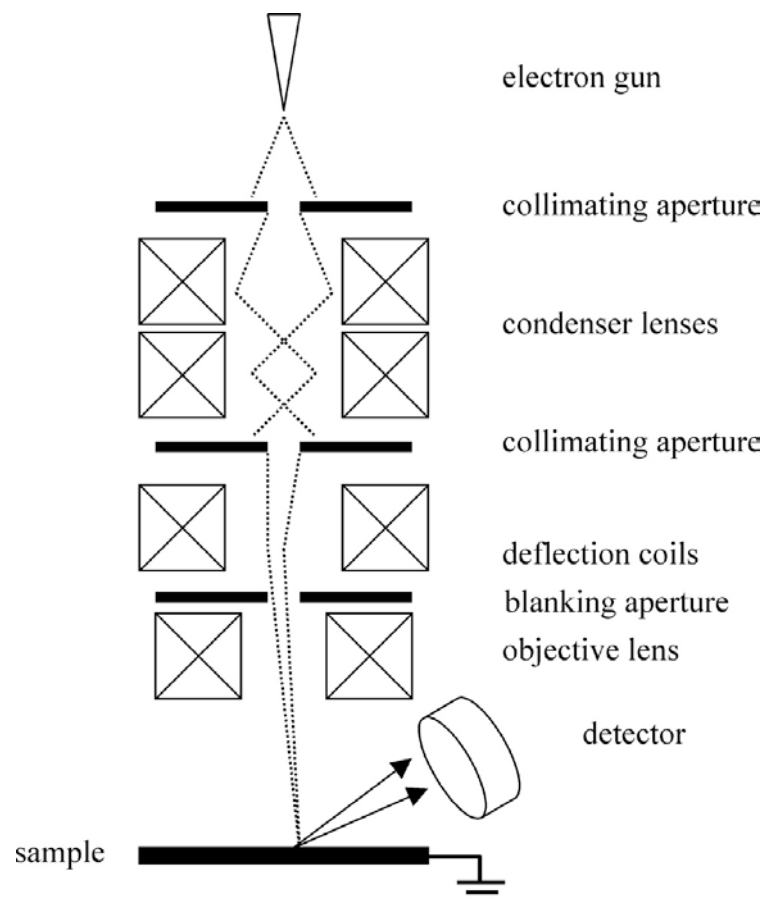


Figure 2.1 Schematic diagram of the SEM showing important elements.

The sample is mounted in a specimen chamber in a high vacuum state of $\sim 10^{-5}$ mBar to prevent moisture or airborne contaminants interfering with the electron beam. When the electron beam strikes the sample, many types of photon and electron are emitted from the surface. Secondary

electrons (SEs) and backscattered electrons (BSEs) are collected for imaging, due to their ability to produce good resolution surface topography - or atomic weight related information in the case of BSEs. SEs result from inelastic scattering of accelerated primary electrons and electrons in a matter. They emit from a shallow depth of between 1 and 10 nm, with relatively low energies ranging from 2 eV to 50 eV. Most SEs are collected in a detector positioned at an angle of about 45° to the axis of the electron beam. The high energy BSEs are produced by elastic scattering events between primary electrons and atomic nuclei. BSEs have a large scattering angle and are thus detected by a through lens detector (TLD) mounted above the last aperture inside the beam column. The number of scattered electrons detected for a certain probe position on a scanned area is converted to the intensity of corresponding pixels on a display, presenting a full frame greyscale image after the completion of a cycle of raster scanning.

2.1.2 Electron beam lithography system

The above-mentioned SEM was equipped with an ELPHY Plus pattern generator (Raith GmbH) and utilised as an electron beam lithography tool. The pattern generator operates by taking remote control of the deflection coils and blanking element of the SEM, allowing the electron beam to raster scan a selected area in a specific dwell time. As EBL is a maskless lithographic technique, an arbitrary pattern and exposure parameters such as write field size, scanning step size and dose are edited using computer-aided design (CAD) software. The pattern generator converts this digital information into an analogue signal and controls the SEM to expose a resist sample to designed patterns at desired doses with a finely-focussed electron beam. The pattern generation uses a 16 bit resolution digital to analogue converter, resulting in pixel resolution of less than 1 nm. However in practice, resolution in patterning is limited by the electron beam spot size, electron scattering and resolution capability of a resist. To achieve optimum lithographic resolution on the tool side, the highest accelerating voltage at the minimum available beam spot size was selected. In this study, an electron beam with an

accelerating energy of 30 keV and beam current of between 20 and 40 pA was used for high resolution patterning.

2.1.3 Plasma etcher and asher

Dry plasma etching is a common technique used to transfer a resist pattern into a substrate material. Etching tools utilised in this work included an electron cyclotron resonance (ECR) plasma etcher and an inductively coupled plasma (ICP) etcher. ECR plasma etching was used in the early experiments, whilst an ICP system was used for the majority of the high resolution etching. The other plasma tool used was a plasma asher, which produces O₂ plasma for the purpose of remove organics contaminants such as resist residue from substrates.

A Plasmalab 80 plus etcher (Oxford Instruments) was used to evaluate the etch resistance of most negative tone resist samples. Using ECR technology, this equipment can generate high-density plasma at relatively low pressures. In contrast to a conventional parallel plate plasma source, ECR plasma is able to provide high-density plasma at low ion energies and thus a high etch rate with low surface damage. A schematic diagram of the ECR plasma etcher is shown in Figure 2.2.

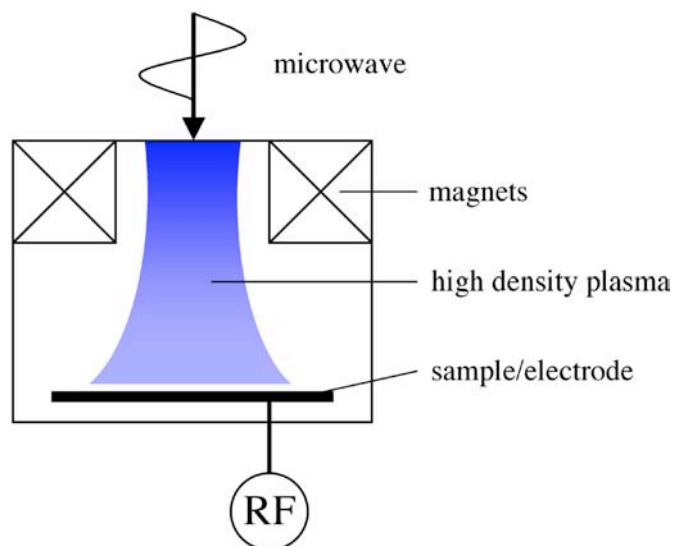


Figure 2.2 Schematic diagram of the ECR plasma etcher.

The ECR system consists of a vacuum chamber, radio frequency (RF) generator, microwave generator and magnetic confinement coils. Process gas is introduced into a vacuum chamber and ionised by applying a radio frequency (RF) signal of 13.56 MHz between two electrodes to generate a plasma. Electrons in the plasma are then accelerated by microwave radiation at a frequency of 2.45 GHz before being confined into a circular motion in the presence of magnetic field. This electron cyclotron resonance configuration allows accelerated electrons to collide with gas molecules, thus producing more electrons, radicals and ions. The etching process commences when the plasma cloud is pulled towards the sample by the negative direct circuit (DC) bias building up at the sample stage.

ECR plasma provides anisotropic etching, typically in a vertical direction. The etching process is a combination of sputtering and associated chemical etching. During sputtering, ions bombard the surface of the sample and knock off surface atoms. Chemical etching involves free radicals impinging on the surface and reacting with surface atoms to form volatile products, which can subsequently be removed by either ion bombardment or desorption. The etching gas used in this study was sulphur hexafluoride (SF₆), a common etchant of silicon. Dissociation of the SF₆ gas in plasma results in the production of an ion and a fluorine radical, as shown in the following:



In the etching process, a volatile product is formed by the following reaction:



The etch rate depends on the ion energy and ion flux impinging on the surface which can be controlled by adjusting RF power, microwave power and process pressure.

A PlasmaPro NGP80 etcher (Oxford Instruments) with ICP technology was mainly used for high resolution pattern transfer. ICP is another high density plasma system in which a plasma is

excited by an RF signal transmitting from a coil instead of parallel plates. In the ICP tool, there are two separate RF generators for an inductive coil and electrodes, with the advantage of this system being that plasma density and ion energy can be independently controlled. A schematic diagram of the ICP plasma etcher is shown in Figure 2.3. An antenna coil is located in the upper part of the plasma chamber. A time-varying RF magnetic field from the coil induces an electric field in the chamber to excite gas molecules into plasma. Electrons and ions are then accelerated to promote collisions and dissociation of gas molecules, leading to an increase in plasma density. Another RF generator is connected to an electrode at the sample stage to control DC bias and thus also the bombardment energy of ions.

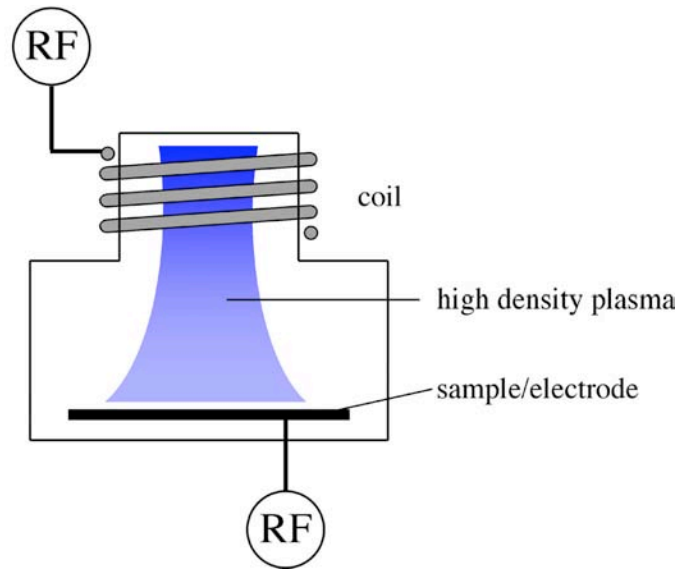


Figure 2.3 Schematic diagram of the ICP etcher system.

As in the ECR system, SF_6 is also used during the ICP etching process. However in addition to SF_6 etching, octafluorobutene (C_4F_8) is added to help control the sidewall angle of the etched structure. Ionisation of C_4F_8 in the plasma produces fluorocarbon molecules which form a polymer layer on the surface, known as a passivation layer, which is more easily removed by ion sputtering than chemical etching. Directional bombardment of ions then continues the vertical etching process, whilst leaving a sidewall protected by the passivation layer. Passivation also improves the etch resistance of the masking resist by reducing damage caused by ion bombardment. By utilising the

combined etching/passivation technique, a high aspect ratio structure with a vertical sidewall can be etched. In practice, etching and passivation processes can be arranged to run successively or simultaneously depending on user demand.

A 100-E plasma processor (Technics Plasma GmbH) was used to remove organic material from substrate by means of dry plasma oxidation. Oxygen plasma is generated at low pressure with an adjustable RF power of between 50 W and 300 W. Highly reactive oxygen radicals in the plasma oxidise organic material at low temperatures under 180 °C. This equipment was mainly used to strip resist layers from samples, being preferable to other wet chemical ashing techniques.

2.1.4 Surface profiler

A Dektak³ ST (Veeco Instruments) surface profiler was used to measure film thickness and step height for all samples in the study. The profiler works by placing a diamond-tipped stylus in contact at right angles to the sample and performing a line scan horizontally across the sample surface at a constant force of 5 to 10 mg. A record of vertical displacement of the tip and position along the scan line are together transformed into a one-dimensional topography of the surface. The profiler is capable of measuring step heights to high levels of precision, with a vertical resolution of approximately 5 nm. One limitation of its usage is that contact profiling can only be applied to a rigid film which can support the weight of the stylus while scanning takes place. Using the stylus on soft material may result in sample damage and error in measurement.

2.2 Resist processing

Most of the resists analysed in this study were chemically amplified (CA) resists. Derivatives of fullerene and additional compounds were formulated following a chemical amplification scheme. Resist materials were mixed at a defined composition ratio in an organic solvent. Resist film was prepared by spin coating techniques and the samples were then processed and analysed through the

steps and methods detailed below. A block diagram summarising sample processing and analysis is given in Figure 2.4.

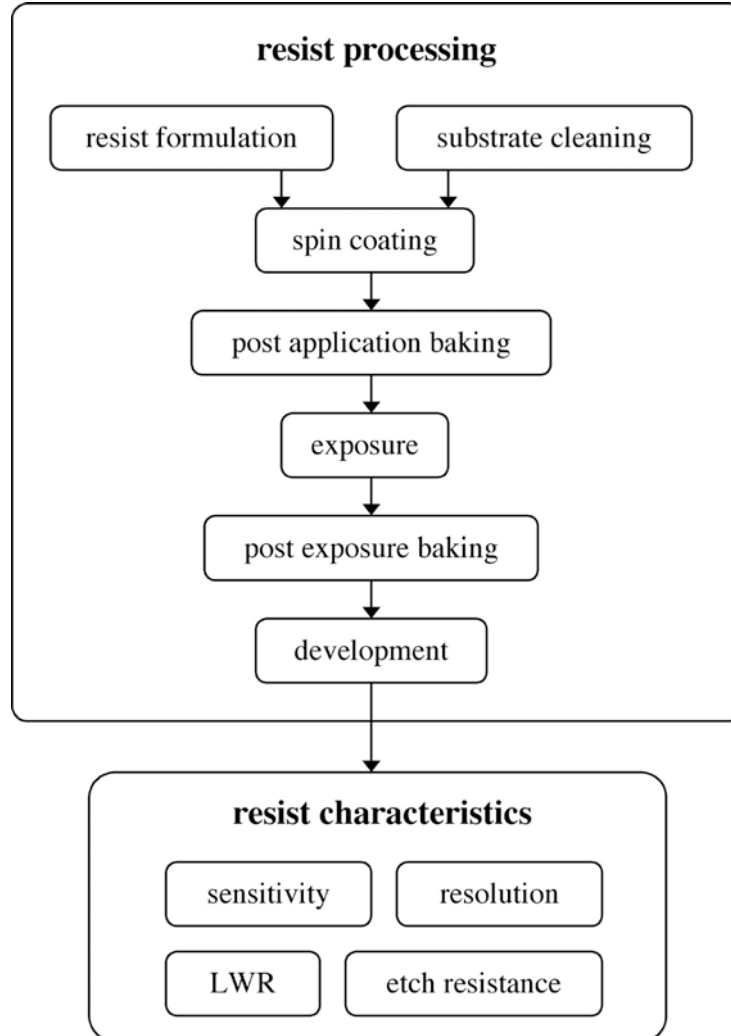


Figure 2.4 Summary of process steps and resist characteristics to be evaluated.

2.2.1 Substrate preparation

Silicon substrates were diced from 4-inch silicon wafers into $2 \times 2 \text{ cm}^2$ chips using a Disco DAD321 automatic dicing saw (Disco). The 4-inch, 100 oriented, n-type (phosphorous-doped) silicon wafers were purchased from Rockwood Wafer Reclaim. Substrate cleaning undertaken was a modified version of the IMEC-clean technique [102]. Silicon chips were ultrasonicated in acetone and isopropanol (IPA) for 10 minutes before being washed in flowing deionised (DI) water (Purite

Neptune, 18.2 M Ω .cm) for another minute. Chips were then immersed in piranha solution, a mixture of sulphuric acid (H₂SO₄, 95-97%) and hydrogen peroxide (H₂O₂, 30%) 1:1 by volume, for 10 minutes and rinsed with DI water. Piranha solution is a strong oxidising agent used to remove organic contaminants and form a thin oxide layer on a substrate. In the next stage, chips were dipped in a weak aqueous solution of hydrofluoric (HF) acid for 1 minute, rinsed in flowing deionised water for 1 minute and then dried with a dry nitrogen blow. HF acid works by etching the oxide layer, removing residual contaminants and terminating silicon with hydrogen, making the surface hydrophobic. Substrates were used within a few hours. An optional hexamethyldisilazane (HMDS) primer can be applied to a cleaned silicon substrate to improve surface adhesion to a spin-coated resist.

2.2.2 Resist preparation and processing

Each compound was dissolved in a suitable solvent at concentrations ranging from 5 to 40 g/l. Compound solutions were stored in a fridge at 8 °C while samples were prepared and processed at room temperature (20 °C). Organic solvents used in this work, including chloroform, anisole and propylene glycol methyl ether acetate (PGMEA), are also known as casting solvents due to their role in resist film preparation. The CA resist solution was prepared by mixing resist components each dissolved in the same solvent to give the desired weight ratio of components. Resists derived from a mixture of solvents were rarely prepared, except where specifically mentioned. The spin coating technique was used for coating resists onto substrates. Using a P-6708D spin coater (SCS), each resist solution was dispensed and spun onto a substrate placed on the vacuum chuck at spin speeds of between 600 and 3,000 revolutions per minute (rpm). The combination of resist concentration and spin speed was adjusted to achieve a smooth resist film ranging from 30 nm to 50 nm in thickness. After spin-coating, resist samples underwent post application bake (PAB) on a conventional hot plate in order to evaporate residual solvent and increase their mechanical strength. The effect of variation in PAB temperature and time was examined to optimise resist performance. A PAB temperature of below 100 C° was generally applied to avoid degradation of the resist film.

Individual resist samples were exposed to an electron beam using the converted SEM described in section 2.1.2. Immediately after exposure, CA resist samples underwent post exposure baking (PEB) to avoid the effects of post exposure delay (PED). PEB is also critical for such samples as thermal energy is used to activate catalysis of photoacids. PEB was typically carried out on a hotplate at 90 °C for 3 minutes. As a final step, resist samples were developed by immersing the sample in a suitable developer, selected according to the type of resist. Organic solvents such as monochlorobenzene (MCB) or a mixture of MCB and isopropanol (IPA) were used for negative tone resists, while an aqueous base solution was used for positive tone resists. The developed samples were finally rinsed in a relatively mild solvent such as IPA and dried with a dry nitrogen blow.

2.3 Resist characterisation

2.3.1 Sensitivity and contrast

Resist sensitivity depends on the energy of the radiation source. In this study, the response of the resists to electron irradiation was evaluated at a beam energy of 20 keV. Resist sensitivity and contrast were determined from their respective response curves as described in the section 1.4.1.1. To produce a response curve, squares with sides of approximately 100 µm were patterned in resist samples using an electron beam at doses ranging between 0.5 µC/cm² and 2,000 µC/cm². After the sample was developed, the remaining film thickness was measured using a surface profiler. A plot of film thickness versus dose was then fitted to a logistic function to represent the response curve. The fitting curve is defined in the form

$$f(x) = m_1 + \frac{m_4 x^{m_2}}{x^{m_2} + m_3^{m_2}}, \quad (2.3)$$

where $f(x)$ is film thickness as a function of dose x , and m_1 , m_2 , m_3 , and m_4 are fitting parameters. The parameters m_1 and m_2 determine the minimum and maximum film thickness, respectively. The parameter m_3 determines the dose at which $f(x = m_3)$ is half of the maximum film thickness, hence

the sensitivity. The contrast γ can be obtained from the first derivation of $f(x)$ with respect to $\log_{10} x$ at $x = m_3$, giving the relation

$$\gamma = \frac{\ln(10)}{4} m_2. \quad (2.4)$$

2.3.2 Resolution

Resolution of resists was evaluated by measuring the minimum feature size of patterns exposed by a finely-focused electron beam at 30 keV. Line patterns with pitch sizes ranging from isolated lines to dense line-space patterns were fabricated in the resist film. Two critical dimensional quantities were measured: line width of isolated lines and pitch size, the distance between two adjacent features of dense patterns as shown in Figure 2.5. Half-pitch size can also be represented. SEM was used to observe resist patterns at high magnification. SEM images of high resolution patterns were taken at an accelerating voltage of 5 kV, or 10 kV in ultra high resolution (UHR) mode with a TLD detector. Feature size was measured using the measurement tool available in the microscope software package.

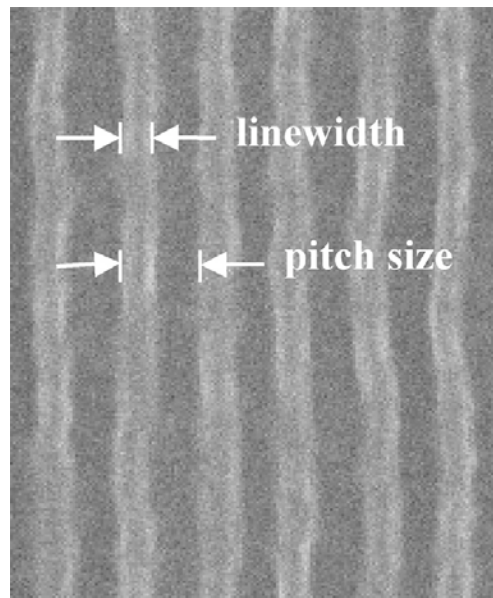


Figure 2.5 SEM image of the line-space pattern of a resist, showing definition of line width and pitch size.

2.3.3 Line width roughness analysis

LWR analysis was performed using LWR_Demokritos, a software package developed at the National Centre for Scientific Research (NCSR) in Demokritos, Greece [103-105]. The software is able to detect edges of a resist line pattern and characterise feature roughness of the resist line from a top-down SEM image, categorised as the off-line analysis. Figure 2.6 presents a screen capture of the graphic output of an LWR calculation using the LWR_Demokritos software. The analysis is based on scaling and fractal concept in which information of the spatial roughness along the edge and the dependence of LWR on the measured length can be extracted rather than performing the conventional calculation for the root mean square value of LWR. Once coordinates of the edge are detected, the correlation among line widths and their distance from a reference line is generated as the height-height correlation function (HHCF). The correlation function provides parameters associated with the line roughness including the *roughness exponent*, the *correlation length*, and the length-independent LWR(3σ) value.

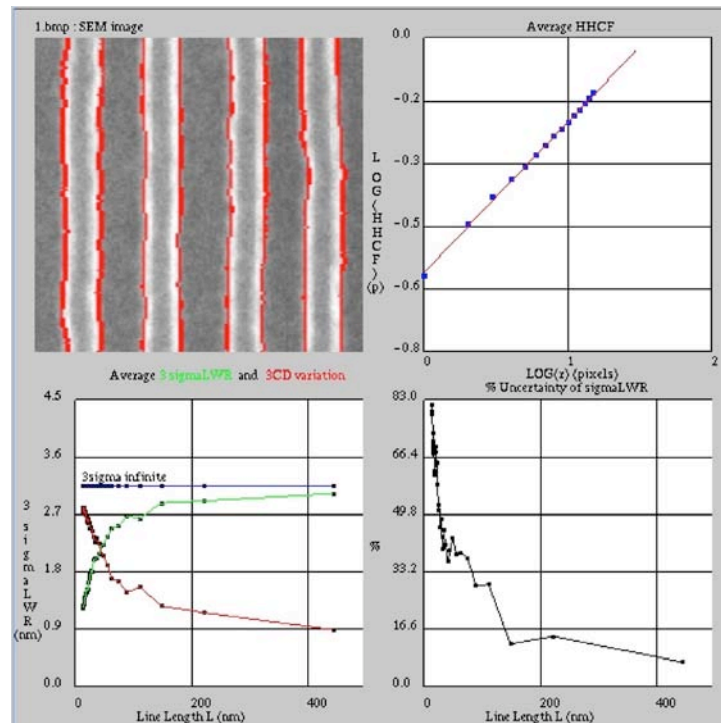


Figure 2.6 Screen capture of the output showing graphical edge detection (upper left), LWR (lower left) and uncertainty (lower right) as a function of measurement length.

The roughness exponent indicates contribution of high frequency fluctuation on LWR. The correlation length is the maximum measured length in which the edge points can be considered correlated. The LWR(3σ) value is extrapolated for the infinite length. It is suggested that measurement length should exceed 10 times the correlation length to minimise uncertainty. In this study, top-down SEM images were taken at 5 kV and a magnification of 400,000 \times for LWR analysis, providing an image resolution of 0.8 nm per pixel and a measurement length of 500 nm.

2.3.4 Etch resistance

Etch resistance of resists to plasma etching was evaluated using either an electron cyclotron resonance (ECR) or an inductively coupled plasma (ICP) system. The former was used for negative tone resists and is detailed in chapter 3, whilst the latter was used for positive tone resists and is discussed in chapter 7. High resolution pattern transfer is detailed in chapter 6. Conditions were set to provide anisotropic etching in which highly vertical etching is achieved. Resist patterns approximately 100 μm in size and of certain film thicknesses were etched under SF_6 gas plasma. As SF_6 is the etching gas for silicon, the etch resistance of the resist can be compared to that of a silicon substrate and they can thus be represented together as the etch selectivity ratio of silicon to resist or the relative etch resistance. More specifically, the relative etch resistance, ER , is the proportion of the total amount of silicon etched to the total amount of resist etched under the same process conditions and is determined by the equation

$$ER = \frac{t_2}{t_1}, \quad (2.5)$$

where t_1 is the thickness of the resist etched and t_2 is the thickness of silicon etched, as shown in Figure 2.7. SAL601 resist (Rohm and Haas), a high etch resistance commercially available novolac resist, was used as a control sample. Etch rates of silicon and resist can be calculated by using the process conditions that a resist film is left after etching so that the loss thicknesses of resist and silicon during the process are measured.

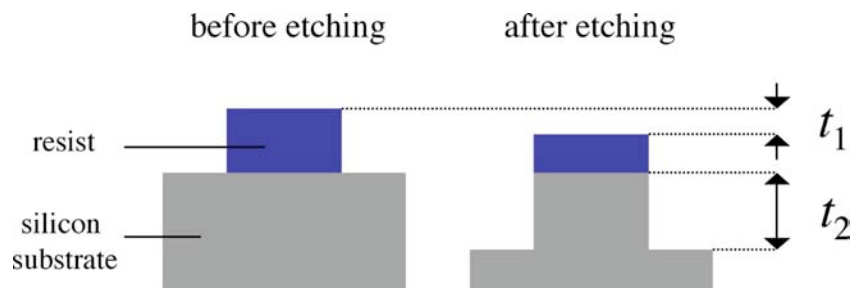


Figure 2.7 Schematic diagram showing the determination of resist/silicon etch selectivity.

Chapter 3

Negative Tone Chemically Amplified Fullerene Based Molecular Resists

This chapter describes the development and characterization of negative tone fullerene based molecular resist for electron beam lithography. Chemical amplification of the fullerene based resist using cationic polymerization of epoxy resin is presented. Variation of resist process conditions was examined in order to optimise lithographic performance of the resists. Evaluation of sensitivity, resolution, line width roughness, etch resistance, and stability to post exposure delay and to aging is presented.

3.1 Resist preparation

Resist materials used in this negative tone resist system composed of the fullerene derivative MF07-01, the photoacid generator PAG07-01, and epoxy crosslinkers (CL), as shown schematically in Figures 3.1 (a)-(d). The MF07-01, Figure 3.1 (a), a mixture of tri, tetra, and penta methanofullerenes with hydroxyl terminated polyether addends, was synthesized and supplied from the Nanoscale Chemistry Research Group, University of Birmingham. The PAG07-01, Figure 3.1 (b), was the photosensitizer UVI-6976, a mixture of triarylsulfonium hexafluoroantimonate salts in propylene carbonate, purchased from Dow. Epoxy novolac resins were used as a crosslinker, purchased from Sigma Aldrich. There were six type of resins with variation in monomer type and molecular weight as well as epoxide functionalities including poly[(phenyl glycidyl ether)-co-formaldehyde], Figure 3.1 (c), with molecular weight of 345 (CL1-1) and 570 (CL1-2) and poly[o-cresyl glycidyl ether)-co-formaldehyde], Figure 3.1 (d), with molecular weight of 540 (CL2-1), 870 (CL2-2), 1080 (CL2-3), and 1270 (CL2-4).

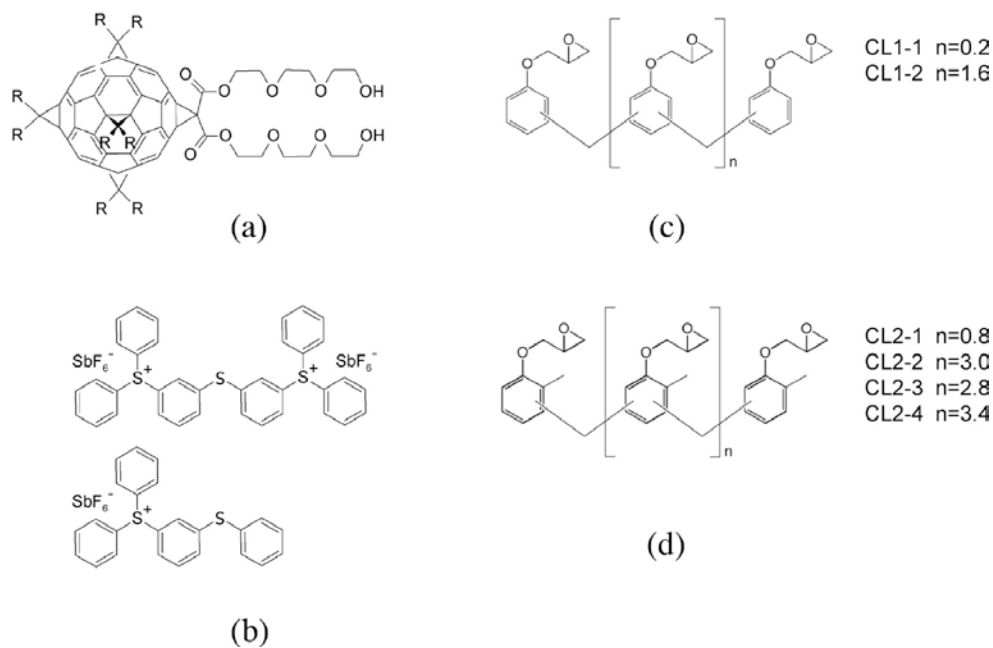


Figure 3.1 Resist materials for the negative tone molecular resists (a) MF07-01, (b) PAG07-01, (c) poly[(phenyl glycidyl ether)-co-formaldehyde] resins, and (d) poly[o-cresyl glycidyl ether)-co-formaldehyde] resins, where n is the number of monomer units in the brackets.

A negative-tone chemically amplified fullerene based resist system was formulated by mixing the fullerene derivative MF07-01, PAG07-01, and an epoxy crosslinker together. The three-component negative-tone resist works by using a cationic polymerisation mechanism via ring-opening of the epoxide functional group. A photoacid reacts with an epoxide ring, causing the ring to open. The highly reactive opened ring can make a bond with -OH group at the end of a pendent of the fullerene derivative and release an acid for a subsequent reaction, resulting in a insoluble three-dimensional cross-linking network in an area exposed to an electron beam.

The resist compounds were dissolved in chloroform. Chloroform was used as a casting solvent used for most samples in this study unless otherwise mentioned. Alternatively solvents such as PGMEA and anisole were also used in order to provide a comparison. The standard composition ratio of the chemically amplified resist was one part of MF07-01 to one part of PAG07-01 to two parts of an epoxy by weight. The resist films were cast on a silicon substrate by spin coating to produce film thickness of between 25 and 50 nm. The standard process conditions are described as follows. Post application bake (PAB) was 75 °C for 10 minutes. Post exposure bake (PEB) was 90 °C for 3 minutes.

The resist samples were developed in MCB:IPA (1:1 by volume) for 10 seconds and rinsed in IPA for another 10 seconds. Resist processing conditions were varied to optimise lithographic performance of the resist as presented in the following sections.

3.2 Sensitivity

The response curves of the pure MF07-01 and chemically amplified (CA) resists to 20 keV electrons are shown in Figure 3.2 (a). The MF07-01 film received no PAB and no PEB. It was developed in MCB:IPA (1:1) for 10 seconds and rinsed in IPA. The sensitivity of the pure fullerene MF07-01 was $610 \mu\text{C}/\text{cm}^2$ with the contrast of 0.7. The CA MF07-01 resists were prepared with PAG07-01 and six different types of epoxy resin at the standard ratio, 50 wt% of epoxy. The samples were processed with the standard process conditions. Sensitivity and contrast of the CA resist are plotted as a function of epoxy molecular weight and represented in Figure 3.2 (b).

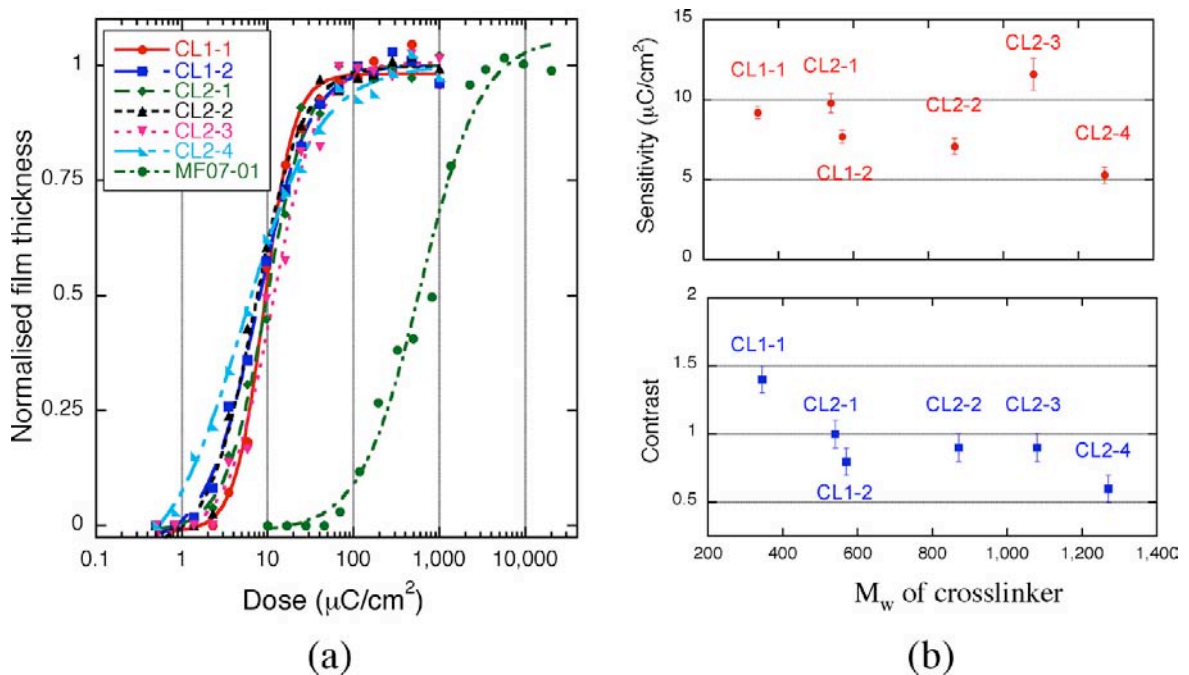


Figure 3.2 (a) Response curves of the fullerene MF07-01 and CA resists formulated with different type of epoxy resin, CL1-1, CL1-2, CL2-1, CL2-2, CL2-3, and CL2-4, at the same composition ratio of 1:2:1 of MF07-01:CL:PAG07-01. The standard process conditions were applied to all samples except that the pure MF07-01 received no PAB and no PEB. (b) Sensitivity and contrast of the CA resists as a function of molecular weight of an epoxy crosslinker.

It can be clearly seen that the chemical amplification enhanced the sensitivity of the MF07-01 resist about two orders of magnitude. The sensitivity of the CA resists was found between 5.3 and 11.6 $\mu\text{C}/\text{cm}^2$ with the contrast between 0.7 and 1.3. The type of crosslinker used showed a slight impact on the resist sensitivity. The sensitivity tended to increase in the resist formulated with a large molecular crosslinker. The maximum sensitivity of 5.3 $\mu\text{C}/\text{cm}^2$ was found in the sample containing CL2-4, the largest epoxy molecule.

3.2.1 Composition ratios

The effects of composition ratios to the resist sensitivity were examined by varying the loading of epoxy or PAG in the CA resist. The response curves of the CA resist with varying CL1-1 loading are shown in Figure 3.3 (a), and plots of sensitivity and contrast as a function of epoxy loading for the resist containing different type of epoxy crosslinkers are shown in Figure 3.3 (b). The ratio of MF07-01 and PAG07-01 in the resist was controlled at 1:1 by weight, and the process conditions were fixed. The non-CA resist containing only MF07-01 and PAG07-01 showed a sensitivity of 421 $\mu\text{C}/\text{cm}^2$ with contrast of 1.0. Addition of the CL1-1 crosslinker caused the response curve shift to a higher sensitivity. Increasing the epoxy CL1-1 levels from 20 wt% to 60 wt% resulted in a significant increase in the sensitivity from 43 $\mu\text{C}/\text{cm}^2$ to 8.8 $\mu\text{C}/\text{cm}^2$ with a slight increase of the contrast from 1.2 to 1.6. A similar trend of relation between the sensitivity and the CL loading, shown in Figure 3.3 (b), was observed for all epoxy resins examined. The resist sensitivity seemed to have reached saturation at about 50 wt% and higher loadings of the epoxy did not significantly improve the sensitivity.

Figure 3.4 (a) shows response curves of the resist MF07-01:CL1-1 (1:1) with varying PAG levels. The resist containing no PAG07-01 showed a sensitivity of 860 $\mu\text{C}/\text{cm}^2$ with a contrast of 0.8. An increase in sensitivity to about 10 $\mu\text{C}/\text{cm}^2$ was observed in the three-component resist with increase of PAG07-01 loadings from 12 to 40 wt%. The contrast also increased to 1.6 with the addition of PAG07-01, and started to decrease to 0.9 when PAG loading exceeded 28.5 wt%. The

saturation of the sensitivity was found at about 25 wt% loading of PAG07-01, the same for all epoxies examined as shown in Figure 3.4 (b).

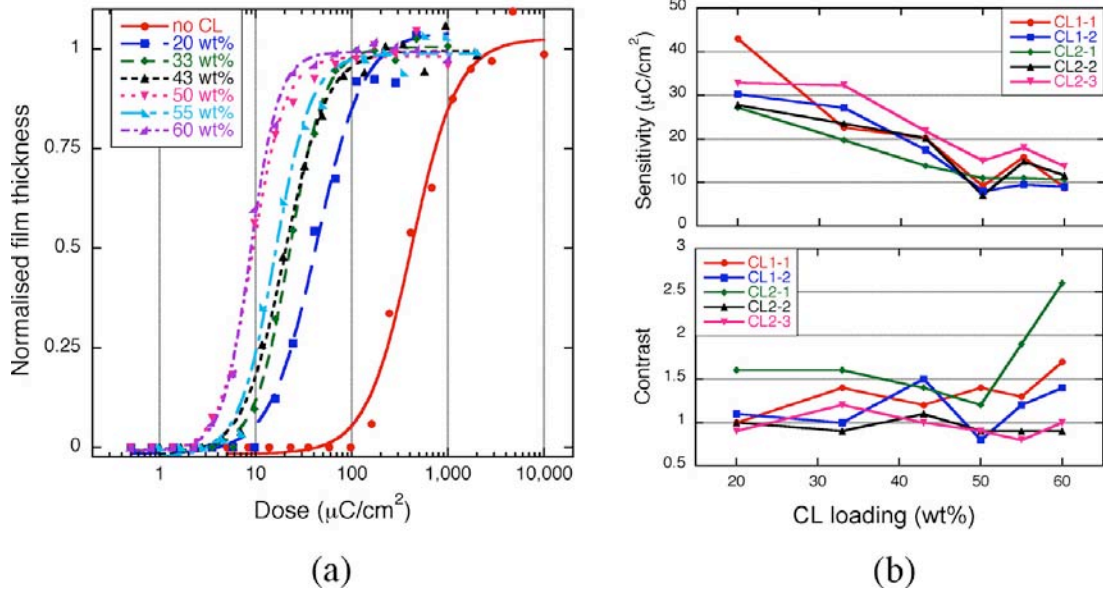


Figure 3.3 (a) Response curves of the CA resist with varying an amount of epoxy CL1-1 from 20 to 60 wt%, whilst the MF07-01:PAG07-01 ratio was fixed to 1:1 by weight. (b) Relation between sensitivity, contrast, and epoxy loading for the resists containing different type of epoxy resin. All samples were processed with the standard conditions.

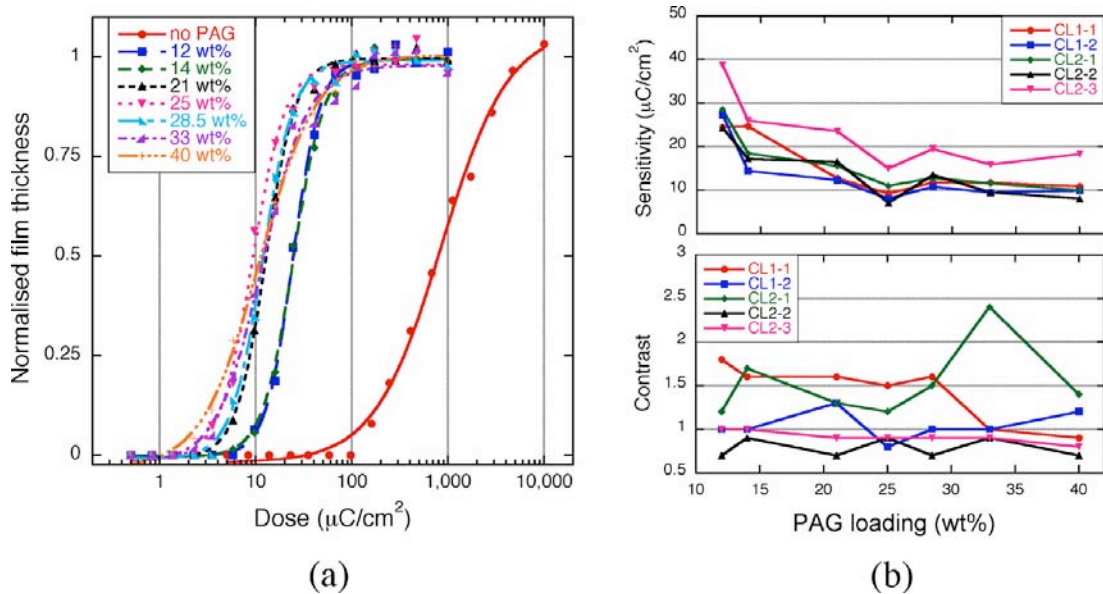


Figure 3.4 (a) Response curves of the CA resist containing CL1-1 with varying PAG07-01 loading from 12 to 40 wt%, whilst the MF07-01:CL1-1 ratio was fixed to 1:2 by weight (b) Relation between sensitivity, contrast, and epoxy loading for the resists containing different epoxy resin. All samples were processed with the standard conditions.

3.2.2 Post application bake and post exposure bake

The effects of PAB and PEB conditions on the resist response were examined for the CA resist MF07-01:CL1-1:PAG07-01 (1:2:1). Sensitivity and contrast of the resist processed with varying PAB temperatures between 70 °C and 120 °C and a fixed PAB time of 10 minutes are shown in Figure 3.5 (a). PEB conditions and development were controlled to the standard condition. A slight increase in the sensitivity from 12 to 9 $\mu\text{C}/\text{cm}^2$ with the increase in PAB temperature can be seen. Figure 3.5 (b) shows sensitivity and contrast of the resist processed with PAB temperature of 75 °C and varying PAB time, whilst PEB conditions and development were fixed. Variation of PAB temperature over a range of 1 to 25 minutes caused a slight change in the sensitivity between 9 and 11 $\mu\text{C}/\text{cm}^2$.

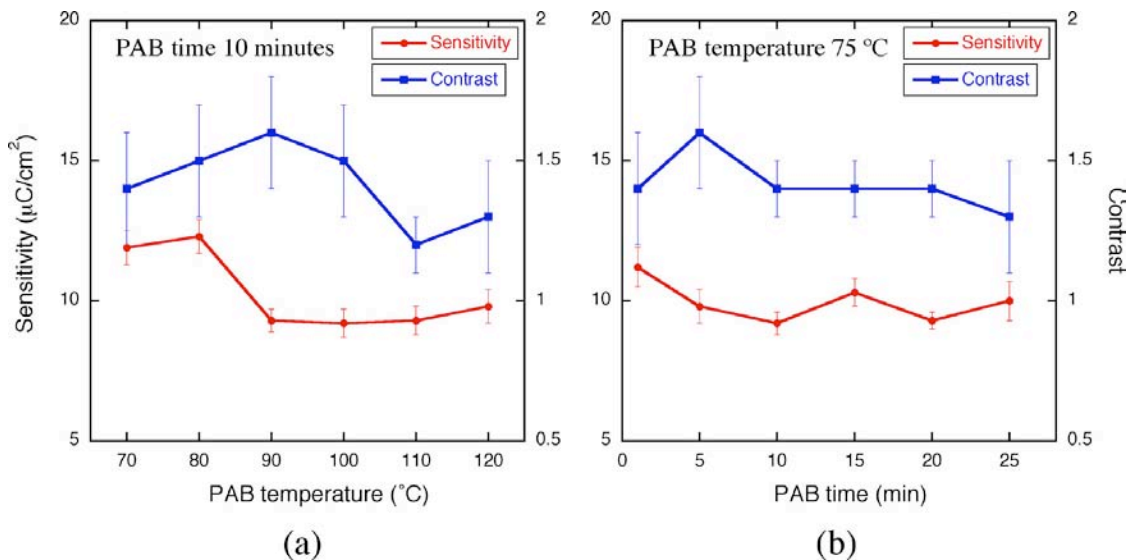


Figure 3.5 Sensitivity and contrast of the CA resist MF07-01:CL1-1:PAG07-01 (1:2:1) processed with varying (a) PAB temperature from 70 °C to 120 °C for 10 minutes and (b) PAB time from 1 to 25 minutes at 75 °C. PEB and development were fixed to the standard conditions.

Results of varying PEB temperature and time are shown in Figures 3.6 (a) and (b) respectively. Other processes were controlled as mentioned above. Varying PEB temperature from 75 °C to 135 °C with a fixed baking time of 3 minutes altered the sensitivity between 10 and 13 $\mu\text{C}/\text{cm}^2$. Varying PEB time from 1 to 9 minutes at 90 °C resulted in a slight change of the sensitivity between 10 and 12 $\mu\text{C}/\text{cm}^2$. In all cases, a significant change in the resist contrast with the variation of baking

conditions was not observed over the range of examination. Change in the resist response started to appear when reducing PEB temperature toward the room temperature (no PEB).

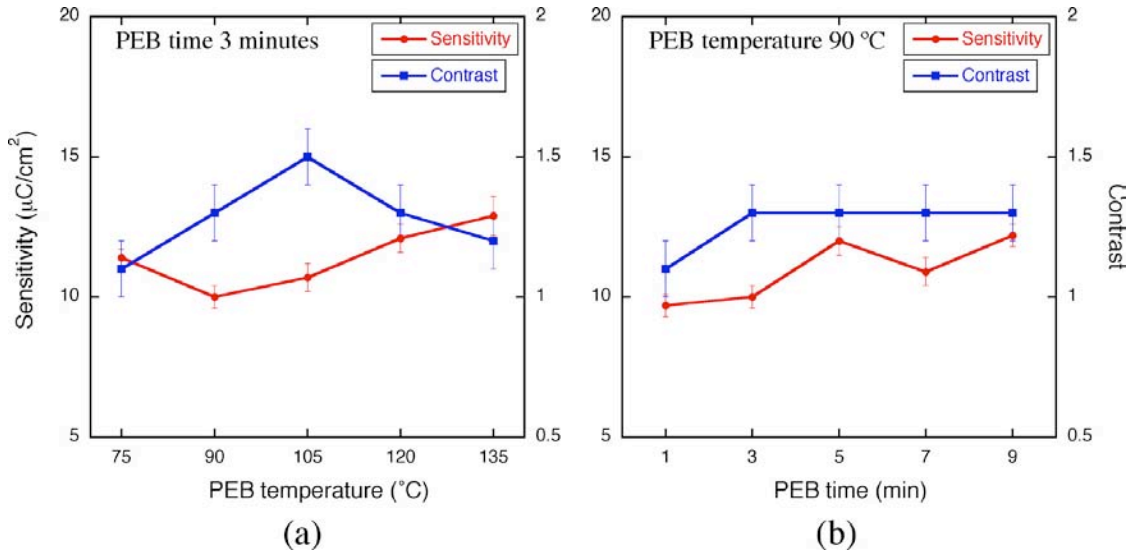


Figure 3.6 Sensitivity and contrast of the CA resist MF07-01:CL1-1:PAG07-01 (1:2:1) processed with varying (a) PEB temperatures from 75 °C to 135 °C for 3 minutes and (b) PEB times from 1 to 9 minutes at 90 °C. PAB and development were fixed to the standard conditions.

Figure 3.7 shows response curve of the resist receiving no PEB or a low PEB temperature up to 60 °C. A decrease in the sensitivity as well as the contrast was observed as PEB temperature decreased. At no PEB, the sensitivity was 20 $\mu\text{C}/\text{cm}^2$ with the contrast of 0.6.

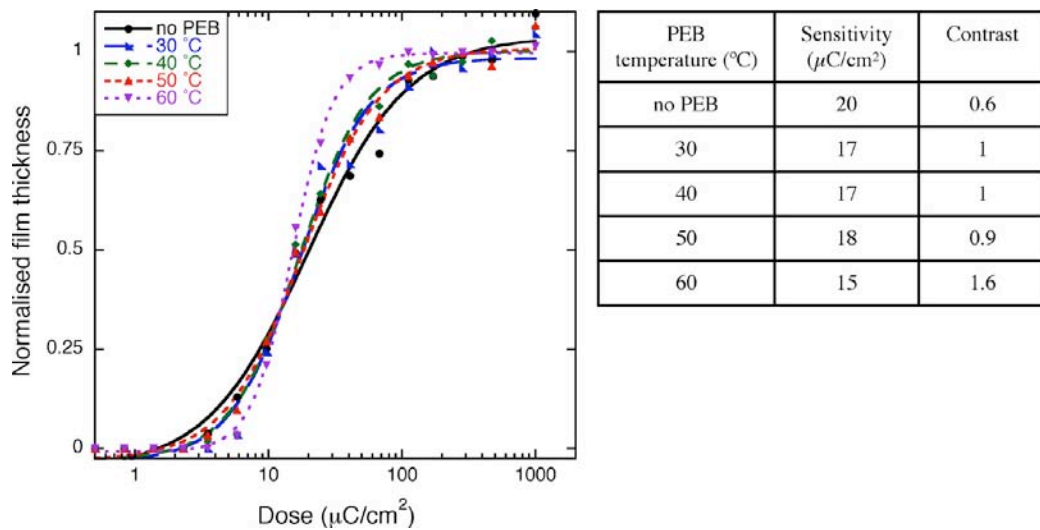


Figure 3.7 Response curves of the CA resist MF07-01:CL1-1:PAG07-01 (1:2:1) processed without PEB or with low PEB temperatures between 30 °C and 60 °C. PAB and Development were fixed to the standard condition.

3.3 Resolution

Resist samples with film thickness of 25 to 30 nm were patterned using a focused electron beam at 30 keV to evaluate the resolution capability of the resist. Single pixel width lines with varying pitch sizes from considerably isolated features to 1:1 line:space dense features were patterned, and the smallest line width and pitch size were measured.

3.3.1 pure MF07-01

The pure MF07-01 acts as a negative tone resist with a capability of high resolution. High resolution patterning was tested for the 30 nm thick MF07-01 film. The sample received PAB of 75 °C for 10 minutes. Development was in an aqueous solution of TMAH at 0.26 N for 10 seconds followed by a rinse in DI water. It is noted that the MF07-01 film is developable in either an organic solvent or an aqueous base solution. 22 nm sparse lines with 400 nm pitch were achieved at a linedose of 10 nC/cm, as shown in Figure 3.8 (a). Dense features with 25 nm half-pitch were achieved at 12 nC/cm, as shown in Figure 3.8 (b). Line edge was very smooth although a little swelling was observed in dense patterns.

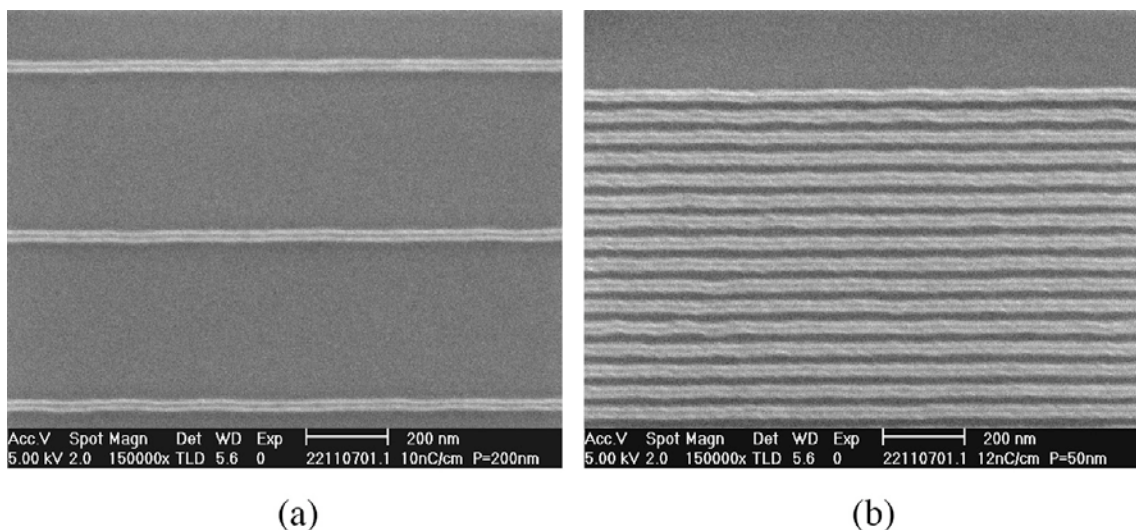


Figure 3.8 High resolution patterns in the non-chemical amplified MF07-01 resist, (a) 22 nm width lines with pitch of 400 nm written with a dose of 10 nC/cm, (b) 25 nm half-pitch lines at a dose of 12 nC/cm. PAB was 75 °C for 10 minutes. Development was in 0.26 N TMAH for 10 seconds followed with a rinse in DI water.

3.3.2 Composition ratios

The chemically amplified MF07-01 resist was prepared at the standard composition ratio of 1:2:1 of MF07-01:CL:PAG07-01 by weight. Six different types of epoxy crosslinker were tested. High resolution features were patterned as described above. The samples were processed with the standard process conditions. Figure 3.9 shows sub 20 nm sparse lines with pitch size of 200 nm patterned in the CA resist formulated with each type of epoxy. Line width of 14 nm at 220 pC/cm, 16 nm at 160 pC/cm, 18 nm at 180 pC/cm, 17 nm at 140 pC/cm, 17 nm at 140 pC/cm, and 19 nm at 100 pC/cm was achieved in the resist containing epoxy CL1-1, CL1-2, CL2-1, CL2-2, CL2-3, and CL2-4, respectively. A little swelling was a common feature. It was suppressed at higher doses. The line roughness was found to be relatively high in samples formulated with a large epoxy molecule such as CL2-3 and CL2-4.

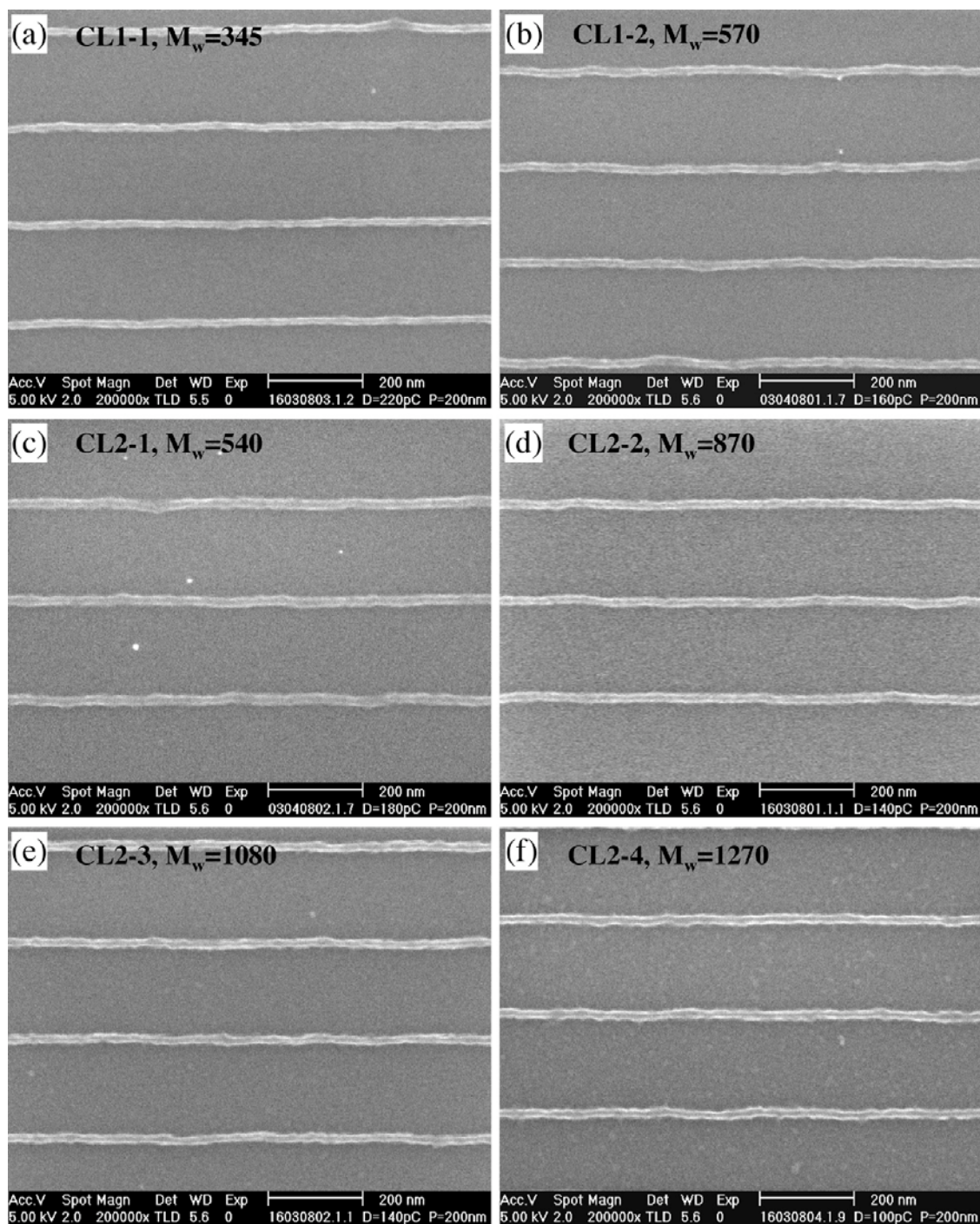


Figure 3.9 Sparse lines with sub 20 nm wide patterned in the CA resist MF07-01:CL:PAG07-01 (1:2:1) containing an epoxy (a) CL1-1, (b) CL1-2, (c) CL2-1, (d) CL2-2, (e) CL2-3 and (f) CL2-4, processed with the standard condition.

The smallest resolved dense lines achievable for each resist are shown in Figures 3.10 (a)-(f). Dense lines with half-pitch of 20 nm were achieved at 130 pC/cm in the resist with CL1-1, Figure 3.10 (a). A larger half-pitch size of 25 nm dense lines was found in other resists at a dose between 140 and 180 pC/cm. It is clearly seen from the results that the resist combining with the smallest epoxy molecule, CL1-1, showed the highest resolution capability among the three-component resists in this study. Edge roughness feature and resist residue in unexposed areas was observed in the resist formulated with a relatively large epoxy molecules.

The highest sparse and dense resolution for this resist system was found in the resist MF07-01:CL1-1:PAG 07-01 (1:2:1) processed with conditions slightly different from the standard. Figure 3.11 (a) shows a sparse line with the smallest line width of 12 nm achieved in a resist receiving PAB of 75 °C for 5 minutes, and Figure 3.11 (b) shows the densest features of 18 nm half pitch achieved in a resist which received a PAB of 75 °C for 10 minutes. Lines were almost resolved with some bridging. It is not currently clear if the resolution was limited by the capability of the exposure tool or the resist.

The resolution was examined for a resist with high PAG loading. The loading of PAG07-01 in the resist formulation was increased to 40 wt% making a composition ratio 1:2:2 of MF07-01:CL1-1:PAG07-01. The resist was patterned and processed with the standard conditions. Figure 3.12 (a) shows that sparse lines with width of as small as 17.5 nm were achieved. However, the resist lost resolution capability in dense features as 25 nm half-pitch dense lines were not resolved due to pattern collapse, Figure 3.12 (b). This could indicate that increasing a proportion of PAG loading in the resist formulation reduces mechanical strength of the resist.

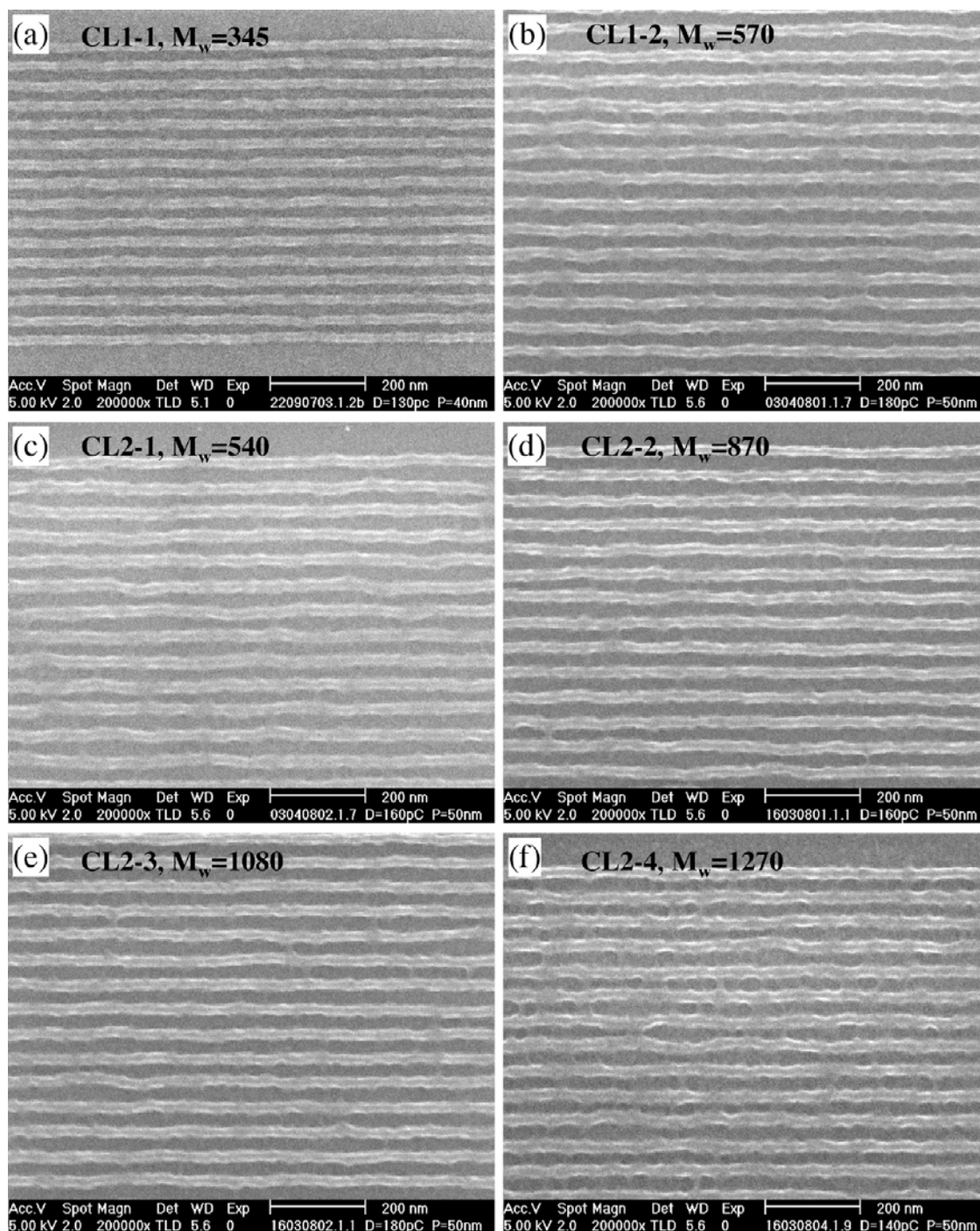


Figure 3.10 Dense feature patterned in the CA resist MF07-01:CL:PAG07-01 (1:2:1) processed with the standard conditions, showing (a) 20 nm half-pitch dense lines in the resist with CL1-1 and 25 nm half-pitch dense lines in the resist with (b) CL1-2, (c) CL2-1, (d) CL2-2, (e) CL2-3 and (f) CL2-4.

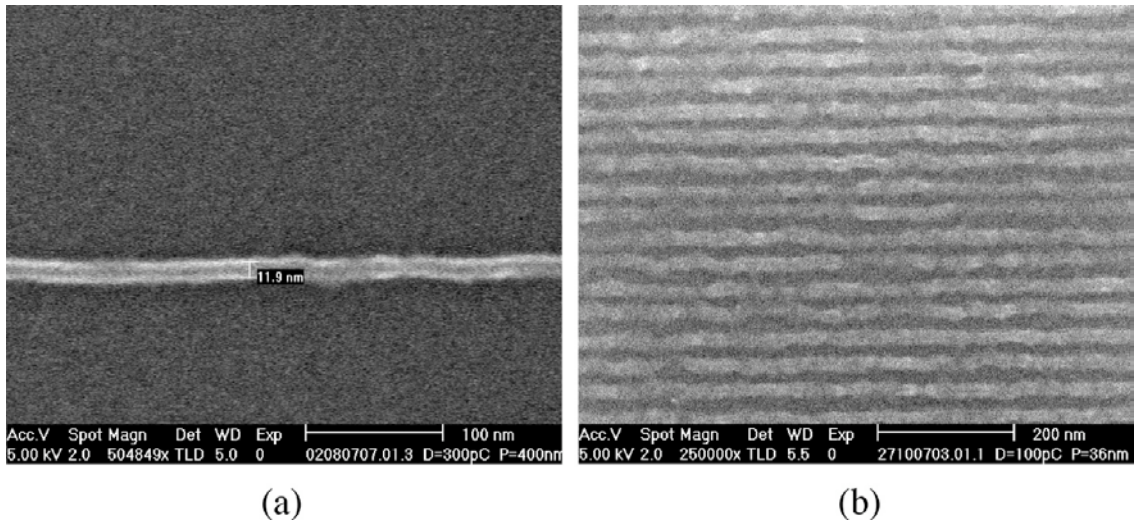


Figure 3.11 The highest resolution features patterned in the resist MF07-01:CL1-1:PAG07-01 (1:2:1), (a) 12 nm line at a dose of 300 pC/cm achieved in the resist processed with PAB of 75 °C for 5 minutes, PEB of 90 °C for 3 minutes, (b) 18 nm half-pitch dense lines at a dose of 100 pC/cm achieved in the resist processed with PAB of 75 °C for 10 minutes, PEB of 90 °C for 1 minute. Development was in MCB:IPA as the standard.

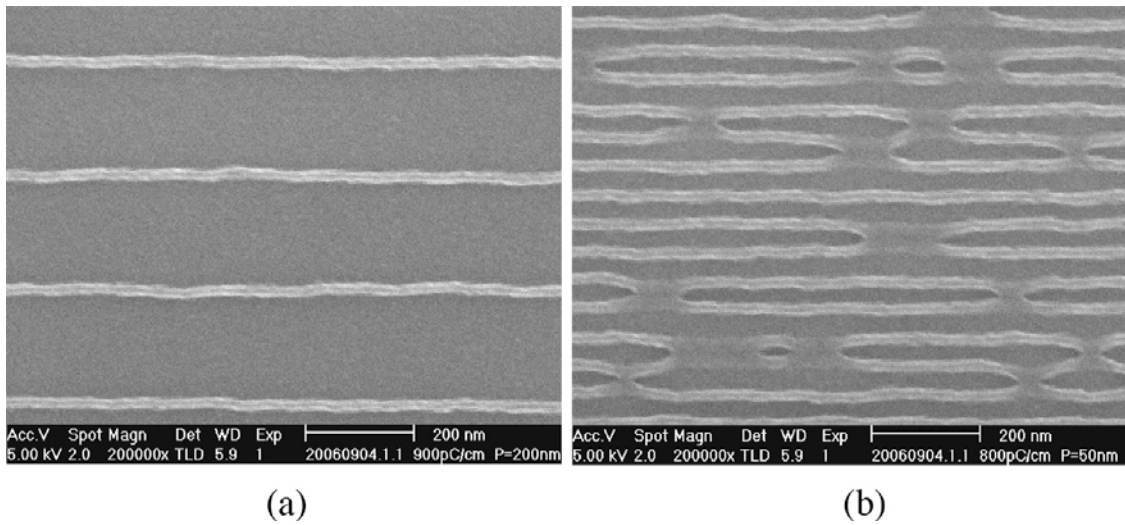


Figure 3.12 Resolution in the resist with high PAG loading showing (a) 17.5 nm sparse lines at 900 pC/cm and (b) 25 nm half-pitch dense lines at 800 pC/cm patterned in the resist MF07-01:CL1-1:PAG07-01 (1:2:2) processed with the standard conditions.

High resolution patterns were written in the resist with high loading of epoxy to test resolution capability. The loading of epoxy crosslinker CL1-1 was increased to 67 wt% to have a composition ratio of 1:6:2 of MF07-01: CL1-1:PAG07-01. Figures 3.13 (a) and (b) shows sparse lines with 17.5 nm line width and dense lines with 20 nm half-pitch achieved in the resist, respectively. The resist was processed with the standard conditions. It has been previously reported [106] that the two component resist CL2-4:PAG07-01 (2:1) gave a resolution about half that achieved in the three-component fullerene resists at the standard ratio. It is interesting that in this study, mixing a smaller amount of the fullerene MF07-01 to the standard three-component CA resist, 11 wt% in this case, still gave the resolution comparable to that of the resist formulated with the standard ratio. It is indicated that even a small amount of the fullerene added to the resist significantly enhanced the resist properties.

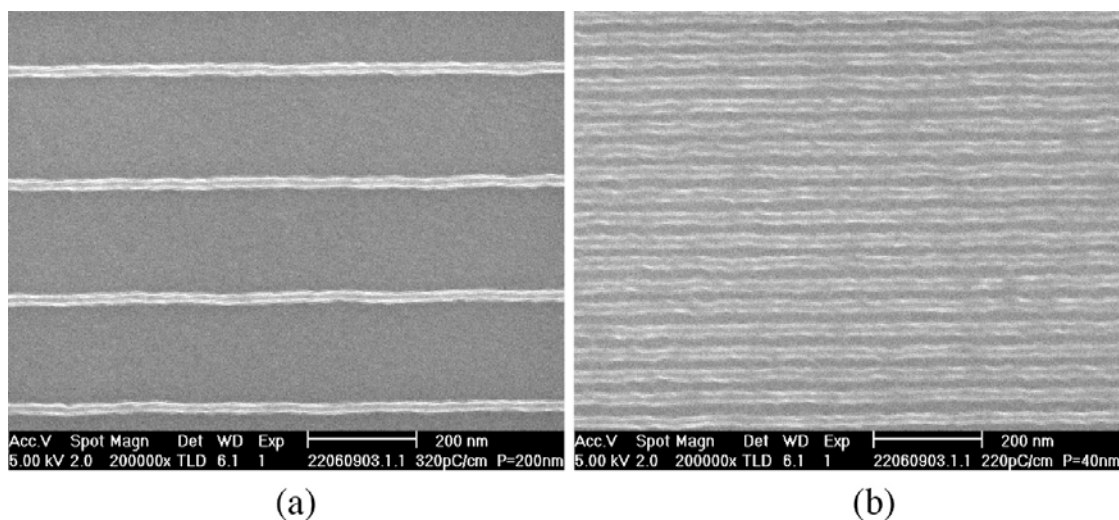


Figure 3.13 Resolution in the resist with high CL loading showing (a) 17.5 nm sparse lines at 320 pC/cm and (b) 20 nm half-pitch dense lines at 220 pC/cm patterned in the resist MF07-01:CL1-1:PAG07-01 (1:6:2) processed with the standard conditions.

3.3.3 Post exposure latitude

The effect of PEB to the resist resolution was examined. A combination of PEB temperatures and times were applied to the resist MF07-01:CL:PAG07-01 (1:2:1) after high resolution patterning, whilst other processes were controlled as the standard. Figure 3.14 shows dense lines with 20 nm half-pitch produced with dose between 120 and 160 pC/cm in the resist formulated with CL1-1. The sample

received PEB of 75 °C, 90 °C or 105 °C for 1 or 5 minutes. It can be seen that dense lines patterns were achieved under a wide range of PEB conditions. The sample that received the intermediate PEB temperature of 90 °C shows the best results among these PEB temperatures.

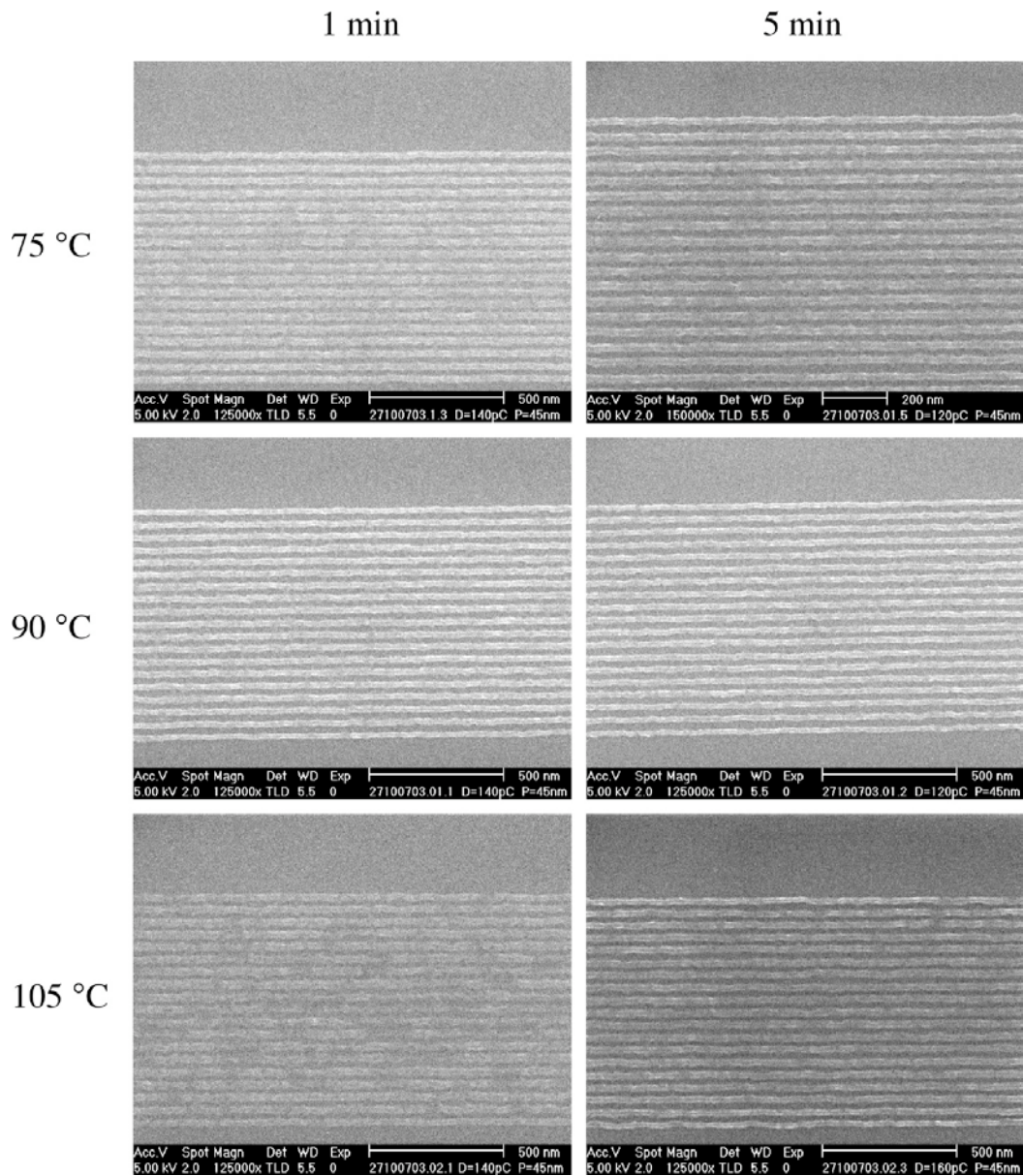


Figure 3.14 20 nm half-pitch dense lines written in the resist MF07-01:CL1-1:PAG07-01 (1:2:1). The resist received PEB temperature of 75 °C (top), 90 °C (middle) or 105 °C (bottom) and PEB time of 1 minute (left column) or 5 minutes (right column).

The effect of PEB conditions on sparse line width for the resist formulated with various types of epoxy is shown in Figure 3.15. It can be seen that no clear trend of line width with varying PEB temperature and time was found. The width of lines slightly altered over a range of PEB temperatures and times examined. The results show that this resist system has a wide PEB latitude for resolution, as well as the sensitivity latitude previously seen. It is one of the major advantage of the fullerene based resist over a typical CA resist in which critical dimensions strongly depend on PEB conditions.

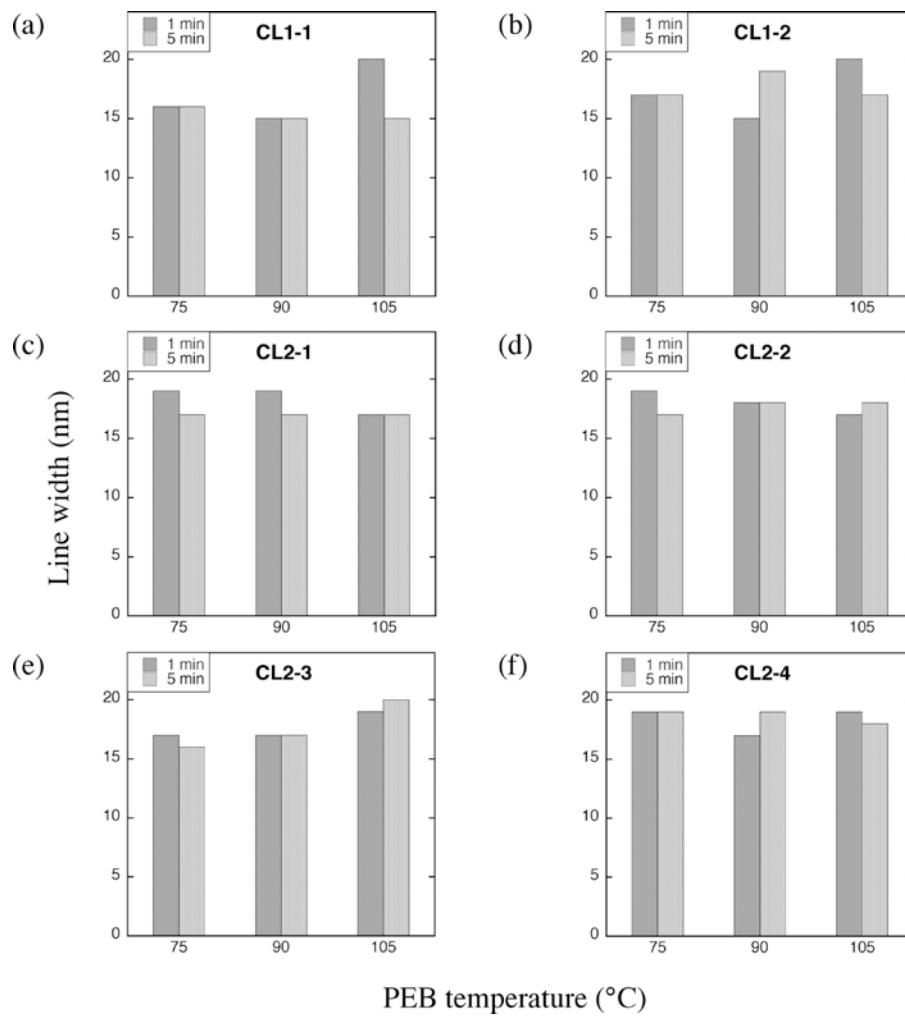


Figure 3.15 A plot of line width as a function of PEB temperature at PEB time of 1 and 5 minutes for the resist formulated with the crosslinker (a) CL1-1, (b) CL1-2, (c) CL2-1, (d) CL2-2, (e) CL2-3 and (f) CL2-4 at the standard ratio. Standard PAB and development conditions were applied in all cases.

It was possible to produce a high resolution pattern in the resist without applying PEB. 17 nm sparse lines and were 25 nm half-pitch dense lines were achieved with little swelling in the sample receiving no PEB before development, as shown in Figures 3.16 (a) and (b) respectively. It can be inferred that catalysis in the resist has a low activation energy. However, it is not yet clear that the crosslinking reaction starts immediately after the generation of an acid, or if elevated temperatures due to exposure to the electron beam drive the reaction.

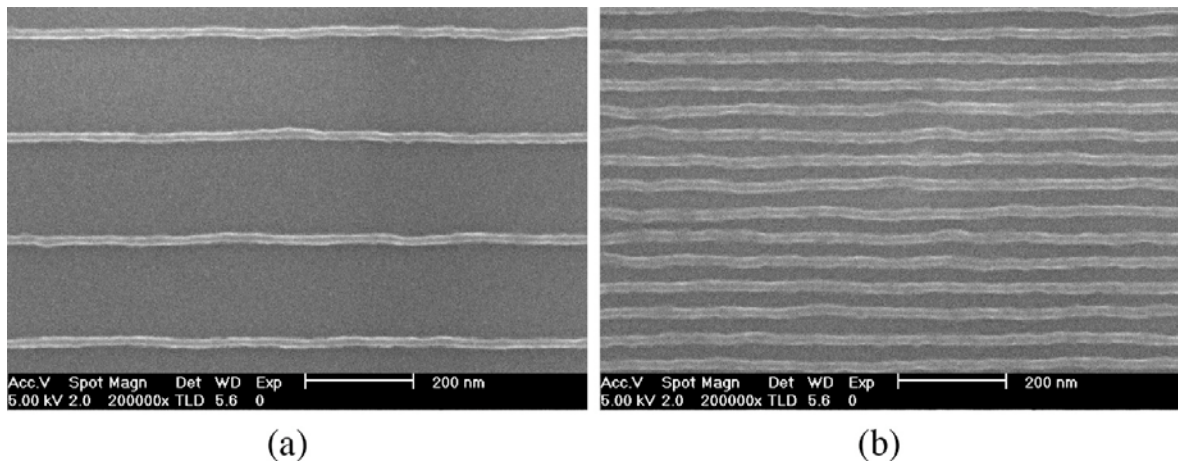


Figure 3.16 Resolution in the resist processed without PEB. (a) 17 nm sparse lines at 480 pC/cm and (b) 25 nm half-pitch dense lines at 240 pC/cm in the resist MF07-01:CL1-1: PAG07-01 (1:2:1). PAB and development was applied as the standard conditions.

3.3.4 Dose latitude

The relation between line width and exposure dose in dense and sparse line patterns was examined to evaluate the dose latitude of the CA resist. The resist MF07-01:CL1-1:PAG07-01 (1:2:1) was processed with the standard conditions. 20 nm half-pitch dense lines pattern were written with a range of doses. The results are presented in Figure 3.17. It can be seen that resolved patterns were achieved across a wide range of doses from 110 pC/cm up to approximately twice that. Lines patterns were tighter at higher doses as the width of each line expanded. More defects were also observed at high doses as the proximity effect became more pronounced.

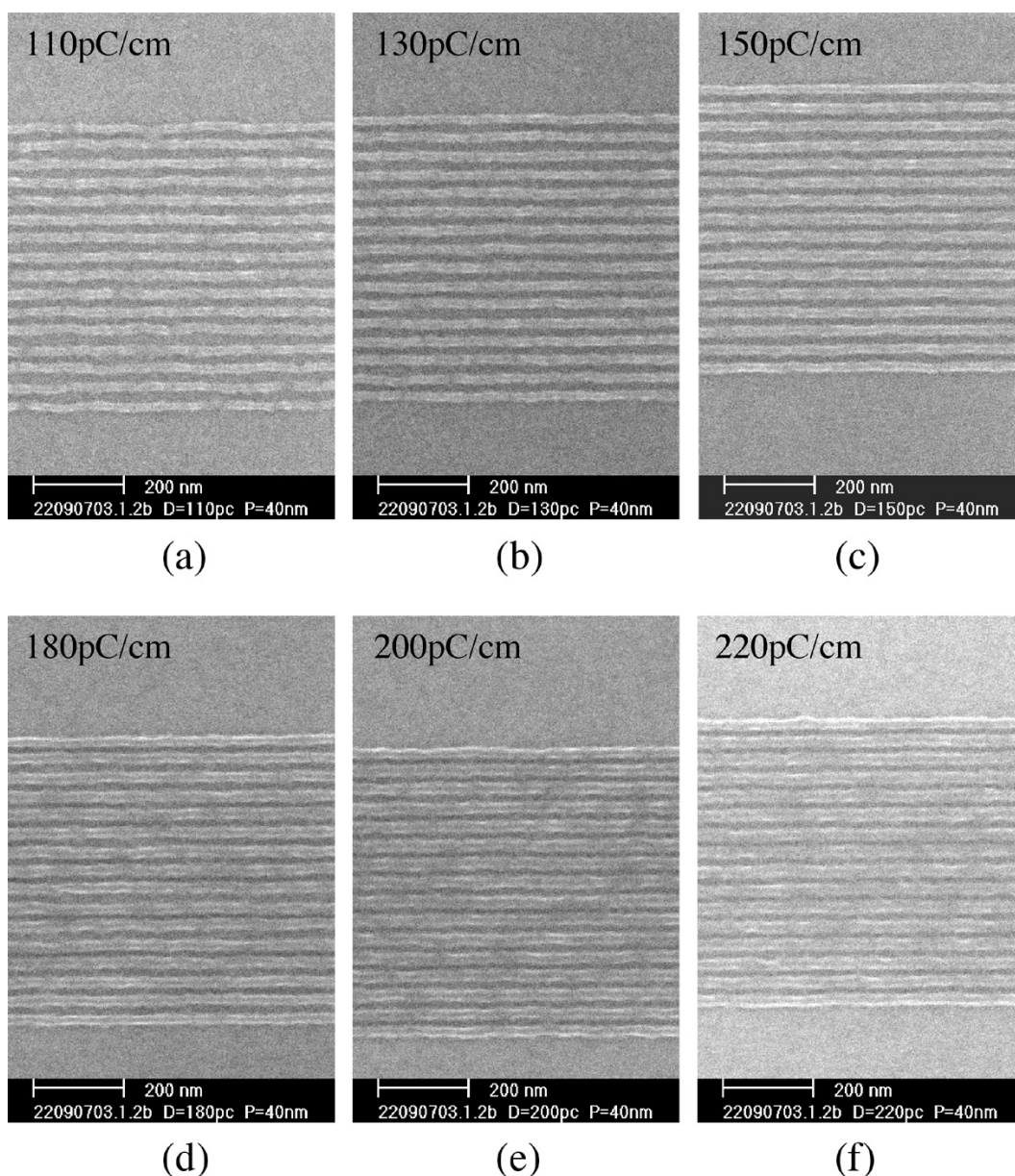


Figure 3.17 20 nm half-pitch dense patterns with varying dose between 110 pC/cm and 220 pC/cm in the resist MF07-01:CL1-1:PAG07-01 (1:2:1) processed with the standard conditions.

Single pixel lines on a 200 nm pitch were written with a range of dose from 100 to 600 pC/cm in the resist formulated with various types of epoxy crosslinker. The width of lines was measured as a function of dose. A linear relation between line width and dose for each resist was illustrated by the linear curve fit in Figure 3.18. It was found that the line width increased linearly with dose at a rate of 1.8 nm, 2 nm, 2.5 nm, 3.1 nm, 2.4 nm, and 3.7 nm per an increment of a line dose of 100 pC/cm for the resist with CL1-1, CL1-2, CL2-1, CL2-2, CL2-3 and CL2-4, respectively, showing some

correlation between epoxy molecular size of an epoxy molecule and the dose latitude of the resist. In addition, by extrapolating the linear curve to intercept the line width axis at 0 pC/cm, an estimation of the resolution limit of this resist of between 9 nm and 13 nm could be made.

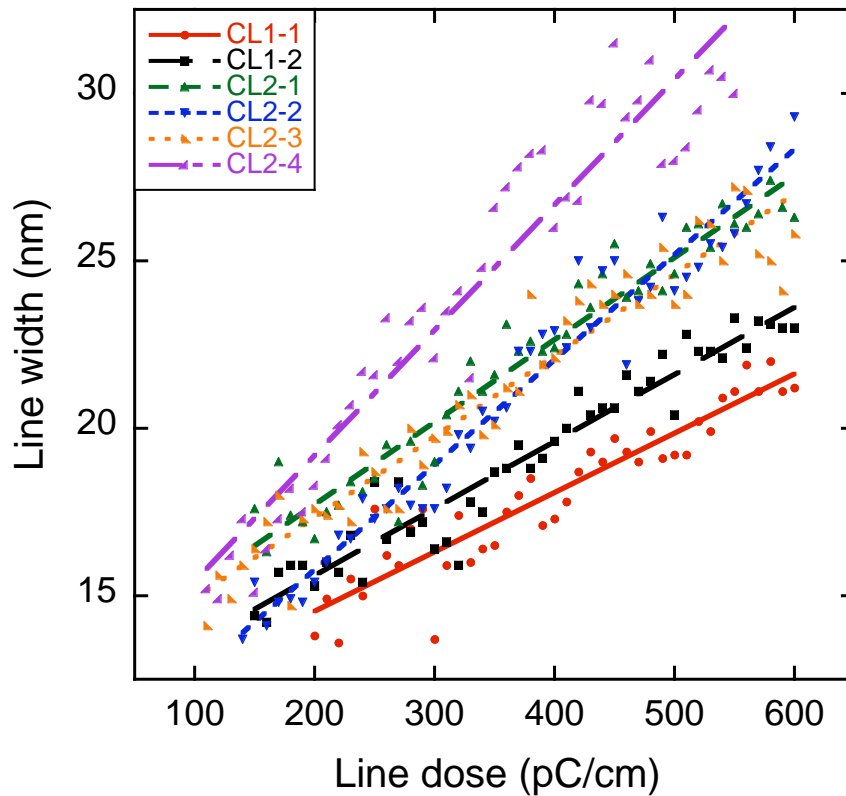


Figure 3.18 Line width of sparse lines as a function of dose with a linear curve fit for the resist MF07-01:CL: PAG07-01 (1:2:1) formulated with various types of epoxy crosslinker. All samples processed with the standard conditions.

3.3.5 Casting solvent

Chloroform is a good casting solvent, but its halogenated nature makes it non-ideal for industrial use. Therefore more environmentally friendly solvents were tested. PGMEA and anisole are considered more suitable to use in manufacturing. Evaluation of the resolution of the resist cast with an alternative solvent is reported in this section. The resist MF07-01:CL1-1:PAG07-01 (1:2:1) was prepared in PGMEA or anisole. The sample cast with PGMEA received PAB of 75 °C for 10 minutes, whilst the one cast with anisole received PAB of 100 °C for 30 minutes. PEB and development conditions were

the same as the standard in both cases. Patterning of dense lines with 25 nm half-pitch was demonstrated as shown in Figure 3.19. The patterns were achieved at 240 pC/cm for the sample cast with PGMEA, Figure 3.19 (a), and at 200 pC/cm for the sample cast with anisole at 200 pC/cm, Figure 3.19 (b). The line patterns were resolved although defects such as edge roughness and swelling were observed.

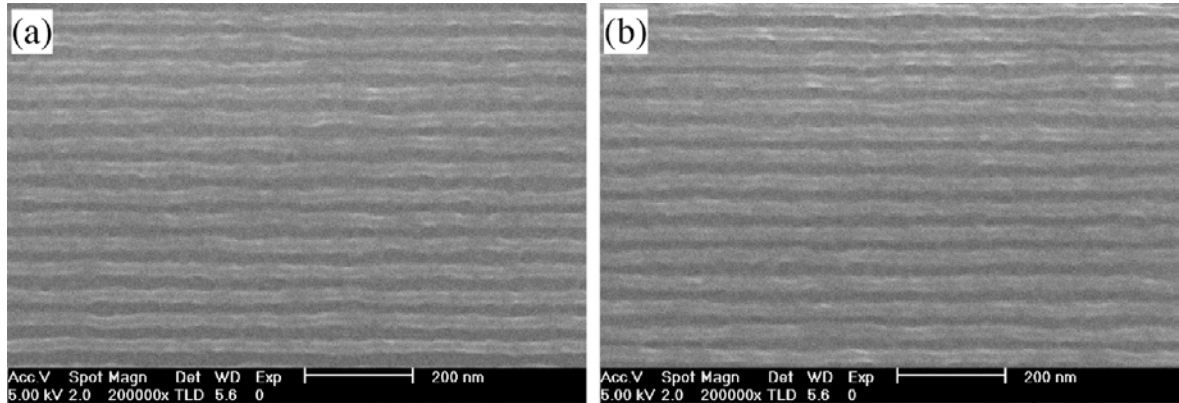


Figure 3.19 A comparison of 25 nm half-pitch dense line patterns in the resist MF07-01:CL1-1:PAG07-01 (1:2:1) cast with (a) PGMEA, and (b) anisole. PAB was varying. PEB was 90 °C for 3 minutes. Development was in MCB:IPA (1:1) for 10 seconds followed by a rinse in IPA.

Plots of sparse line width with varying doses in Figure 3.20 shows a comparison of the result between alternative solvents and chloroform. It can be seen that using PGMEA and anisole both show a slight reduction in the resolution capability of the resist. Although a line width as small as 15 nm was achievable, the line width increased with dose at a rate of 2.6 nm and 3.6 nm per 100 pC/cm for the resist cast with PGMEA and anisole, respectively, a little higher than that of the chloroform sample.

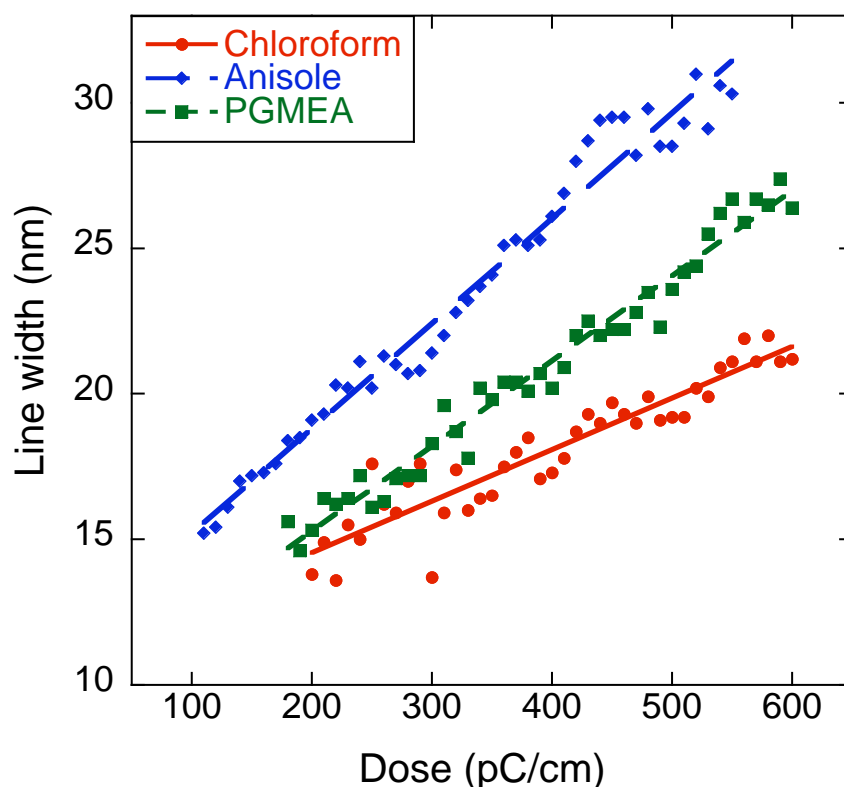


Figure 3.20 A comparison of line width of sparse lines as a function of dose for the resist MF07-01:CL1-1: PAG07-01 (1:2:1) cast with chloroform, PGMEA, anisole. A plot was presented with a linear curve fit.

3.3.6 Developer

As demonstrated in the previous section, solvent can play a role on the resist resolution. In this section, various combinations of casting solvent and developer were examined for the resist resolution. Samples of resist MF07-01:CL1-1:PAG07-01 (1:2:1) were prepared from chloroform, PGMEA, or anisole. PAB was varied to suit each solvent as described above. The sample was patterned at high resolution, followed by PEB of 90 °C for 3 minutes. It was developed in anisole, xylene, PGMEA, anisole:IPA (1:1) or MIBK:IPA(1:3) for 10 seconds and rinsed in IPA. A mixture of IPA and water and an aqueous TMAH solution were also tested as a developer. The sample was developed in IPA:water (1:1) for 30 seconds or 0.26 N TMAH for up to 60 seconds, followed by a rinse in DI water. The results are shown in Figure 3.21. It is clearly seen that the selection of casting solvent and developer significantly affected the resolution capability of the resist. Incompatibility between a

casting solvent and developer resulted in defects such as swelling and residue. For anisole casting, xylene or MIBK:IPA could be used as well as MCB:IPA. Although the pure MF07-01 is developable in an aqueous base solution, this CA fullerene based resist system prefers organic solvents as a developer because it is formulated with an epoxy resin, a lipophilic compound. The resist was almost fully developed in IPA:water, leaving some residue on the substrate. It could not be developed in the TMAH solution.

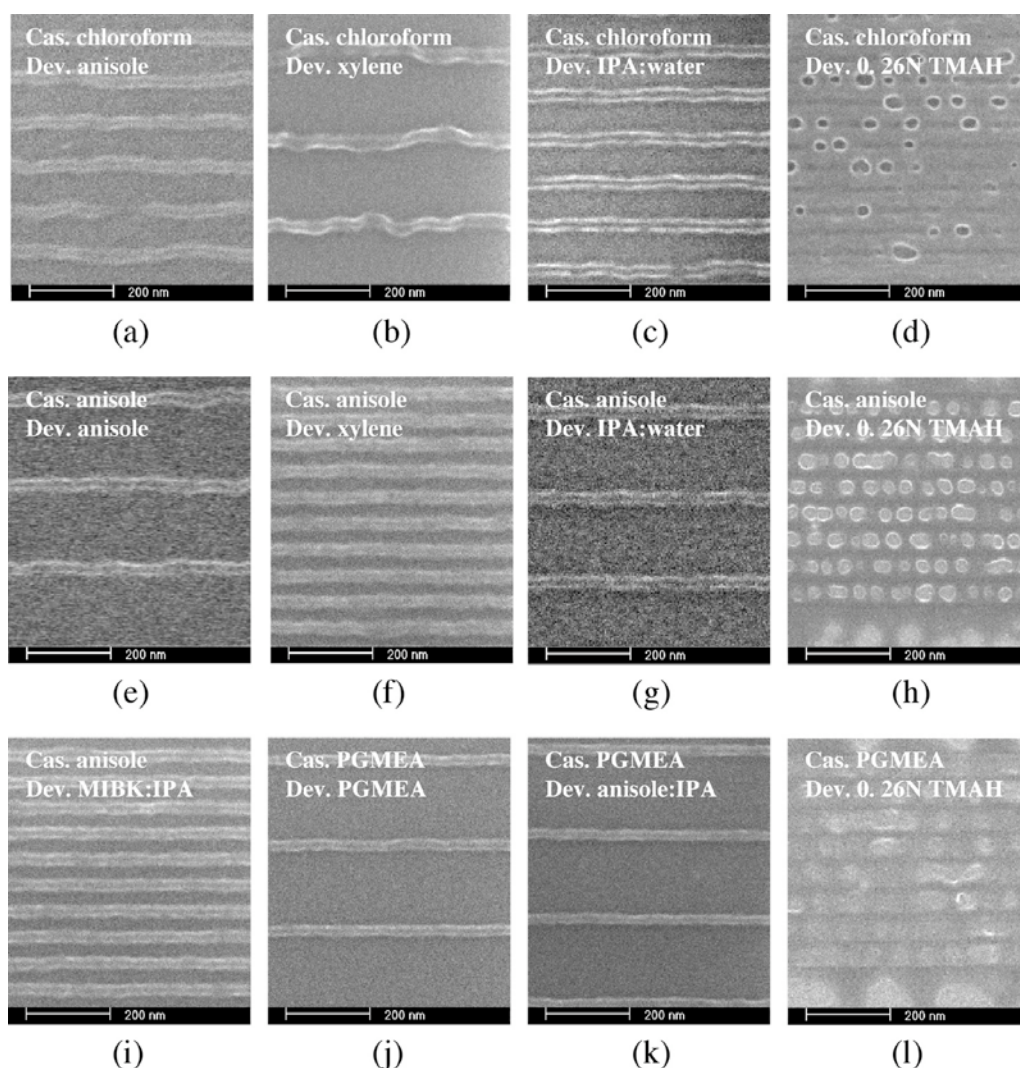


Figure 3.21 High resolution patterns achieved in the CA resist MF07-01:CL1-1:PAG07-01 (1:2:1) cast and developed with a pair of solvent-developer of (a) chloroform-anisole, (b) chloroform-xylene, (c) chloroform-IPA:water (1:1), (d) chloroform-0.26 N TMAH, (e) anisole-anisole, (f) anisole-xylene, (g) anisole-IPA:water (1:1), (h) anisole-0.26 N TMAH, (i) anisole-MIBK:IPA (1:1), (j) PGMEA-PGMEA, (k) PGMEA-anisole:IPA (1:1), or (l) PGMEA-0.26 N TMAH.

3.4 Line width roughness

Line width roughness (LWR) analysis of the resist patterns was carried out using the method described in section 2.3.3. Single pixel sparse and dense lines with pitch size of 200 nm and 50 nm respectively were written in the non-chemically amplified MF07-01 resist and chemically amplified MF07-01 resists formulated with various epoxy crosslinkers at the standard composition ratio of 1:2:1 parts of MF07-01:CL:PAG07-01. The pure MF07-01 resist received PAB of 75 °C for 10 minutes and the sample was developed in 0.26 N TMAH solution for 10 seconds followed with rinsing in DI water, whilst all CA resist samples were processed with standard conditions. Figure 3.22 shows a comparison of LWR results between sparse and dense lines for all resists.

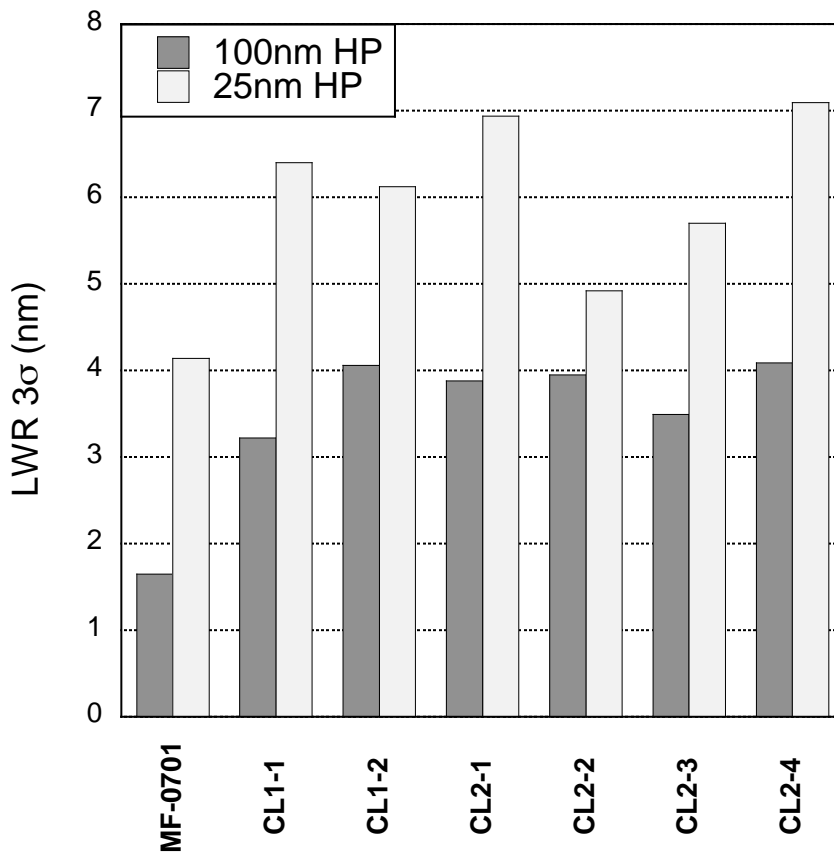


Figure 3.22 A comparison of LWR(3σ) values of sparse (100 nm half pitch) and dense lines (25 nm half pitch) patterned in the pure MF07-01 resist and in the chemically amplified resists containing different epoxy crosslinkers.

The LWR(3σ) value was measured for lines exposed with sufficiently low doses and averaged from five lithographic lines in the same sample. It can be seen that LWR(3σ) of sparse lines were lower than those of dense lines, and LWR(3σ) of CA resists were relatively high in comparison with that of the pure material. Sparse lines in the MF07-01 resist showed the LWR(3σ) as low as 1.6 nm, and the LWR(3σ) increased to about 4 nm in dense feature. LWR(3σ) for sparse lines in CA resists was between 3 and 4 nm, and it was between 5 and 7 nm in dense lines. A correlation between the type of crosslinker and LWR was not clearly observed here. Effects of resist compositions, exposure dose, and other processing parameters to LWR of the CA MF07-01 resists were investigated and are reported in chapter 5.

3.5 Etch resistance

The resistance of the negative tone fullerene resists to plasma etching was evaluated using the ECR plasma etcher. The chemically amplified resists were prepared with 6 different epoxy crosslinkers at the same weight ratio of 1:2:1 MF07-01:CL:PAG07-01. The samples received no PAB or PAB of 75 °C for 10 minutes to examine the effect of baking. The resist films of about 50 nm thick were patterned and processed under the standard conditions. The samples were etched with SF₆ etchant at a flow rate of 5 sccm and pressure of 1 mT for 5 minutes. Plasma etching was performed at 25 °C with RF power of 17 W, microwave power of 250 W, and a DC self bias of about 110 to 115 V. Variations of resist film thickness and etched depth in the silicon substrate by the anisotropic etching process were measured. Calculation of the etch resistance of the resist to silicon was performed using the method described in section 2.3.4. The commercial resist SAL601 (Rohm and Haas) was etched together with the fullerene resist in each case as a control sample and its ER was normalised to 3 times that of silicon.

Etch resistances of the fullerene based resists and SAL601 are compared and shown in Figure 3.23. It can be seen that an epoxy type and PAB conditions had no insignificant impact on the etch

resistance of the resist. The etch resistance of the fullerene resist containing CL1-1, CL1-2, CL2-1, or CL2-4 varied between 2.5 and 2.8 times that of silicon, a little below that of the SAL resist.

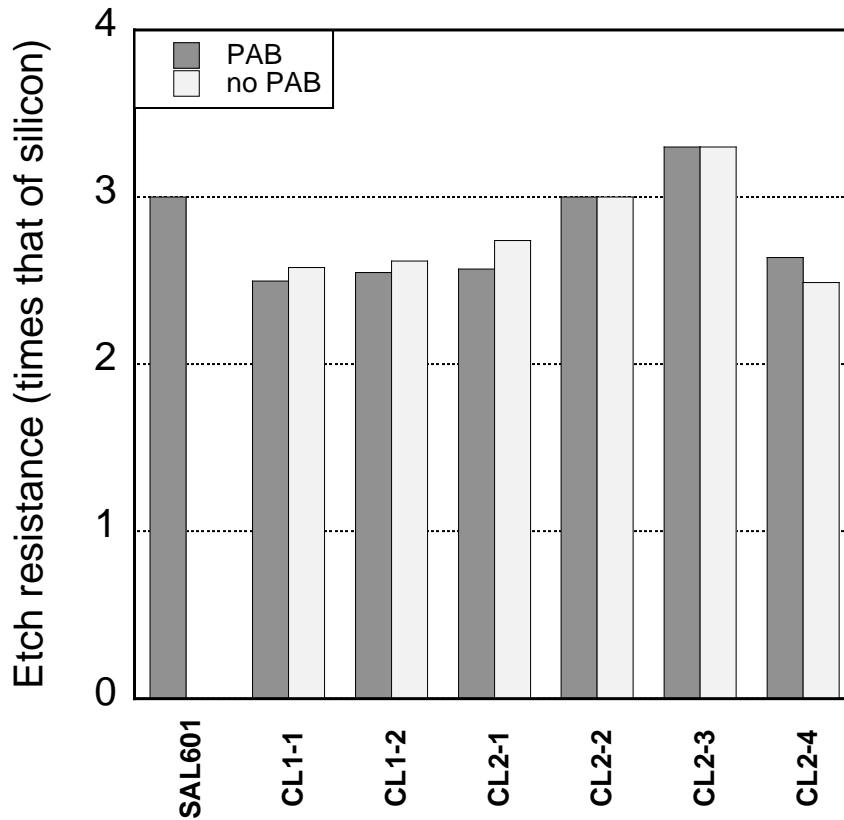


Figure 3.23 Etch resistance to plasma etching of SAL601 and the CA MF07-01 resists relative to the etch resistance of silicon. The CA MF07-01 resists were prepared with varying types of an epoxy and PAB conditions. The resist composition ratio was controlled with one part of fullerene per 2 parts of epoxy and one part of PAG. PAB was 75 °C for 10 minutes. PEB was 75 °C for 3 minutes. Development was in MCB:IPA (1:1) for 10 seconds followed with a rinse in IPA.

Transfer of high-resolution resist pattern to the silicon substrate using ECR plasma etching was demonstrated. Sparse and dense resist patterns with feature sizes of 20 nm were etched to fabricate silicon nanostructures, as shown in Figure 3.24. The sample was etched for 2 seconds under the same plasma conditions as those described above. Etched lines were resolved but with high roughness on the sidewalls. The ECR etching system and etching conditions used were found too aggressive for such high-resolution features. The etching process had to be completed in a very few

seconds to avoid over etching, as such small structures can be easily damaged by even a small variation of anisotropy. A more robust pattern transfer technique using ICP etching was studied and the results are reported in chapter 6.

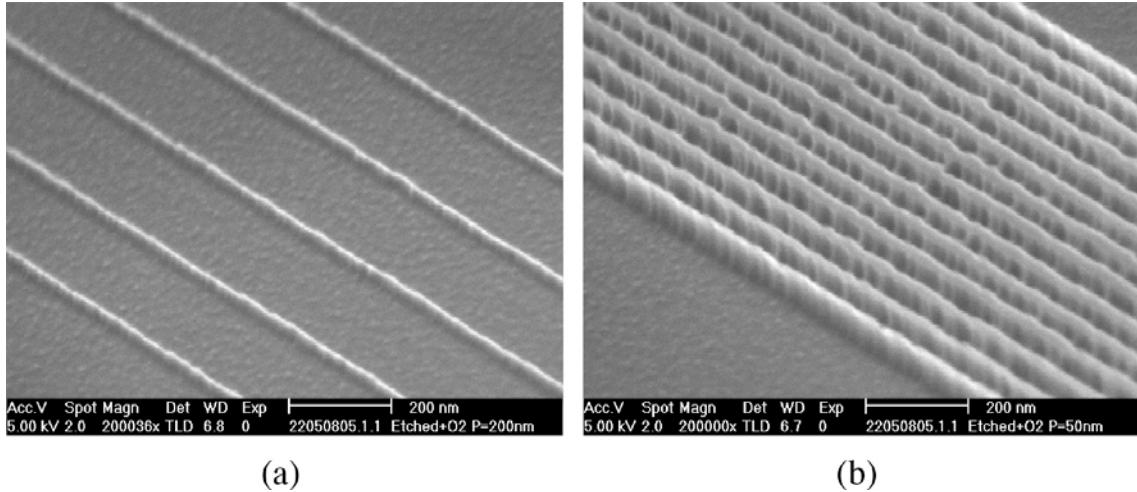


Figure 3.24 (a) Sparse and (b) 25 nm half pitch silicon structures with 50 nm height achieved from etching of 30 nm thick resist pattern by ECR plasma etching. The residual resist was removed by O₂ plasma.

3.6 Post exposure delay

Effects of post exposure delay (PED) to sensitivity and resolution of the CA MF07-01 resist were investigated. The resist MF07-01:CL1-1:PAG07-01 (1:2:1) was prepared with PAB of 75 °C for 10 minutes. The sample was exposed to electrons and then left under ambient cleanroom conditions: 20 °C and humidity of 50%, for up to 24 hours before receiving PEB of 90 °C for 3 minutes and development in MCB:IPA (1:1). Response curves of resists receiving PED are shown in Figure 3.25. The sensitivity slightly reduced from 25 $\mu\text{C}/\text{cm}^2$ for the sample without a delay to 32 $\mu\text{C}/\text{cm}^2$ for the sample with a 24-hour delay. A decrease in the contrast from 1.1 to 0.7 was also observed.

The resolution capability of the resist subjected to PED was evaluated. Figure 3.26 shows 25 nm half-pitch dense lines written in the sample with varying PED time. It can be seen that a well resolved dense line pattern was achievable even though a delay of 24 hours was introduced.

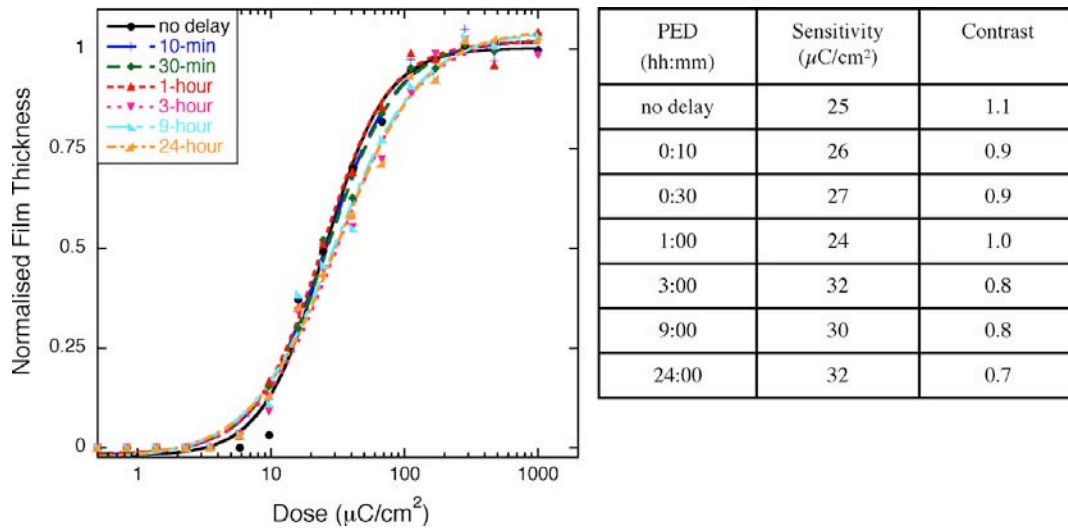


Figure 3.25 Response curves of the CA resist MF07-01:CL1-1:PAG07-01 (1:2:1) receiving PED for up to 24 hours. The resists were cast with chloroform and received PAB of 75 °C for 10 minutes. After applying PED, the sample were processed with PEB of 90 °C for 3 minutes, developed in MCB:IPA (1:1) for 10 seconds, and rinsed in IPA.

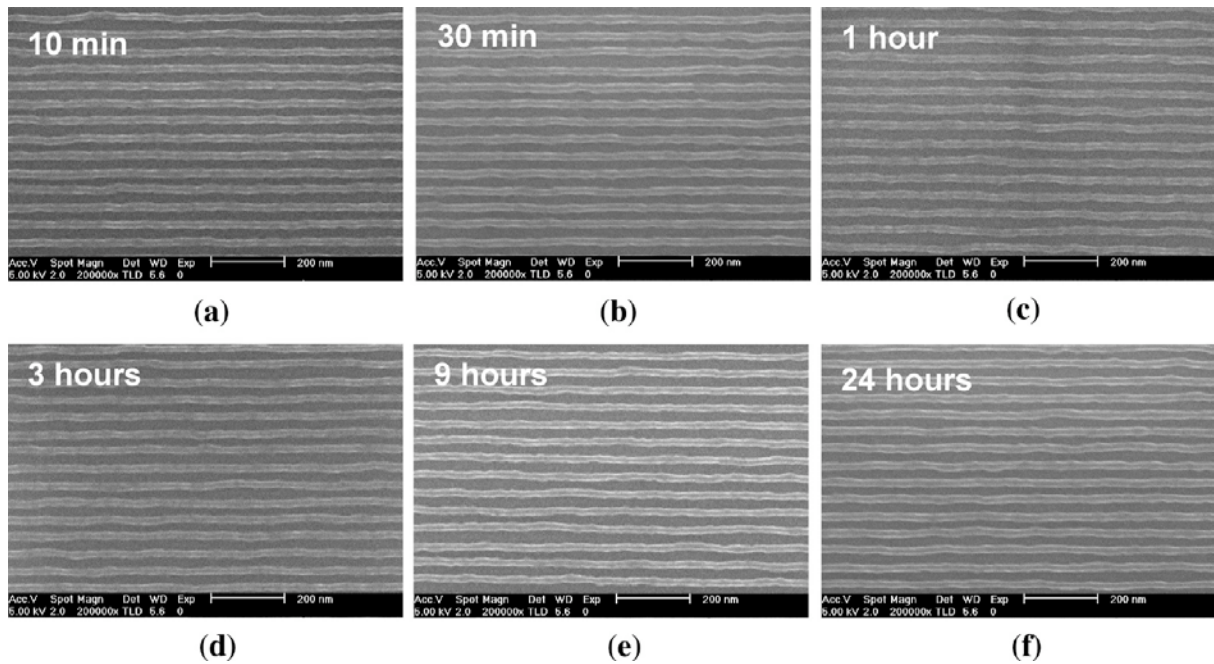


Figure 3.26 25 nm half pitch dense lines written in the resist received PED of (a) 10 minutes, (b) 30 minutes, (c) 1 hour, (d) 3 hours, (e) 9 hours, and (f) 24 hours. PAB, PEB and development were applied as the standard conditions.

3.7 Aging effects

Aging effects in the CA fullerene based resist were studied. The resist MF07-01:CL2-4: PAG07-01 (1:2:1) were prepared in chloroform. Samples were divided into five sets as follows and summarised in Table 3.1. Set 1 was spun on a substrate, post application baked at 75 °C for 10 minutes and stored in a cleanroom under ambient conditions. Set 2 was spun on a substrate and stored in a cleanroom under ambient conditions. Set 3 was spun on a substrate, baked and stored in a vacuum desiccator at ambient temperature. Set 4 was spun on a substrate and stored in a vacuum desiccator at ambient temperature. Set 5 was stored as a mixed resist solution in a refrigerator at 8°C, and spun on a substrate shortly before exposure. Exposure was performed after samples had been aged for between 3 days and 30 days. A freshly prepared resist sample was exposed in each case as a control. All samples received PEB of 90 °C for 3 minutes and were developed in MCB:IPA(1:1) as the standard conditions. Response curves of samples in set 1 and a plot of the resist sensitivity as a function of sample age for all sets are shown in Figures 3.27 (a) and (b), respectively.

Table 3.1 Storage conditions of resist samples to examine the aging effects.

Set	Resist sample	PAB	Storage conditions
1	Spin coating film	Yes	In a cleanroom under ambient conditions
2	Spin coating film	No	In a cleanroom under ambient conditions
3	Spin coating film	Yes	In a vacuum desiccator under ambient temperature
4	Spin coating film	No	In a vacuum desiccator under ambient temperature
5	Dissolved in chloroform	No	In a refrigerator at 8 °C

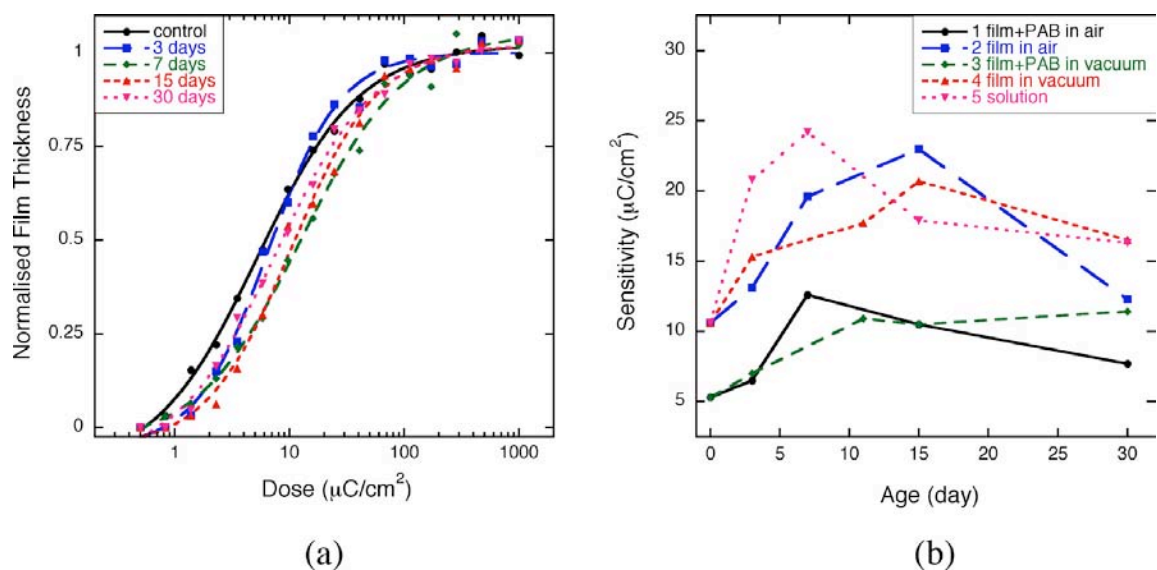


Figure 3.27 Effects of aging on the sensitivity of the resist MF07-01:CL2-4:PAG07-01 (1:2:1). (a) Response curves of the resist film baked at 75 °C for 10 minutes and stored under ambient cleanroom conditions for between 3 and 30 days before exposure. A freshly prepared sample was exposed as a control. (b) Sensitivity of the resist sample as a function of age.

It can be seen that the sensitivity initially decreased from between 5 and 10 $\mu\text{C}/\text{cm}^2$ to between 15 and 25 $\mu\text{C}/\text{cm}^2$ within one or two weeks then started increasing gradually in all cases. The results suggest that introduction of chloroform and airborne impurities play an insignificant role to aging, and pre-exposure crosslinking in aged samples is believed to be involved in the aging process.

High resolution patterns were written in aged samples. A comparison of semi-dense lines with a half-pitch of 50 nm written in samples in set 2, 4, and 5 is shown in Figure 3.28. It can be seen that high resolution features could be achieved in a sample stored under ambient conditions for 7 days, as a solution for 7 days or in vacuum for 11 days. Degradation in a 30-day aged sample was observed as the line pattern was covered with residue, regardless of the storage conditions. The presence of insoluble residue might relate to the shift toward higher sensitivity in an aged sample. The lithographic capability of the resist lasts for nearly 2 weeks after mixing. The film life and shelf life could not be accurately specified due to a lack of data, but it seems likely that an additional stabilising agent will be required.

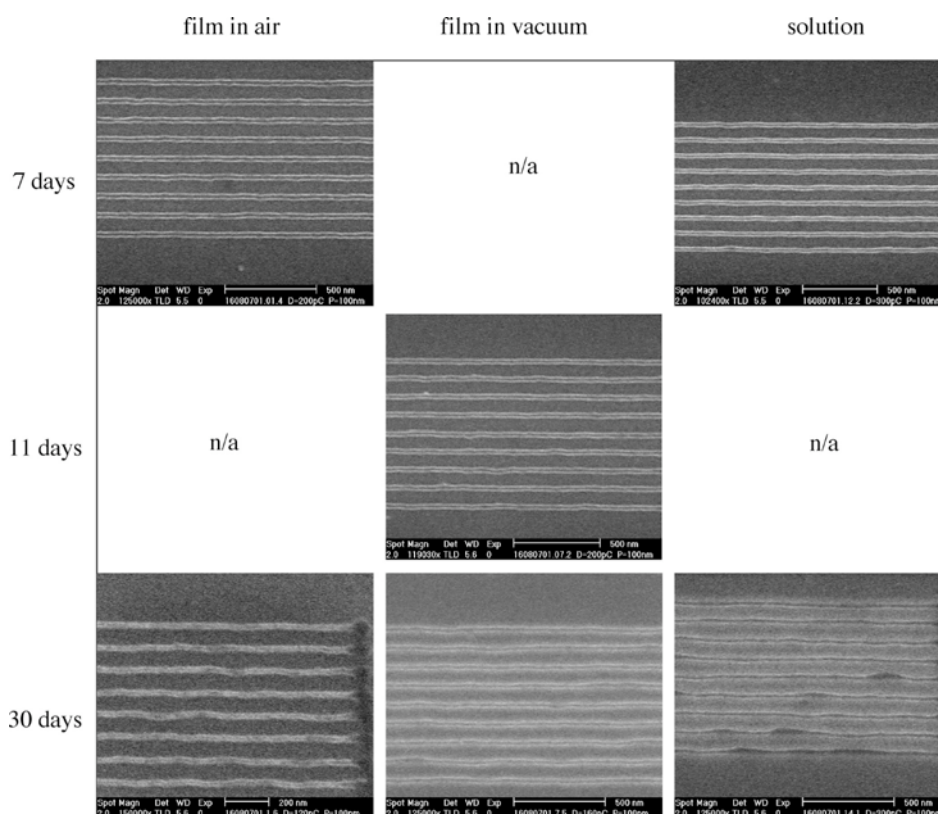


Figure 3.28 Semi-dense lines at half-pitch of 50 nm in the resist sample aged for 7 days, 11 days, and 30 days. Three sets of the sample were stored as a film in air, a film in a vacuum desiccator, and a 3-component resist solution at 8 °C. All samples were processed without PAB.

3.8 Conclusions

Negative tone chemically amplified fullerene based molecular resists were developed for electron beam lithography. A success of chemical amplification of the fullerene derivative MF07-01 by adding with a PAG and an epoxy novolac crosslinker was demonstrated. The sensitivity of the 3-component chemically amplified resist was 5 - 10 $\mu\text{C}/\text{cm}^2$ at 20 keV, about two orders of magnitude enhancement from that of the pure MF07-01. Sparse resolution of sub 20 nm and dense resolution of 25 nm half-pitch were reproducible in a number of resist formulations. The highest sparse resolution of 12 nm, and dense resolution of 20 nm half-pitch were demonstrated in the resist formulated with an epoxy CL1-1. The best resist formulation and processing conditions for the high-resolution, fullerene based, e-beam resist are summarised in Table 3.2. The resists are capable of being processed at a wide range of PAB and PEB conditions without a strong significant change in resolution or sensitivity. In

addition, high resolution features can be produced in the resist film in the absence of the PEB process or after a post exposure delay of up to 24 hours. A remarkably low LWR(3σ) was found in the non-chemically amplified MF07-01 resist: 1.6 nm and 4 nm in sparse and dense features respectively. Chemical amplification resulted in a slight increase in LWR. The CA resists showed LWR(3σ) of 3 - 4 nm in isolated lines, whilst the relatively high value of 5 - 7 nm was found in the 25 nm half-pitch features - considerably above the LWR requirement in the ITRS roadmap. The etch resistance of the resists to SF₆ plasma, using an ECR plasma source, was between 2.5 and 3.2 times that of silicon, comparable to SAL601 under the same etching conditions. The CA fullerene resist exhibited degradation during storage. The film life and shelf life of the resist formulated with CL2-4 in chloroform were approximately two weeks under ambient cleanroom conditions. The source of degradation is unclear, at this time.

Table 3.2 The best resist formulation and processing conditions for the high-resolution, negative-tone, chemically amplified, fullerene based resist.

Resist formulation	
Fullerene derivative	MF07-01
Crosslinker	Epoxy novolac resin CL1-1
PAG	PAG07-01
Fullerene weight ratio (parts)	1
Crosslinker weight ratio (parts)	2
PAG weight ratio (parts)	1
Casting solvent	Chloroform
Processing conditions	
PAB temperature	75 °C
PAB time	5-10 minutes
PEB temperature	90 °C
PEB time	3 minutes
Developer	MCB:IPA (1:1 by volume)
Development time	10 seconds
Rinse	IPA

Chapter 4

Effects of Base Quenchers

A base quencher is often added to chemically amplified resist formulation to improve resolution capability of the resist. A base can neutralise a photoacid, and thus help control acid diffusion. This chapter describes a study of the effects of base quencher additives on negative tone chemically amplified fullerene-based molecular resists. Various base and photoactive quenchers were added to the three-component resist formulation previously presented in Chapter 3. The sensitivity and resolution capability of the resists on the addition of a quencher were evaluated.

4.1 Sample preparation

The base quenchers were selected from commercially available materials (Sigma Aldrich) and they are shown in Figure 4.1. The quenchers used in this work were 1,8-diazabicyclo[5.4.0]undec-7-ene (BA-1 in Figure 4.1 (a)), 4-phenylpyridine (BA-2 in Figure 4.1 (b)), diphenylamine (BA-3 in Figure 4.1 (c)), 1-piperidineethanol (BA-4 in Figure 4.1 (d)), N-methyl pyrrolidinone (BA-5 in Figure 4.1 (e)), and triphenylsulfonium triflate (PAG03-01 in Figure 4.1(f)). It should be noted that PAG03-01 is typically used as a photoacid generator, but it was used here as a photo-active quencher.

The resist was prepared by mixing the fullerene derivative MF07-01, epoxy novolac resin CL1-1, and photoinitiator PAG07-01 at one part, four parts, and two parts by weight, respectively. It should be noted that the large of concentration of crosslinker and PAG in the resist formulation here was necessary in order to maintain resist sensitivity since the MF07-01 compound used in the experiments reported in this chapter tended to exhibit poorer sensitivity than reported in Chapter 3, most likely due to its age. The quencher was then added to the resist at between 0.5 wt% and 8 wt% to the total weight of the resist.

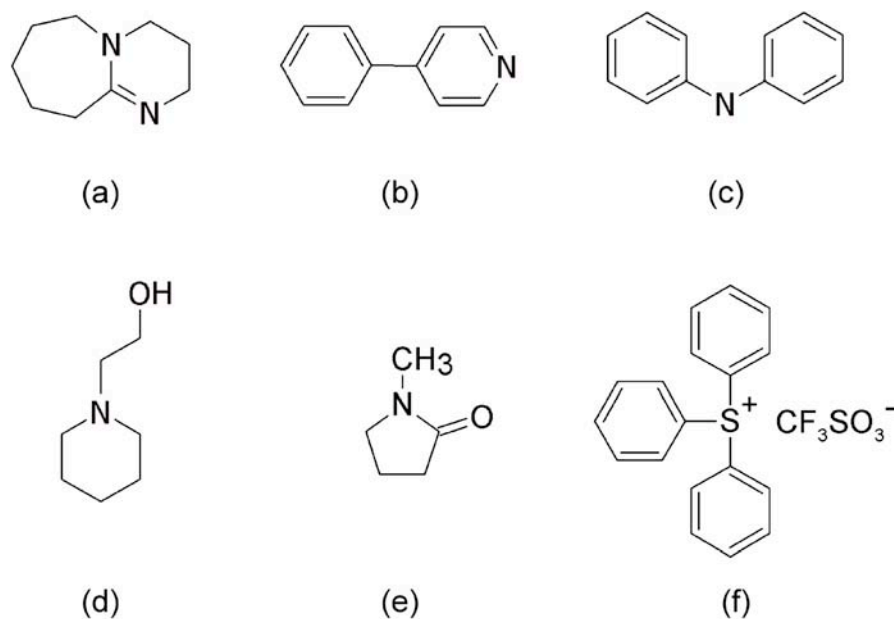


Figure 4.1 Base additives (a) 1,8-diazabicyclo[5.4.0]undec-7-ene (BA-1), (b) 4-phenylpyridine (BA-2), (c) diphenylamine (BA-3), (d) 1-piperidineethanol (BA-4), (e) N-methyl pyrrolidinone (BA-5), and (f) triphenylsulfonium triflate (PAG03-01).

The molar ratio of the quencher to PAG07-01 could not be precisely calculated because PAG07-01 was a proprietary mixture of triarylsulfonium salts with an unknown molecular weight distribution. However, loading the quencher up to 8 wt% should be sufficiently high to allow the quencher to take full effect. The process conditions were controlled as follows: the casting solvent was chloroform; PAB was 75 °C for 10 minutes; PEB was 90 °C for 3 minutes, the development process occurred in MCB:IPA (1:1) for 10 seconds followed by a rinse in IPA.

4.2 Sensitivity

The response to the 20 keV electrons of the fullerene resists with the added quenchers were examined. Sensitivity and contrast of the resist were plotted versus additive levels as shown in Figure 4.2. The sensitivity of the three-component resist without an additive was between 14 and 16 $\mu\text{C}/\text{cm}^2$, with the contrast of between 0.9 and 1.1. The response of the resist with BA-1 is shown in Figure 4.2 (a). BA-1 is a strong amine base. Addition of a BA-1 to the resist at even small level can significantly affect

resist sensitivity. A decrease in the sensitivity to between 40 and 75 $\mu\text{C}/\text{cm}^2$ and a slight decrease in the contrast to 0.8 were observed as the additive level increased. Addition of the weak amine bases BA-2, BA-3 and BA-4 to the resist caused little change in the sensitivity and the contrast, even at a high loading level of 8 wt%, as shown in Figures 4.2 (b), (c), and (d), respectively.

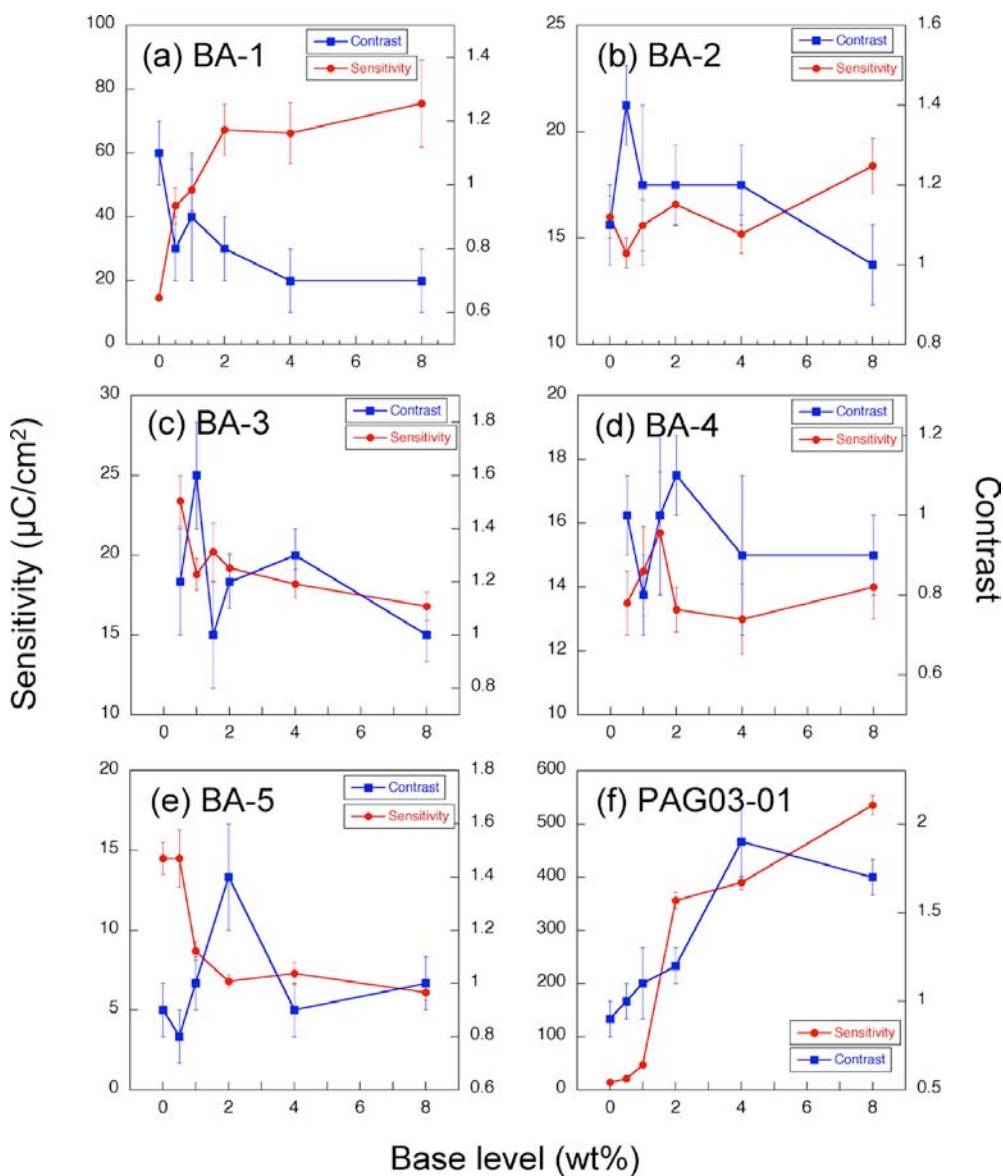


Figure 4.2 Sensitivity and contrast as a function of levels of base quencher for the CA fullerene resists added with (a) BA-1, (b) BA-2, (c) BA-3, (d) BA-4, (e) BA-5, and (f) PAG03-01 at loadings of 0.5 wt% to 8 wt%.

The response of the weak base samples show little change in sensitivity in a variation of less than 5 $\mu\text{C}/\text{cm}^2$. A slight increase of the contrast to 1.4 and 1.5 was found at 0.5 wt% BA-2 and 1 wt% BA-3, respectively. The weak amide base BA-5, known as a common atmospheric poison of a chemically-amplified resists [107], had a strange effect on the resist response in an unexpected manner, as shown in Figure 4.2 (e), where the resist sensitivity increased from 14.5 $\mu\text{C}/\text{cm}^2$ to 6 $\mu\text{C}/\text{cm}^2$ as the level of BA-5 level was increased to 8 wt%. The PAG03-01, examined here as a quencher, acted as a very effective quencher in this resist system. A significant reduction in the sensitivity from 14 $\mu\text{C}/\text{cm}^2$ in the resist without the quencher to 540 $\mu\text{C}/\text{cm}^2$ with the quencher at 8 wt% is shown in Figure 4.2 (f). The contrast was also improved to 1.8-2.0 at high quencher levels. It is suggested by Henderson [108] that of a triflate anion (CF_3SO_3^-) in unexposed PAG03-01 can react with an opened epoxide ring without regeneration of an acid, thus quenching acid like base dose, whilst photo-decomposition of PAG03-01 produces triflic acid ($\text{CF}_3\text{SO}_3\text{H}$) which can cause epoxide ring opening and regenerate an acid for a subsequent reaction, as a typical PAG.

4.3 Resolution

The high resolution capability of the resists containing the quenchers was evaluated by examining sparse and dense line patterns written in the resist samples with the quenchers BA-1, BA-2, BA-3, BA-4, and BA-5 added at varying base levels. All of the samples were processed under the same conditions. Sparse features at a pitch of 200 nm were written in the resist with the quenchers. The results are shown in Figure 4.3. Sub 20 nm line widths were achieved for all loadings of BA-1, BA-2, BA-3, and BA-4 from 0.5 wt% to 8 wt%. An increase in the width of sparse lines up to 35 nm was observed in the resist with BA-5 greater than 0.5 wt%.

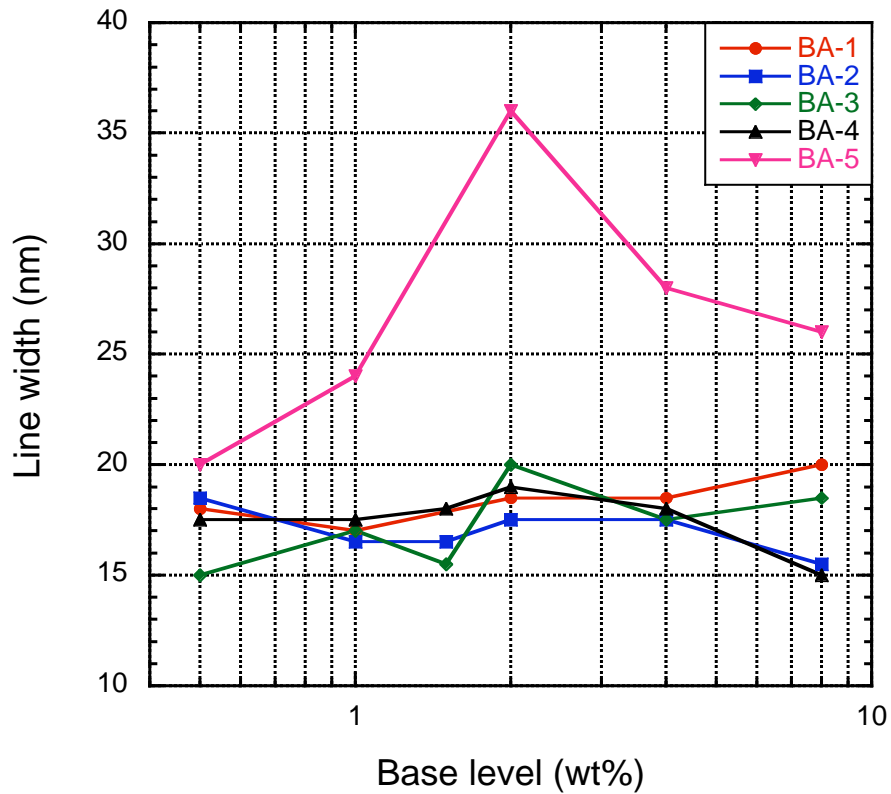


Figure 4.3 Width of sparse line patterns in the resists with BA-1, BA-2, BA-3, BA-4, and BA-5 at varying base levels from 0.5 wt% to 8 wt%.

Dense lines patterns in the resist with the base quenchers at 1 wt% were compared with the patterns in the resist without a quencher, as shown in Figure 4.4. A resolution of 22.5 nm half pitch was achieved in the resist without a quencher, Figure 4.4 (a), as well as for the resists with quenchers BA-1, BA-2, and BA-3, Figures 4.4 (b), (c), and (d), respectively. In the resists with BA-4, Figure 4.4 (e), and BA-5, Figure 4.4 (f), 25 nm and 30 nm half pitches were achieved, respectively. It can be seen that a slight increase in line width roughness was seen upon addition of the base quenchers.

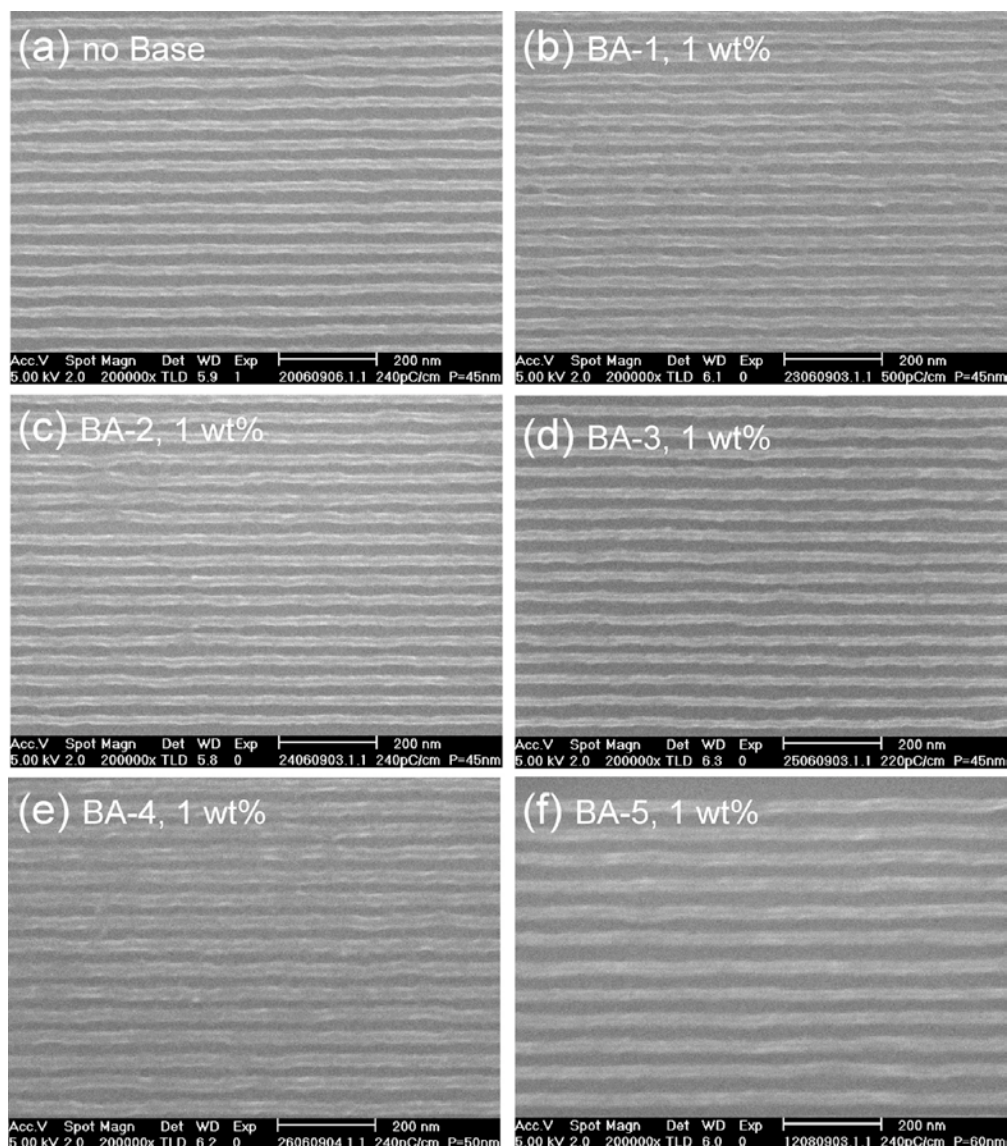


Figure 4.4 Dense patterns: 22.5 nm half pitch line space in the resist (a) without quencher at a line dose of 240 pC/cm, (b) with the BA-1 1 wt% at a line dose of 500 pC/cm, (c) with the BA-2 1 wt% at a line dose of 240 pC/cm, (d) with the BA-3 1 wt% at a line dose of 220 pC/cm; (e) 25 nm half pitch line space in the resist with BA-4 1 wt% at a line dose of 240 pC/cm; (f) 30 nm half pitch line space patterned in the resist with BA-5 1 wt% at a line dose of 240 pC/cm.

The capability of the selected quenchers to suppress acid-assisted crosslinking reactions was further investigated using a defocused electron beam. Patterning a line feature with a defocused beam allows a gradient of dose, giving a low contrast features - blurring the feature edge. A comparison of distribution of energy deposited in the resist between focused and defocused beam is shown in Figure 4.5. Sidewall angle of the resist feature could then be measured to examine the effect of the quencher

as the dose varies gradually. The defocusing level was determined by varying the vertical distance between the ideal focus plane of the electron beam and the resist surface.

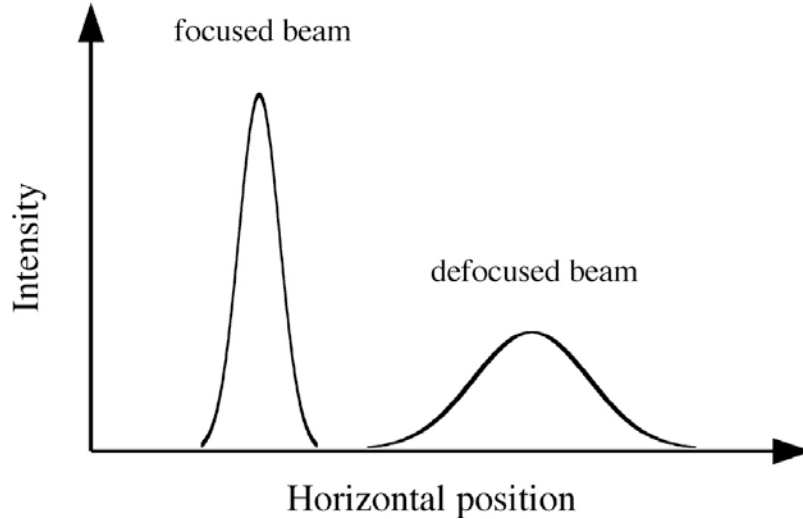


Figure 4.5 Energy distributions of focused e-beam and defocused e-beam.

Sparse lines with a 200 nm pitch were written in the resist without a quencher and with 1 wt% BA-2, BA-3 or BA-4. All samples received a PAB of 70 °C for 10 minutes to prevent film degradation, whilst the other processes were the same as described above. Each sample was then imaged in cross-section. The sidewall angle, the angle between the resist sidewall and the silicon substrate, was measured at line doses of 240 pC/cm, 300 pC/cm, and 360 pC/cm. The variation in the sidewall angles with the vertical shift of focus point are shown in Figure 4.6. It can be seen in Figure 4.6 (a) for the resist without a quencher that the angle reduced from 90° to 50° as the focus point was shifted to 25 µm above the film. In the resist films containing base additives, Figures 4.6 (b), (c) and (d), the sidewall is less affected by defocusing up to a considerable shift of focus. In particular, additive BA-2 was the most effective at suppressing the effects of defocusing.

Figures 4.7 (a)-(d) show the cross-sections of lines written in the resist without a quencher and that with the quencher BA-2 at 1, 2 and 4 wt% added. Lines were written with the focused beam and with the focus shifted by 10, and 20 µm in each case. It can be seen that the line width and sidewall angle in the resist with 1 wt% BA-2 suffered less from the defocusing. However, adding more BA-2 beyond this point did not improve the resist profile further.

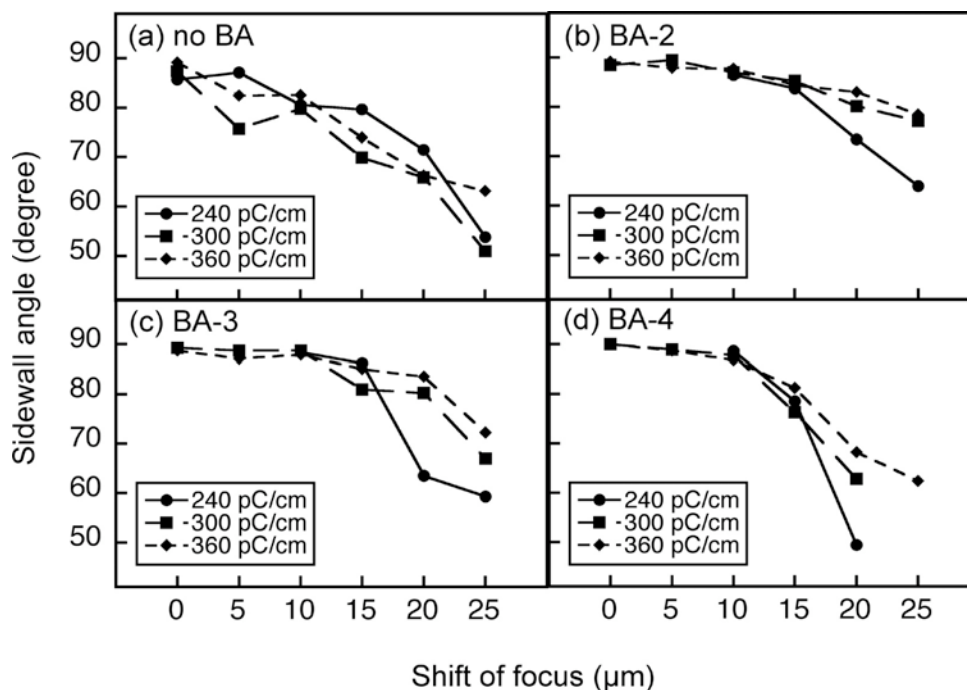


Figure 4.6 Sidewall angles of the 200 nm pitch lines as a function of the vertical shift of focus in the resist (a) without a base, (b) with BA-2 1 wt%, (c) with BA-3 1 wt%, (d) with BA-4 1 wt%.

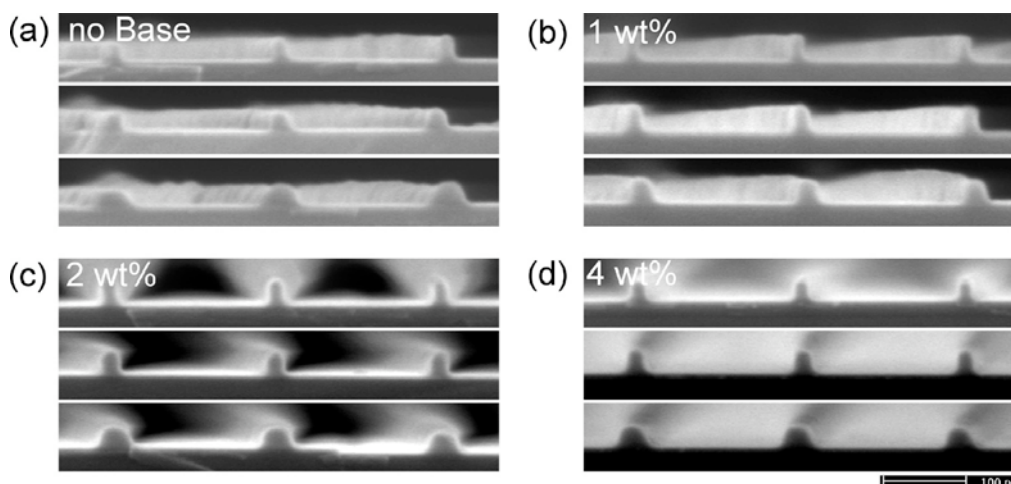


Figure 4.7 Cross-section of sparse lines in the resist (a) without a base, (b) with BA-2 at 1 wt%, (c) 2 wt%, (d) 4 wt%, written with a focused beam (top) and with the focus shifted 10 μm (middle), and 20 μm (bottom).

4.4 Conclusions

The effect of adding various quenchers on the sensitivity and resolution of a negative tone chemically amplified fullerene-based resist was studied. The quenchers included strong and weak amine bases, an amide base, and a triflate salt PAG. Some quenchers, such as the strong base BA-1 and PAG03-01,

significantly decreased resist sensitivity. In contrast, addition of the amide base quencher BA-5 increased resist sensitivity but degraded the high resolution capability. The weak amine bases BA-2, BA-3, and BA-4 had relatively small effect on both the sensitivity and resolution. It was found that in the case of sparse line patterning with a defocused electron beam, the addition of weak amine bases at low concentrations could suppress the acid reaction at the feature edge. The best additive formulation and processing conditions for the chemically amplified fullerene based resist are summarised in Table 4.1.

Table 4.1 The best additive formulation and processing conditions for the 4-component, negative-tone, chemically amplified, fullerene based resist.

Resist formulation	
Fullerene derivative	MF07-01
Crosslinker	Epoxy novolac resin CL1-1
PAG	PAG07-01
Base additive	BA-2
Fullerene weight ratio (parts)	1
Crosslinker weight ratio (parts)	2
PAG weight ratio (parts)	1
Base additive level (% wt)	1.0
Casting solvent	Chloroform
Processing conditions	
PAB temperature	75 °C
PAB time	10 minutes
PEB temperature	90 °C
PEB time	3 minutes
Developer	MCB:IPA (1:1 by volume)
Development time	10 seconds
Rinse	IPA

Chapter 5

Line Width Roughness Analysis

This chapter describes the line width roughness (LWR) analysis of the chemically amplified negative tone fullerene-based molecular resists. All experiments were carried out with the MF07-01 resists presented in Chapter 3. Several lithographic parameters concerning materials and processes were investigated in order to characterise and optimise LWR.

5.1 Effects of resist formulation

Samples with various types of epoxy resin, casting solvent, concentration of PAG, or concentrations of base quencher were patterned and processed to measure LWR of the sparse line feature. Average values of line width and the corresponding LWR are reported at various exposure doses.

5.1.1 Crosslinkers

The impact of the epoxy crosslinker type in the resist formulation was investigated using six epoxy novolac resins. The epoxy resins were different in structure, weight and the number of epoxide functional groups per molecule, as summarised in section 3.1. The resist composition was fixed at the same weight ratio for all samples, 1:2:1 of MF07-01:CL:PAG. Resists at such a ratio previously demonstrated the optimum combination of high resolution and sensitivity. Resist processing conditions were the same for all samples in this chapter unless otherwise noted. Samples were cast with chloroform. PAB was 75 °C for 10 minutes. PEB was 90 °C for 3 minutes. Development was in MCB:IPA (1:1) for 10 seconds followed by a rinse in IPA. Single pixel lines were written with a pitch size of 200 nm, sparse features, in the resist with a variation in line dose between 100 pC/cm and 600 pC/cm. Resist thickness was approximately 30 nm. LWR(3σ) and the average width of the written lines were plotted against the line doses, as shown in Figures 5.1 (a) and (b), respectively. Both line

width and LWR increased with exposure doses in the observed range, showing a strong positive correlation between line width, LWR and exposure dose. The line width-dose relationship was approximately linear. The minimum line width achievable in each resist was between 13 nm and 18 nm. The average LWR, calculated from the sparse lines receiving sufficiently low doses, was between 2.6 nm and 3.8 nm. The resist containing CL1-1, which has the lowest molecular weight, showed the best resolution and lowest LWR. The resist containing CL2-4, which has the highest molecular weight, showed the poorest resolution of any exposure dose. This shows the impact of the molecular size of the crosslinker to the quality of lithographic resolution in this resist system. There was no significant difference between the use of the phenyl type and the o-cresyl type epoxy crosslinkers.

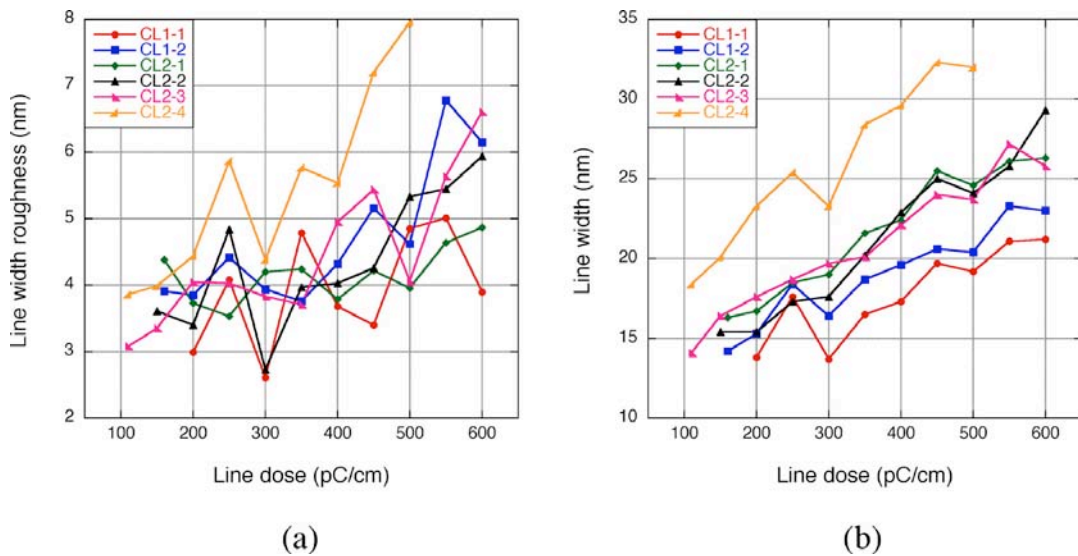


Figure 5.1 (a) LWR(3σ) and (b) line width as a function of exposure dose in the resists formulated with six different epoxy novolac resins.

5.1.2 Acid levels

The impact of the PAG level in the resist on LWR was also investigated. PAG07-01 was used in the experiments. The resists were composed of MF07-01 and CL1-1 at a fixed weight ratio of one part to two parts with a varying amount of PAG from 14 wt% to 40 wt% of the total resist weight. The resist film thickness was between 31 nm and 35 nm. The resist processing conditions were controlled as previously described. The line width and LWR(3σ) of the sparse lines versus exposure dose of the

resists with varying PAG levels are shown in Figures 5.2 (a) and (b). Due to significant differences in resist sensitivity with varying PAG concentrations, each resist received a different range of doses giving a line width from the minimum value to approximately 25 nm. It can be seen from the line width-dose relationship in Figure 5.2 (b) that resists exhibited a smaller exposure latitude, higher rate of increasing line width with exposure dose at higher PAG level. The same trend was observed in the LWR-dose relationship where LWR increased more quickly with increasing exposure dose at higher level. A relatively low LWR was found in the resists with intermediate PAG levels, 25 wt% to 29 wt%. The lowest LWR was 2.3 nm in the resist containing 29 wt% PAG, as shown in Figure 5.2 (c). Increasing the PAG level to 40% caused an increase in LWR to 3.4 nm and a decrease in the PAG level to 14% also caused an increase in LWR to 3.7 nm. This indicates the complexity of material impacts on resist performance.

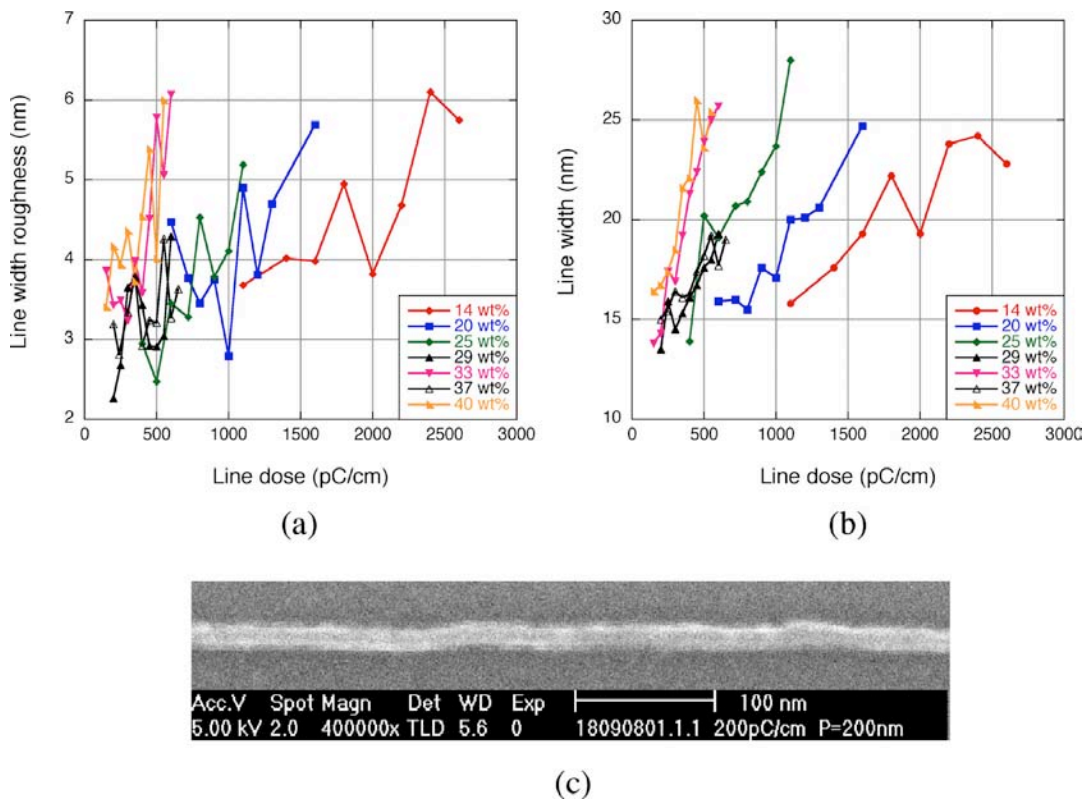


Figure 5.2 (a) Line width and (b) LWR(3σ) as a function of exposure dose in the resists formulated with varying PAG levels ranging from 14 wt% to 40 wt%. (c) The sparse line with 14 nm width and LWR(3σ) of 2.3 nm in the resist with 29 wt% PAG.

5.1.3 Base quencher levels

Addition of a quencher to a CA resist is a simple technique of improving resolution and lowering LWR by allowing a base additive to neutralize excessive photoacids that have diffused out of the exposure area. The effect of a base additive on LWR was investigated by introducing different amounts of tripropylamine (TPA) to the resist formulation. The resist MF07-01:CL1-1:PAG07-01 at the standard ratio of 1:2:1 was prepared with TPA added at levels ranging from 1 wt% to 10 wt% of the resist weight. All samples were processed using the same conditions. The film thickness was between 30 nm and 34 nm. The LWR(3σ) and the average line width as a function of line dose are shown in Figures 5.3 (a) and (b). Addition of small amounts of the base provided relatively low LWR. The average LWR at sufficiently low doses was about 3 nm. The lowest LWR was 2.1 nm at 600 pC/cm in the resist with an additional 1 wt% base, as shown in Figure 5.3 (c).

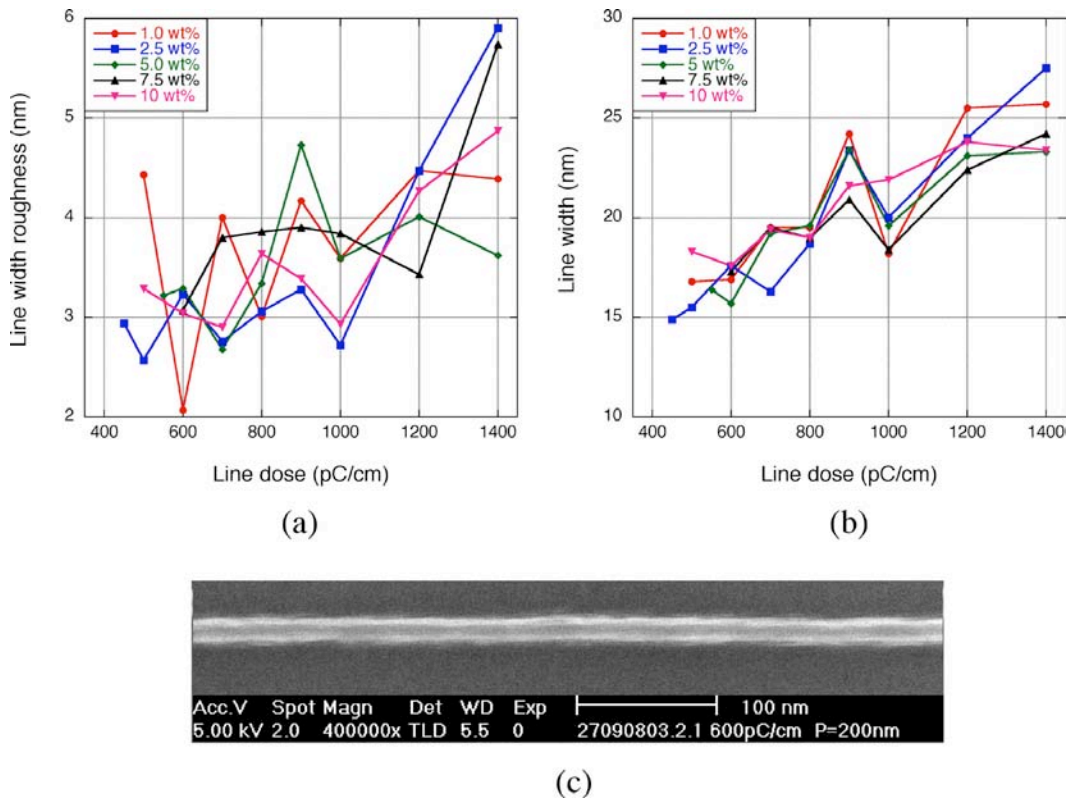


Figure 5.3 (a) LWR(3σ) and (b) line width as a function of exposure dose in the resists with varying base quencher levels ranging from 1 wt% to 10 wt%. (c) The sparse line with 17 nm width and LWR(3σ) of 2.1 nm in the resist with 1 wt% base.

5.1.4 Casting solvent

Some residue of casting solvent remaining in the film, even after PAB, can contribute to acid mobility in the resist, and thus acid diffusion. The LWR was measured for the resist cast with different solvents. Resist MF07-01:CL1-1:PAG07-01 at a 1:2:1 ratio was prepared with chloroform, anisole or PGMEA. Each resist sample received a sufficient PAB temperature and time to remove the residual as much solvent as possible, subject to the condition that the resist film was not degraded upon baking. The resist cast with chloroform received a PAB of 75 °C for 10 minutes. The resist cast with anisole received a PAB of 100 °C for 30 minutes. The resist cast with PGMEA received a PAB of 75 °C for 15 minutes. The other processes were as previously stated. The results are shown in Figures 5.4 (a) and (b). It can be clearly seen in Figure 5.4 (b) that the type of solvent significantly affected the resolution capability of the resist. The resist cast with chloroform shows the smallest line width followed by those cast with PGMEA and anisole successively. The difference between the LWR of the resists cast with each solvent, as shown in Figure 5.4 (a), was less pronounced. The resist cast with chloroform showed the smallest LWR value of about 3 nm at sufficiently low doses, between 200 pC/cm and 300 pC/cm. The LWR in the resist cast with PGMEA was slightly higher than the others.

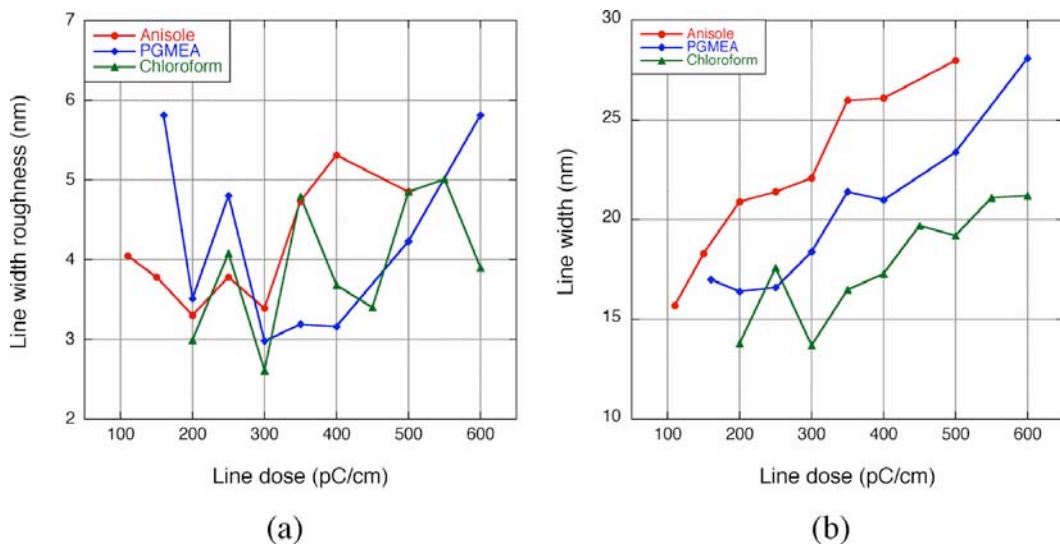


Figure 5.4 (a) LWR(3 σ) and (b) line width as a function of exposure dose in the resists cast with chloroform, anisole or PGMEA.

5.2 Effects of resist processing

The impacts of lithography processes on LWR, including PAB, PEB, and development, were investigated, and results are reported in this section. The sample processing conditions were varied as stated below. Line width and LWR of sparse lines as a function of exposure dose are represented.

5.2.1 Post application bake

The PAB process, which is used to remove the solvent from the resist film, suppresses the effect of residual solvent in the resist film. Resist samples MF07-01:CL1-1:PAG07-01 at a 1:2:1 ratio cast by chloroform received no PAB or a PAB temperature of 75 °C for between 1 and 20 minutes. The other processes were controlled. Film thickness slightly reduced with increasing the PAB time from 39 nm to 35 nm, presumably due to solvent removal. The LWRs as a function of exposure doses are shown in Figure 5.5. The PAB condition had a small effect on LWR. The resist with PAB showed a slightly lower LWR in comparison to that without PAB. The average value of LWR at doses between 600 pC/cm and 1100 pC/cm was below 3 nm in the samples with PAB, whereas it was above 3 nm in that the sample without PAB. The resist with a PAB of 75 °C for 5 minutes gave the lowest LWR of 2.2 nm at 1000 pC/cm.

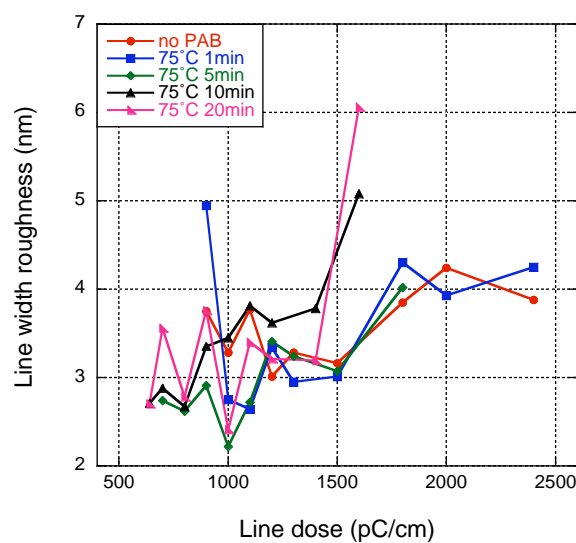


Figure 5.5 LWR(3σ) as a function of exposure dose in the resists which received varying PAB conditions.

5.2.2 Post exposure bake

The impact of the PEB process was examined with the resist MF07-01:CL2-4:PAG07-01 at a 1:2:1 ratio. The samples received a combination of PEB temperatures and times. The other processes were controlled. The PEB temperatures were 75 °C, 90 °C, and 105 °C, whilst the PEB times were 1 minute or 5 minutes. The results are shown in Figure 5.6. The resist which received a PEB of 75 °C for 1 minute had the highest LWR values over the range of line doses examined. It is obvious that increasing either PEB time to 5 minutes or PEB temperature reduced LWR. No significant further change in LWR was achieved when PEB temperature was at least 90 °C or duration was 5 minutes. The lowest LWR was 3.1 nm at 120 pC/cm in the resist with a PEB of 105 °C for 1 minute.

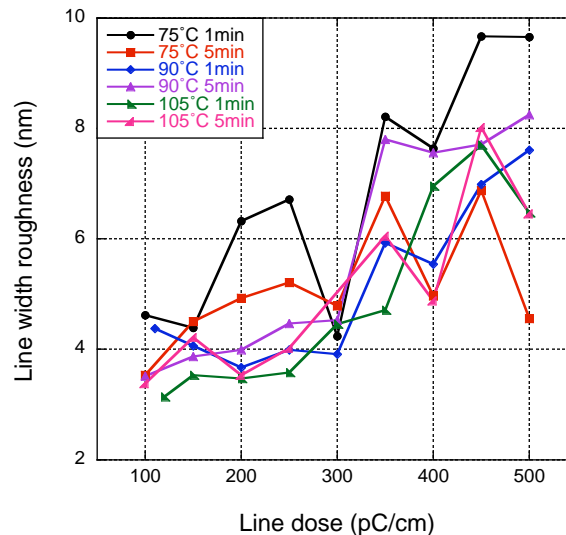


Figure 5.6 LWR(3σ) as a function of exposure dose in the resists which received a variation of PEB temperatures and times.

5.2.3 Development

A number of organic solvent developers were examined for LWR analysis. Resist samples of MF07-01:CL1-1: PAG07-01, at a 1:2:1 ratio and cast using chloroform, were processed under the same PAB and PEB conditions. The resists were exposed and developed with various developer solvents including:

anisole for 10 seconds,

xylene for 10 seconds,
a mixture of anisole:IPA (1:1) by volume for 10 seconds,
a mixture of methyl isobutyl ketone (MIBK):IPA (1:3) by volume for 10 seconds,
a mixture of MCB:IPA (1:1) by volume for 10 seconds,
and MCB for 5 seconds.

A 10-second rinse in IPA followed for all samples. The relationship of line width-dose and LWR-dose are shown in Figures 5.7 (a) and (b). The effect of the developer solvent on line width and LWR was very pronounced. Development in xylene or MIBK:IPA (1:3) showed the worst results with poor resolution and high LWR. The best line width achieved in the resists developed in xylene and MIBK:IPA (1:3) was above 20 nm, whilst the other developers provided the line widths of between 15.5 nm and 16.5 nm at the optimum dose between 600 pC/cm and 800 pC/cm. The resists developed in xylene and MIBK:IPA (1:3) also had high LWR values - about double those found in the samples developed in the other solvents. LWR values lower than 3 nm at the optimum doses were achieved when the sample was developed in anisole, MCB or MCB:IPA (1:1). The smallest LWR of 2.4 nm was found at 1000 pC/cm in the sample developed in anisole, as shown in Figure 5.7 (c).

5.3 Film thickness

The impact of film thickness on LWR was also investigated. The resist samples MF07-01:CL1-1:PAG07-01 at a 1:2:1 ratio were prepared with different film thicknesses ranging from 24 nm to 73 nm. The samples were patterned with sparse lines and processed under the standard conditions. The LWR-dose relationship is shown in Figure 5.8 (a). It was found that that LWR was lower in the thickest resist film. The sample with the 24 nm film thickness showed the highest LWR in which the minimum LWR was 3 nm at 300 pC/cm. The line pattern written in the 62 nm thick sample showed the lowest LWR values of 1.9 nm at a relatively high dose of 1100 pC/cm, as shown in Figure 5.8 (b).

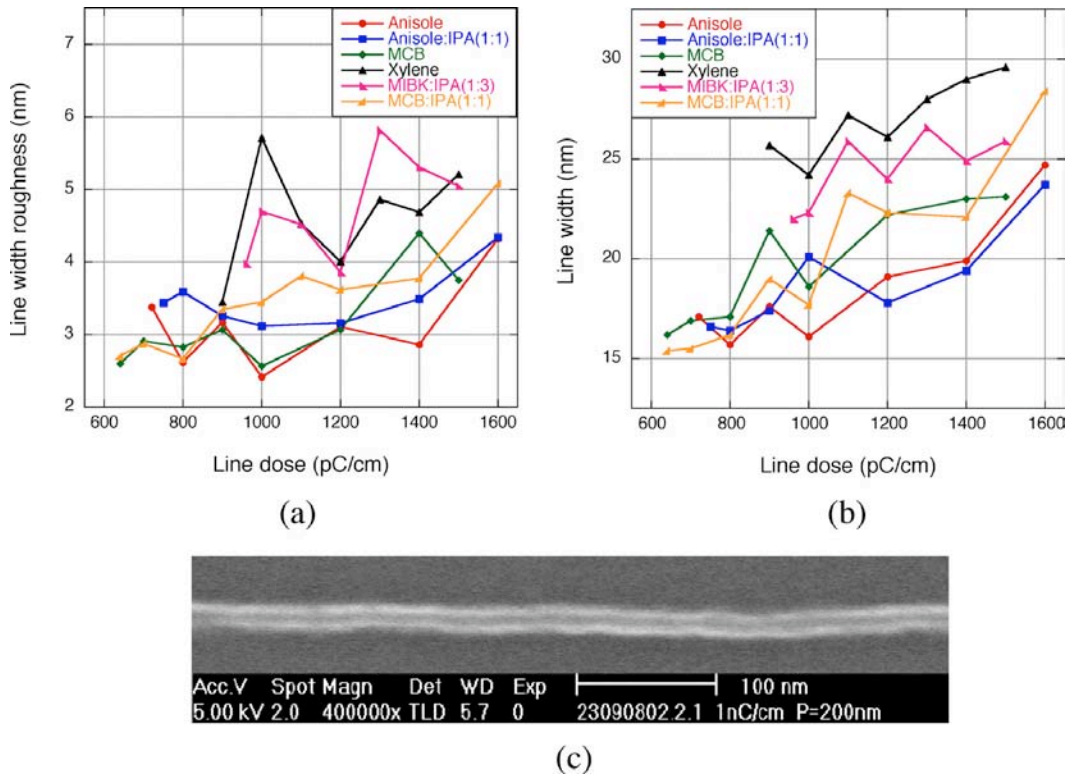


Figure 5.7 (a) LWR(3σ) and (b) line width as a function of exposure dose in the resists processed with different developer solvents. (c) The sparse line with 16 nm width and LWR(3σ) of 2.4 nm in the resist developed in anisole for 10 seconds and rinsed in IPA.

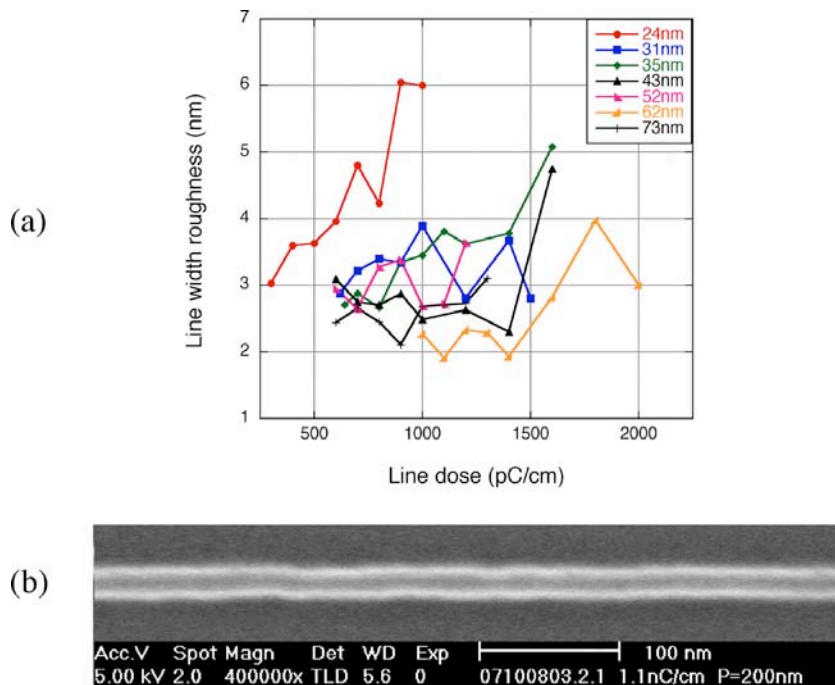


Figure 5.8 (a) LWR(3σ) as a function of exposure dose in the resists with different thicknesses. (b) The sparse line with 21 nm width and LWR(3σ) of 1.9 nm in the 62 nm thick resist.

5.4 Pitch size

The LWR of resist patterns with a range of pitch sizes was measured. The experiment was performed with the resist MF07-01:CL1-1:PAG07-01 at a 1:2:1 ratio. Single pixel lines with pitch sizes of 400 nm, 200 nm, 100 nm, 80 nm, 60 nm and 50 nm were written in the 30 nm thick sample. The line dose was varied from 200 pC/cm to 320 pC/cm. The resist was processed under standard conditions. The results are shown in Figure 5.9. The LWR increased dramatically when the pitch size became smaller than 100 nm, from about 3 nm in the sparse lines to 6 nm or above in 50 nm pitched lines at any dose examined.

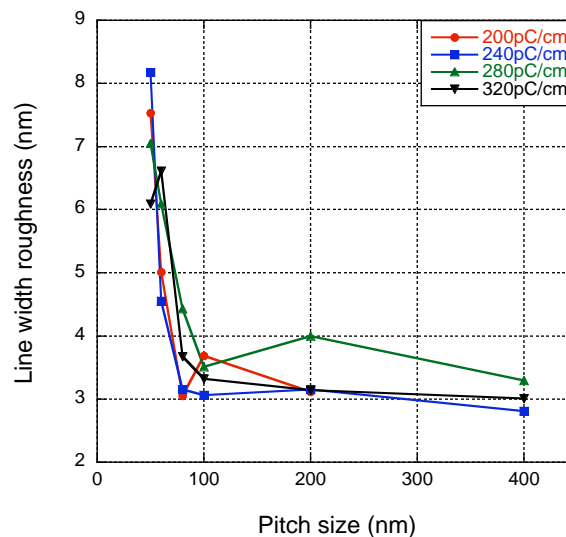


Figure 5.9 LWR(3σ) as a function of pitch size in the resist MF07-01:CL1-1:PAG07-01 (1:2:1).

5.5 Conclusions

LWR analysis for the negative tone chemically amplified fullerene-based molecular resist was undertaken. The impacts of exposure dose, epoxy crosslinker, PAG concentration, casting solvent, PAB, PEB, developer solvent, film thickness, and pitch size on LWR were investigated. The LWR(3σ) of the features as well as the line width generally increased with exposure dose. The smallest feature size and LWR could be achieved simultaneously at a sufficiently low exposure dose. The LWR value of the sparse lines was typically between 3 nm and 4 nm at optimum doses. An LWR

as low as about 2 nm was achieved in some circumstances. The reduction of LWR was also achieved by selecting different materials and the optimisation of processes such as formulation of the resist with the low molecular weight crosslinker, optimising PAG levels, the additional of a small amount of base quencher, the application of sufficient PAB and PEB and processing with appropriate solvents. However, LWR increased in dense features and in thin films. The best resist processing conditions for LWR reduction in the negative-tone, chemically amplified, fullerene based resist are summarised in Table 5.1, where film thickness and feature density is controlled.

Table 5.1 The best resist processing conditions for LWR reduction at equal film thickness and feature density.

Resist formulation	
Fullerene derivative	MF07-01
Crosslinker	Epoxy novolac resin CL1-1
PAG	PAG07-01
Base additive	Tripropylamine (TPA)
Fullerene weight ratio (parts)	1
Crosslinker weight ratio (parts)	2
PAG weight ratio (parts)	1 to 1.25
Base additive level (%wt)	1.0 (at PAG level of 25 wt%)
Casting solvent	Chloroform
Processing conditions	
PAB temperature	Nearly independent
PAB time	Nearly independent
PEB temperature	≥ 90 °C
PEB time	≥ 1 minute
Developer	Anisole
Development time	10 seconds
Rinse	No

Chapter 6

Plasma Etching for High Resolution Pattern Transfer

This chapter presents a systematic study of the reactive ion etching (RIE) of chemically amplified negative-tone fullerene-based molecular resist for high resolution and aspect ratio silicon nanostructure. The transfer of high-resolution resist patterns to silicon substrates using inductively coupled plasma (ICP) etching is reported. The effects of process parameters such as gas flow rate, gas pressure, ICP power, and radio frequency (RF) power on the pattern transfer process were investigated to optimise the etch rate, selectivity to the resist, and anisotropy of the etched structure.

6.1 Experimental setup

All etching experiments were performed using the Plasma Pro ICP system equipped with an ICP65 source from Oxford Instruments. The etcher system was described in section 2.1.3. The etching and passivation gases used were SF_6 and C_4F_8 respectively. Negative tone resist MF07-01:epoxy:PAG07-01 samples with a film thickness of 30 to 35 nm were prepared using the standard process. A slight variation in the resist formulations and resist processing was allowed as it was found in previous studies that the resist composition ratios and baking conditions had little impact on the etch resistance of the MF07-01-based resist [109]. Micro- and nanoscale resist patterns were written in the samples using electron beam lithography.

The samples were continuously etched under a mixed $\text{SF}_6/\text{C}_4\text{F}_8$ gas plasma process. Variations in the film thickness and silicon etch depth were measured before and after etching. In this way, the plasma etch rate of silicon and the etch selectivity of silicon to resist were calculated. Variations in the

process parameters such as gas flow rate, gas pressure, ICP power and RF power were examined to investigate their effect on the silicon etch rate, selectivity to resist and anisotropy.

6.2 Effects of etching gas flow rate

Figure 6.1 shows the etch rate of silicon and the etch selectivity to the resist at SF₆ flow rates varying between 15 and 35 sccm, whilst the C₄F₈ flow rate was fixed at 30 sccm. The samples were etched for 20 seconds with an RF/ICP power of 20/220 W, a pressure of 15 mT and a temperature of 20 °C. It can be seen that the etch rate increased with an increase in SF₆ flow rate, from 1 nm/s at 15 sccm up to 6.8 nm/s at 35 sccm. An increase in selectivity up to 6.2 at this flow rate was also observed. The increase in the gas flow rate resulted in an increase in the etching ion flux impinging on the sample, thus enhancing the silicon etch rate. The anisotropy of the structure was achieved by varying the SF₆ flow rate.

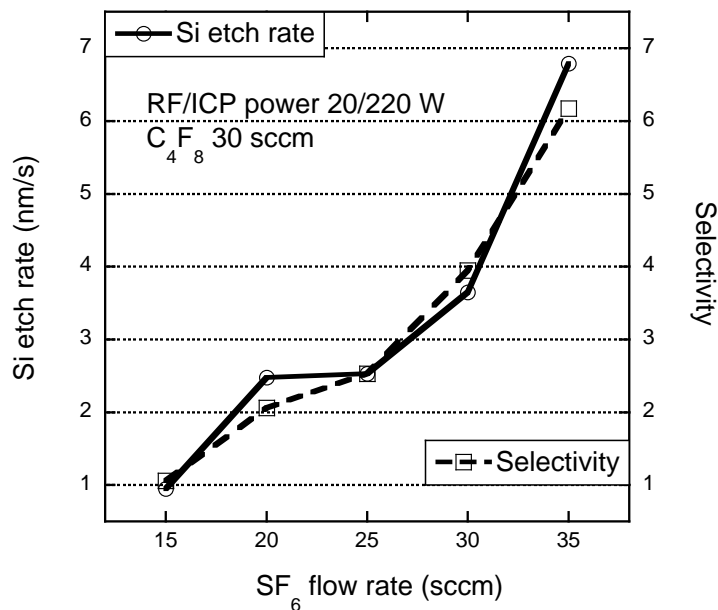


Figure 6.1 Effect of SF₆ flow rate on the etch rate of silicon and the selectivity to the resist. All samples were etched for 20 seconds with 30 sccm C₄F₈ flow, 20/220 W RF/ICP power and 15 mT at 20 °C.

The effect of the etching gas flow rate on the anisotropy is shown in Figure 6.2. The samples were etched for 20 seconds at an SF₆ gas flow between 25 and 35 sccm whilst other parameters were controlled. It can be seen that the sidewall angle changed as the gas flow rate varied, and that good anisotropy was achieved at the SF₆ flow rate of 25 sccm under these etching conditions. At the higher flow rates, the lateral etching rate became considerable, causing undercutting of the features.

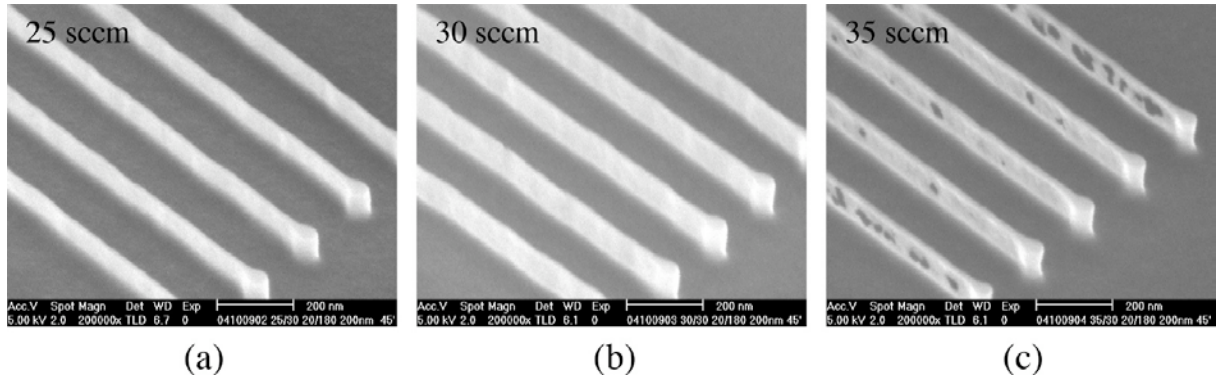


Figure 6.2 Effect of the SF₆ flow rate on the anisotropy of the silicon structure. The SF₆ flow rate was (a) 25 sccm, (b) 30 sccm, and (c) 35 sccm. All samples were etched for 20 seconds with 30 sccm C₄F₈ flow, 20/180 W RF/ICP power and 15 mT at 20 °C. Residual resist was removed by O₂ plasma ashing.

6.3 Effects of gas pressure

Figure 6.3 shows the etch rate of silicon and the selectivity to the resist as the pressure of the process gases varied between 15 and 35 mT. The samples were etched for 20 seconds with an SF₆/C₄F₈ flow of 20/30 sccm and an RF/ICP power of 20/220 W, at a temperature of 20 °C. It can be seen that both the etch rate and the selectivity decreased with an increase in process pressure, reaching the minimum at 30 mT, with an etch rate was only 1 nm/s and selectivity of 1.6. The increase in pressure resulted in an increase in the density of the plasma species, thus increasing the plasma activity. In a mixed gas process, the etching and passivation processes are competitive. The reduction in etch rate and selectivity implies that passivation of the silicon surface is the dominant process at high pressure. In spite of these disadvantages, applying high pressure can help to suppress the aspect-ratio-dependent etching (ARDE) which leads to lower etching rate in denser feature. Etching at high pressure also led to the suppression of the transfer of resist footing features into the silicon structure, as illustrated in

Figures 6.4 (a) and (b). At the pressure of 15 mT the resist footing was transferred to the silicon, Figure 6.4 (a), whilst the footing feature was clearly suppressed at high pressure of 30 mT, Figure 6.4 (b).

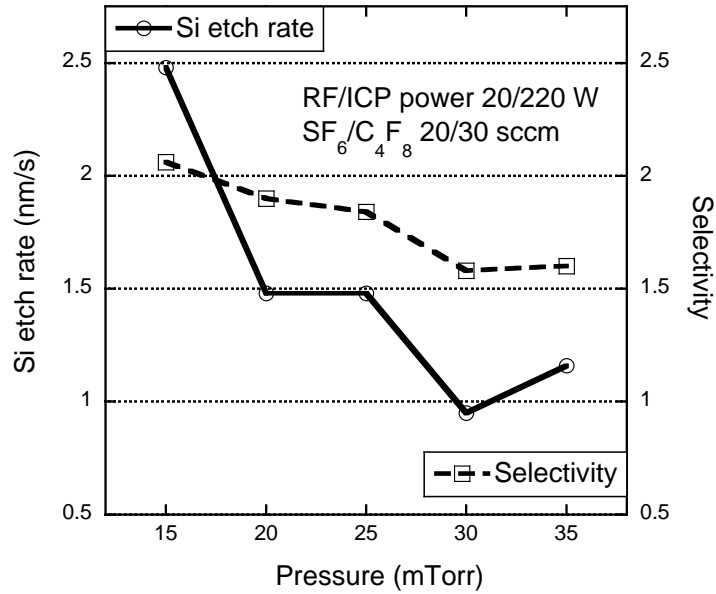


Figure 6.3 Effect of pressure on the etch rate of silicon and the selectivity to the resist. All samples were etched for 20 seconds with 20/30 sccm SF₆/C₄F₈ flow and 20/220 W RF/ICP power at 20 °C.

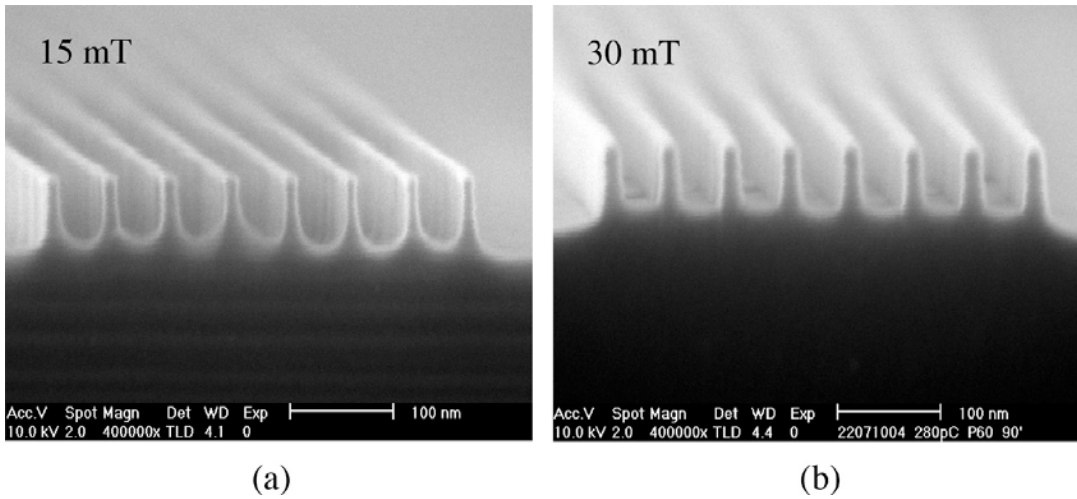


Figure 6.4 Comparison of footing features in 60-nm pitch silicon structure in samples etched at (a) 15 mT and (b) 30 mT, with 25/30 sccm SF₆/C₄F₈ flow and 20/220 W RF/ICP at 20 °C for 20 seconds. Residual resist was removed by O₂ plasma ashing.

6.4 Effects of ICP power

Figure 6.4 shows the etch rate of silicon and the selectivity to the resist as the ICP power is varied between 120 and 220 W. The samples were etched for 20 seconds with an SF₆/C₄F₈ flow of 25/30 sccm, RF power of 20 W, pressure of 15 mT, and a temperature of 20 °C. It can be seen that the etch rate initially rose with an increase in ICP power. The maximum etch rate of 7.3 nm/s was observed at 160 W. Increasing the ICP power beyond this point resulted in a drop in the etch rate. The same trend was also found in the relation between selectivity and ICP power. The maximum selectivity of 6 was found at 180 W. The increase in the ICP power promotes the ionisation of gases, and increases the plasma density. The resonance of the etch rate and the selectivity at intermediate ICP powers indicates the domination of the silicon etching process over passivation. However the undercutting of features was not found in this range of ICP powers under the conditions described, as shown in Figure 6.5. Applying too high ICP power leads to roughening the top surfaces of the silicon structures in addition to the disadvantage of lowering the etch rate and the selectivity. Figure 6.6 illustrates the damage to a silicon structure in a sample etched with an ICP power of 260 W and a relatively low SF₆ flow of 20 sccm, whilst other parameters were as described above.

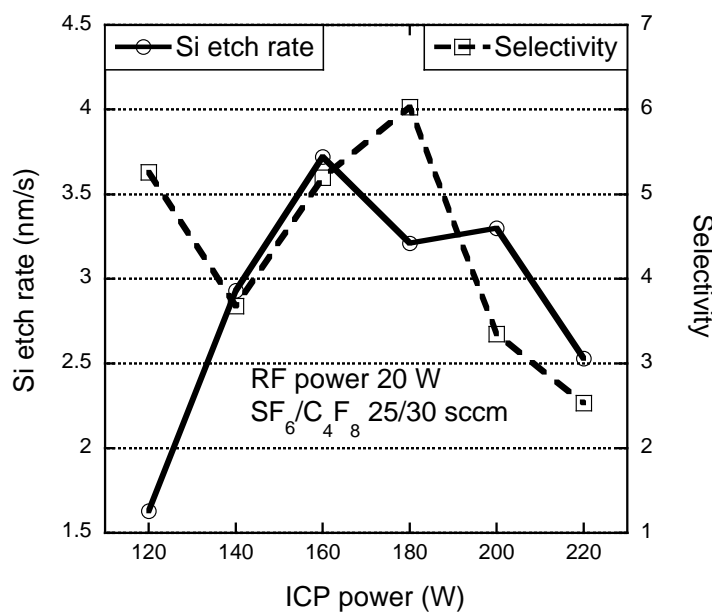


Figure 6.4 Effect of ICP power on the etch rate of silicon and the selectivity to the resist. All samples were etched for 20 seconds with 25/30 sccm SF₆/C₄F₈ flow, 20 W RF power and 15 mT at 20 °C.

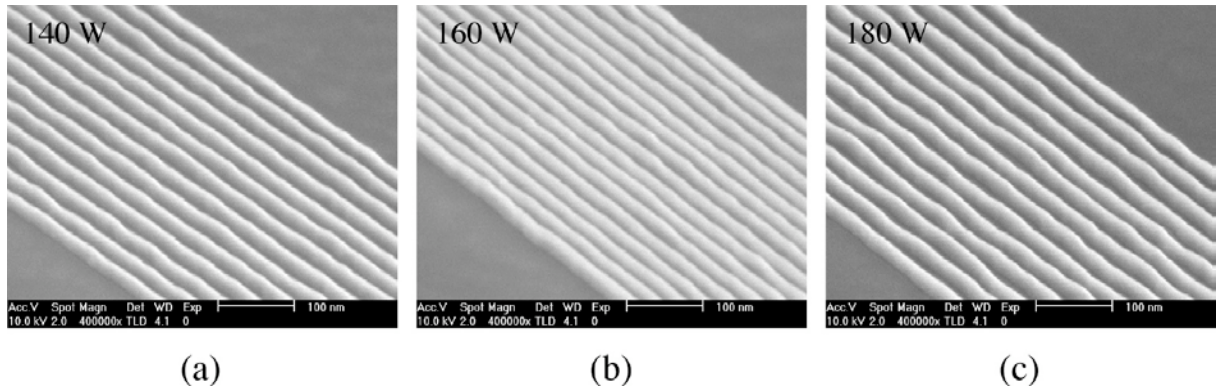


Figure 6.5 Dense silicon structures in samples processed with an ICP power of (a) 140 W, (b) 160 W, and (c) 180 W. All samples were etched for 20 seconds with 25/30 sccm $\text{SF}_6/\text{C}_4\text{F}_8$ flow, 20 W RF power and 15 mT at 20 °C. Residual resist was removed by O_2 plasma ashing.

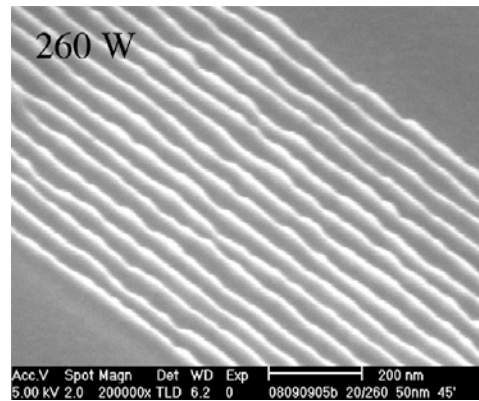


Figure 6.6 Damage of dense silicon structure when etched at high ICP power of 260 W. The process conditions were 20/30 sccm C_4F_8 flow, 20 W RF power, 15 mT, 20 °C, and 20 seconds of etching. Residual resist was removed by O_2 plasma ashing.

6.5 Effects of RF power

Figure 6.7 shows the etch rate of silicon and the selectivity to the resist as RF power was varied from 20 to 45 W. The samples were etched for 20 seconds with an $\text{SF}_6/\text{C}_4\text{F}_8$ flow of 25/30 sccm, ICP power of 180 W and a pressure of 15 mT, at 20 °C. It can be seen that the etch rate of silicon increased with RF power before levelling off at about 5.6 nm/s with an RF of 40–45 W. A slight change in selectivity between 2.6 and 3.3 was observed over the range of power examined. The RF power contributes to the energy of the ions bombarding the sample. Increasing the RF power results in an increase in sputtering rate and anisotropy. However, applying an RF power of more than 20 W under the conditions given above showed no improvement in anisotropy. Positively sloped sidewalls were found at a wide range

of RF powers, as illustrated in Figure 6.8. In addition, sidewall roughness and surface roughness were clearly observed in the samples processed at an RF power above 30 W.

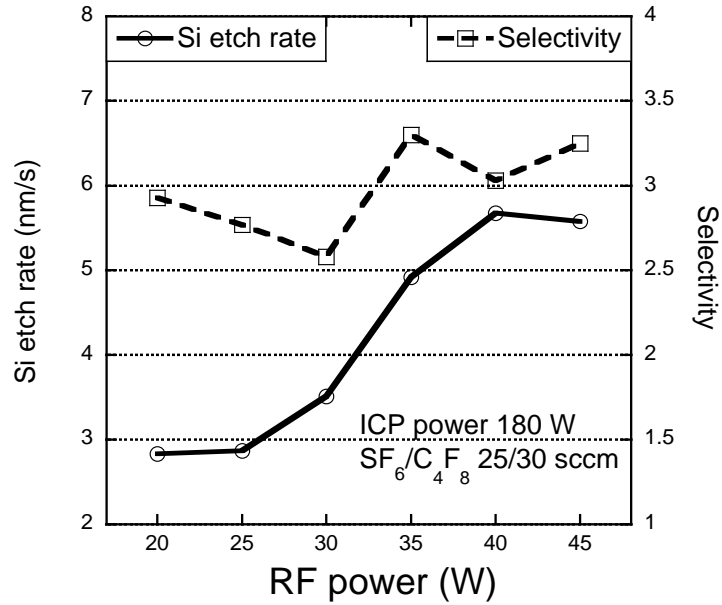


Figure 6.7 Effect of RF power on the etch rate of silicon and selectivity to resist. All samples were etched for 20 seconds with 25/30 sccm SF₆/C₄F₈ flow, 180 W ICP power and 15 mT at 20 °C.

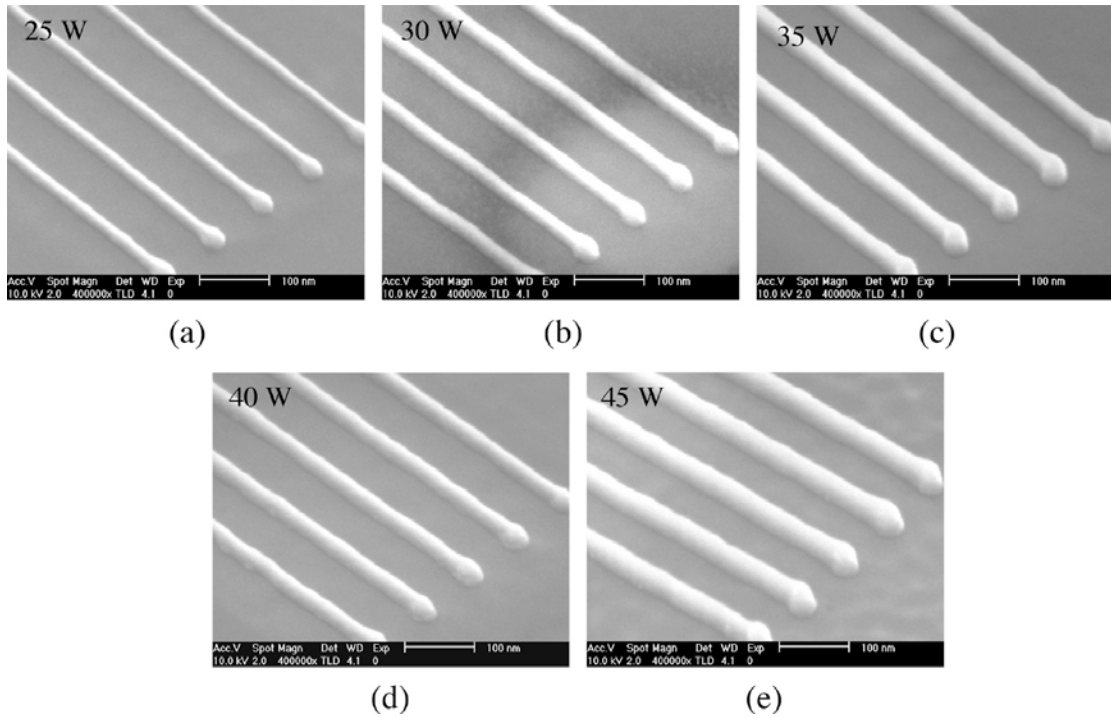


Figure 6.8 Etched silicon structures in the samples processed with RF power of (a) 25 W, (b) 30 W, (c) 35 W, (d) 40 W, and (e) 45 W.

6.5 Conclusions

The transfer of a high-resolution resist patterns to a silicon substrates using plasma etching was described and demonstrated. The etch rate of silicon and selectivity to the negative-tone fullerene-based resist were characterized under a mixed SF₆/C₄F₈ etching process with varying etching parameters including gas flow rate, pressure, ICP and RF power. The etch rate increased with an increase in SF₆ flow rate and RF power, a decrease in pressure and at intermediate ICP power. The selectivity of the resist changed in the same way as the silicon etch rate. It was strongly dependent on the SF₆ flow rate and ICP power. The anisotropy and sidewall profile could be carefully controlled via all etching parameters. The anisotropic etching of a 20-nm-wide silicon structures with the maximum selectivity of 6 was demonstrated, using the etching conditions summarised in Table 6.1.

Table 6.1 Mixed SF₆/C₄F₈ etching conditions for silicon giving anisotropic pattern transfer to silicon with high etch sensitivity to resist.

SF ₆ flow rate (sccm)	25
C ₄ F ₈ flow rate (sccm)	30
Pressure (mT)	15
ICP power (W)	180
RF (electrode) power (W)	20
Temperature (°C)	20

Chapter 7

Positive Tone Chemically Amplified Fullerene Based Molecular Resists

This chapter describes the development and characterization of positive tone chemically amplified fullerene based molecular resist for electron beam lithography. A fullerene derivative was designed so as to allow chemical amplification via a deprotection scheme to work as highly sensitive positive tone resists. Various resist formulations and the effects of additives such as a base quencher and a dissolution inhibitor are presented. Evaluation of the lithographic performances including sensitivity, resolution capability, dissolution characteristics in an aqueous base solution and etch resistance is presented.

7.1 Resist Preparation

The resist materials used in this study consisted of fullerene derivatives, photoacid generators (PAG) and additive compounds. The chemical structures are shown in Figure 7.1. The five fullerene derivatives studied in this work were supplied from the Nanoscale Chemistry Research Group, University of Birmingham. These compounds were methanofullerenes with polyether addends protected by an acid-labile group. The derivative MF-THP was a mixture of multiple adduct methanofullerenes protected by a tetrahydropyran (THP) group, Figure 7.1 (a). The other derivatives were monodispersed compounds. They were multiple adduct methanofullerenes protected by a *tert*-butylacetylcarbonyl (*t*BAC) group, Figure 7.1 (b). MF-*t*BAC(1), MF-*t*BAC(2), MF-*t*BAC(3) and MF-*t*BAC(6) derivatives were mono, di, tri, and hexa adduct derivatives, respectively.

The PAGs and other additive compounds were commercially available (Sigma Aldrich), Figures 7.1 (c)-(g). The PAGs used in the study were PAG07-01 (UVI-9676, Dow), a mixture of

triarylsulfonium hexafluoroantimonate salts, PAG03-01, triphenylsulfonium triflate, and PAG03-02, diphenyliodonium triflate. The selected base additive was BA-3. PAG04-04, tris(4-*tert*-butylphenyl) sulfonium perfluoro-1-butanesulfonate, a compound typically used as a photoacid generator, was used here as a dissolution inhibitor.

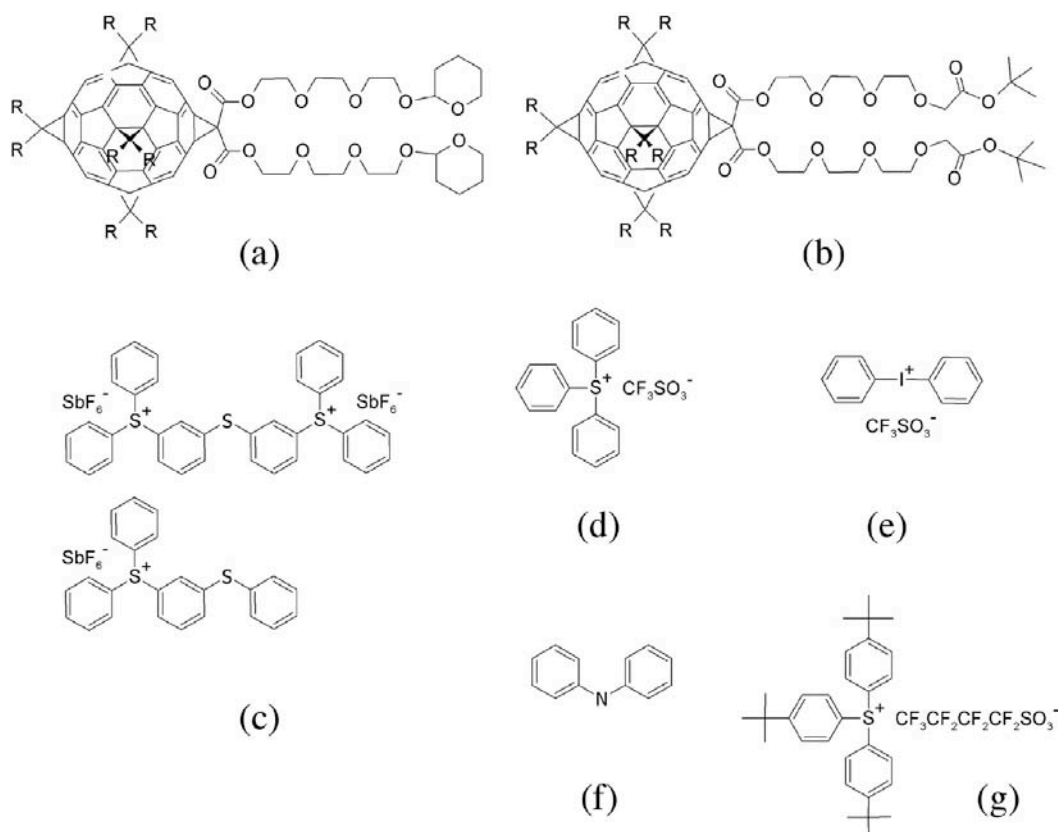


Figure 7.1 Resist materials for the positive tone molecular resists (a) MF-THP, (b) MF-*t*BAC, (c) PAG07-01, (d) PAG03-01, (e) PAG03-02, (f) BA-3, and (g) PAG04-04.

The resists were formulated as positive tone resists. The fullerene derivatives were chemically amplified via an acid-catalysed deprotection scheme by blending the pure material with a PAG at an appropriate weight ratio. The lipophilic protecting groups, THP and *t*BAC functional groups, in principle, make the fullerene derivatives insoluble in an aqueous base solution. Upon irradiation and baking at an elevated temperature, the cleavage of the acid-labile group is initiated causing a polarity change of the derivative so that it becomes soluble in a basic solution. A base quencher was added to

the resist formulation to limit acid diffusion. An optional dissolution inhibitor was used to promote greater solubility difference between exposed and unexposed areas.

Resists were prepared in the following organic solvents: chloroform, PGMEA, Ethyl lactate, 2-heptanone, anisole, and cyclohexanone. Chemically amplified (CA) resist solutions were mainly prepared in PGMEA, unless stated otherwise. A mixture of solvents was occasionally used to increase solubility of a PAG. Spin-coated resist films were prepared to have thickness between 30 nm and 60 nm. PAB was applied unless film degradation was observed upon baking as noted. However a problem was found with PEB process, therefore it was eliminated, as described in section 7.3. The resist samples were developed in an aqueous solution of tetramethyl ammoniumhydroxide (TMAH) at concentrations of 0.26 N or less, or in pure water.

7.2 MF-THP-based resists

The MF-THP derivative dissolved readily in chloroform or PGMEA. Spin-coated films of pure material on hydrogenated silicon were rough. Adding PAG07-01 to the MF-THP resist did not improve the film quality. A positive image was achieved when the CA MF-THP resist was exposed to electrons at moderate doses, whereas a negative image was evidenced at high doses. It was also found that unexposed CA MF-THP film was removed too quickly when developed in 0.26 N TMAH solution, giving poor contrast between the exposed and unexposed areas, and hence a poor resolution capability. As a result, characterisation of the MF-THP-based resists was not continued.

7.3 MF-*t*BAC-based resists

Most spin-coated films of the MF-*t*BAC-based resists were smooth, but with some crystallisation apparent. It was not possible to achieve a uniform resist film with the tri-adduct MF-*t*BAC(3) and this material was rejected from further experiments. The PAB process can be applied to the hexa-adduct MF-*t*BAC(6) resist films, but it caused pinholes and degradation in other resists. The PEB process was found to be incompatible with the CA MF-*t*BAC resists and therefore it was not applied to most of the

samples. PEB caused large-scale defects in exposed patterns independent of PAG type, as shown in Figure 7.2. A dose to clear was found at a range of TMAH concentrations. It was found that developer strength affected the resist in many aspects. The developer strength and development time were adjusted for each resist formulation and are reported in the following sections.

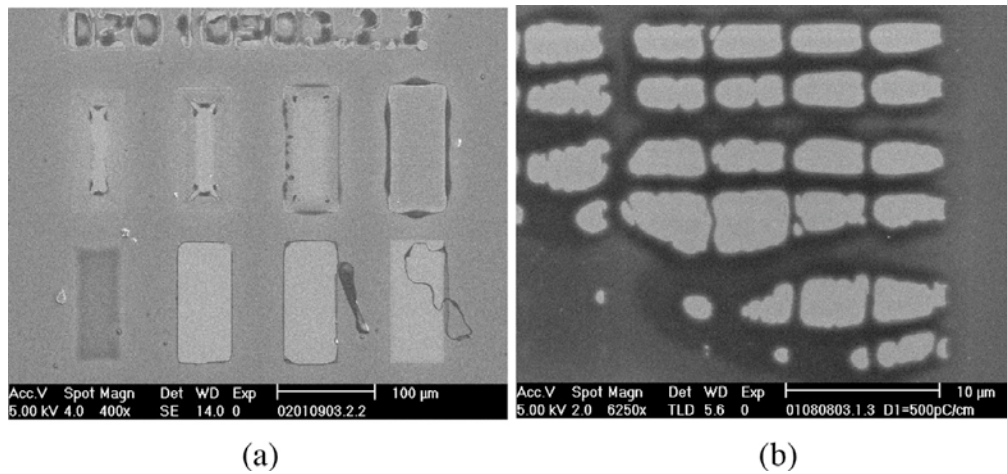


Figure 7.2 Defects in the resist MF-*t*BAC(6):PAG07-01 (50:50 wt%) processed with (a) PAB at 90 °C for 60 seconds, PEB of 105 °C for 90 seconds, and development in 0.026 N TMAH for 10 seconds followed by a rinse in DI water. (b) No PAB, PEB of 90 °C for 180 seconds, and development in 0.26 N TMAH for 10 seconds followed by a rinse in DI water.

7.3.1 Sensitivity

Two-component chemically amplified resists based on MF-*t*BAC(1), MF-*t*BAC(2), or MF-*t*BAC(6) were prepared by adding various PAGs and the optional additives. The response of the resists to electron irradiation was measured at a beam energy of 20 keV following the method described in section 2.3.1.

7.3.1.1 CA MF-*t*BAC(1) resists

The response curves of the CA MF-*t*BAC(1):PAG07-01 resists with varying PAG levels between 50 wt% and 67 wt% are shown in Figure 7.3. The resists were not subjected to baking processes. They were developed in 0.26 N TMAH for 60 seconds and rinsed in DI water. It was found that the exposed resists were relatively insoluble in the developer and that a dose to clear was not achieved in a positive tone region. At high doses above 100 $\mu\text{C}/\text{cm}^2$, the resists acted as negative tone resists.

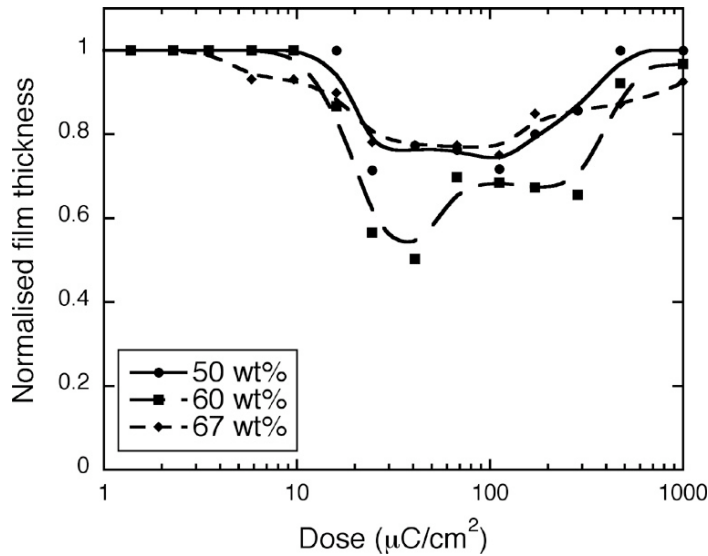


Figure 7.3 Response curves of the CA MF-*t*BAC(1):PAG07-01 resist with PAG loadings of 50 wt%, 60 wt%, and 67 wt%. No clearing dose was found.

7.3.1.2 CA MF-*t*BAC(2) resists

Response curves of the CA MF-*t*BAC(2) resists with added PAG07-01, PAG03-01, and PAG03-02 are shown in Figures 7.4 (a)-(c), respectively. Figure 7.4 (a) shows the response curves of the CA MF-*t*BAC(2):PAG07-01 resists containing 44 wt%, 50 wt%, and 60 wt% PAG. The resists did not receive any baking process. They were developed in 0.26 N TMAH for 10 s and rinsed in DI water. An increase in resist sensitivity together with a reduction in the contrast was observed as the PAG levels increased. The sensitivities were $136 \mu\text{C}/\text{cm}^2$, $114 \mu\text{C}/\text{cm}^2$ and $123 \mu\text{C}/\text{cm}^2$, with contrasts of 2.5, 1.8 and 1.3 at PAG07-01 loadings of 44 wt%, 50 wt%, and 60 wt%, respectively. The sensitivity could not be improved further below $100 \mu\text{C}/\text{cm}^2$ by increasing more PAG.

Figure 7.4 (b) shows the response curves of CA MF-*t*BAC(2):PAG03-01 resists containing 10 wt%, 20 wt%, and 33 wt% of PAG. The resists were cast with anisole, and did not receive baking. The samples were developed in a diluted TMAH at 0.026 N for 5 s and rinsed in DI water. It can be seen that the sensitivity dramatically increased from $78 \mu\text{C}/\text{cm}^2$ to $21 \mu\text{C}/\text{cm}^2$ and $11.2 \mu\text{C}/\text{cm}^2$ as the PAG loading increased from 10 wt% to 20 wt% and 33 wt%, respectively. A slight decrease in the contrast from 2.9 down to 2.5 at 33 wt% PAG was also observed.

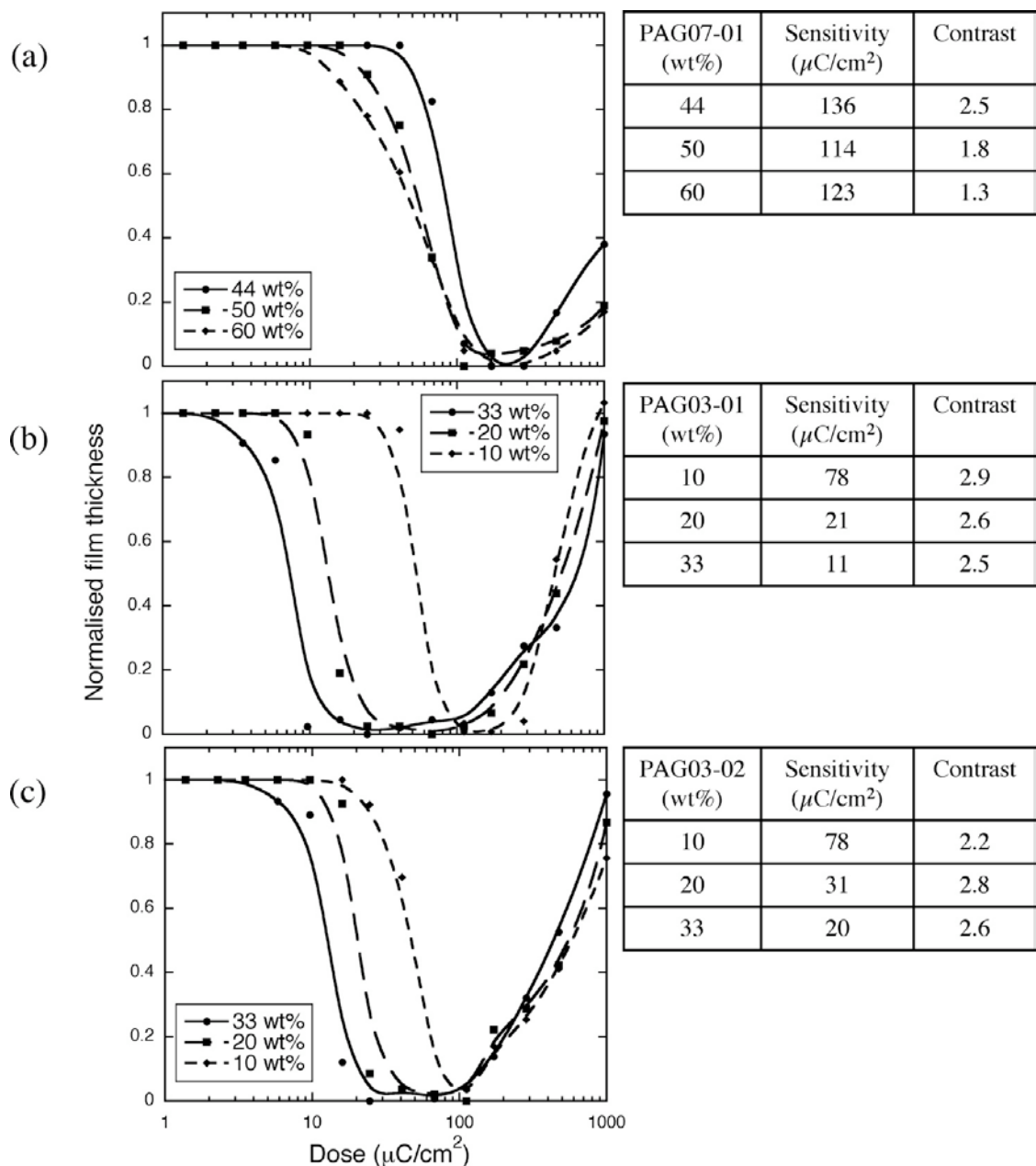


Figure 7.4 Response curves of (a) CA MF-*t*BAC(2):PAG07-01 resist with PAG loadings of 44 wt%, 50 wt%, and 60 wt%, (b) CA MF-*t*BAC(2):PAG03-01 resist and (c) CA MF-*t*BAC(2):PAG03-02 resist with PAG loadings of 10 wt%, 20 wt%, and 33 wt%.

Response curves of CA MF-*t*BAC(2):PAG03-02 resists containing 10 wt%, 20 wt%, and 33 wt% of PAG are shown in Figure 7.4 (c). The resists were cast with a mixture of anisole and cyclohexanone. The samples received no PAB and PEB, and were developed in 0.026 N TMAH for 5

s and rinsed in DI water. The sensitivity of these resists increased from 78 $\mu\text{C}/\text{cm}^2$ to 31 $\mu\text{C}/\text{cm}^2$ and 20 $\mu\text{C}/\text{cm}^2$ with a slight improvement in the contrast from 2.2 to 2.8 and then 2.6 as the PAG03-02 levels increased from 10 wt% to 20 wt% and 33 wt%, respectively.

It can be clearly seen that the resists exhibited dual tone behaviour. They had a positive tone at intermediate doses and a negative tone at higher doses. A negative tone behaviour of the CA MF-*t*BAC(2) resists was observed at onset doses of approximately 100-300 $\mu\text{C}/\text{cm}^2$ depending on the type of PAG added to the resist.

7.3.1.3 CA MF-*t*BAC(6) resists

Response curves of the chemically amplified MF-*t*BAC(6):PAG07-01 resist are shown in Figure 7.5. The resist samples were MF-*t*BAC(6):PAG07-01 at the PAG loading of 38 wt%, 44 wt%, 50 wt%, and 55 wt%. The samples received PAB of 100 °C for 30 minutes. The PEB process was not applied for all samples. The development was in DI water for 10 seconds. The CA MF-*t*BAC(6) resists showed a higher sensitivity than the CA MF-*t*BAC(2) resists at the same loading level of PAG07-01. The resist sensitivity was 141 $\mu\text{C}/\text{cm}^2$ with a contrast of 2 at 38 wt% PAG loading. Increasing PAG levels to 55 wt%, the sensitivity of the resist also increased to 70 $\mu\text{C}/\text{cm}^2$, and the contrast decreased to 1.6. The PAB process was found to be important for enhancing the sensitivity of the resist. The sensitivity of the resist MF-*t*BAC(6):PAG07-01 (50:50 wt%) was 80 $\mu\text{C}/\text{cm}^2$ with PAB of 100 °C for 30 minutes and 155 $\mu\text{C}/\text{cm}^2$ without PAB. The sensitivity was also improved by developing in a diluted TMAH solution. The sensitivity of the resist MF-*t*BAC(6):PAG07-01 (50:50 wt%) improved to 49 $\mu\text{C}/\text{cm}^2$ with development in 0.026 N TMAH for 10 seconds, followed by a quick rinse with DI water. However the development in TMAH was found to be too aggressive for high resolution patterning in this resist system, giving a poor resolution as described in section 7.3.2.

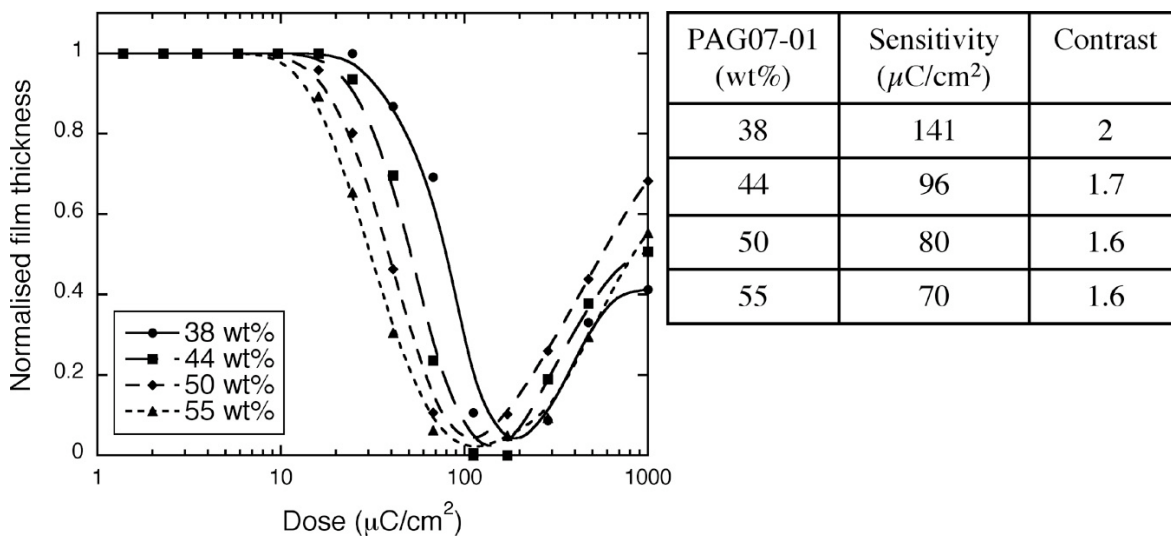


Figure 7.5 Response curves of CA MF-*t*BAC(6):PAG07-01 resist with PAG loadings of 38 wt%, 44 wt%, 50 wt%, and 55 wt%.

The effect of a base additive to resist sensitivity was examined using the amine base BA-3. The base was added to the MF-*t*BAC(6):PAG07-01 (50:50 wt%) at 1 wt%, 2 wt%, and 4 wt% to the total resist weight. A PAB of 100 °C for 30 minutes was applied. All samples were exposed and developed in DI water for 10 seconds without receiving PEB. The response curves are shown in Figure 7.6. Addition of the base BA-3 caused a slight decrease in resist sensitivity but little increase in contrast. The sensitivity decreased from 80 $\mu\text{C}/\text{cm}^2$ in the resist without the base to 78 $\mu\text{C}/\text{cm}^2$, 81 $\mu\text{C}/\text{cm}^2$ and 90 $\mu\text{C}/\text{cm}^2$ with 1 wt%, 2 wt% and 4 wt% added base, respectively. The contrast was found to increase from 1.6 to 1.7.

The effect of a dissolution inhibitor on resist sensitivity was also examined. The additive PAG04-04 is a multiple functioning PAG. It acts as a dissolution inhibitor in an aqueous base solution due to the integration of the *tert*-butylphenyl functional group to the triphenyl sulfonium molecule. Samples were prepared by adding one part of a mixture of PAG07-01 and PAG04-04 to one part of the fullerene MF-*t*BAC(6) by weight. The proportions of PAG04-04 in the resist varied from 2.5 wt% to 25 wt%. The samples were baked, exposed and developed in DI water for 10 seconds. The response curves are shown in Figure 7.7. A slight increase in both sensitivity and contrast with more PAG04-04

were clearly seen. The sensitivity increased from $78 \mu\text{C}/\text{cm}^2$ at 2.5 wt% of the additive to $51 \mu\text{C}/\text{cm}^2$ at 25 wt% of the additive. The maximum contrast of 1.9 was found additive loadings above 12.5 wt%.

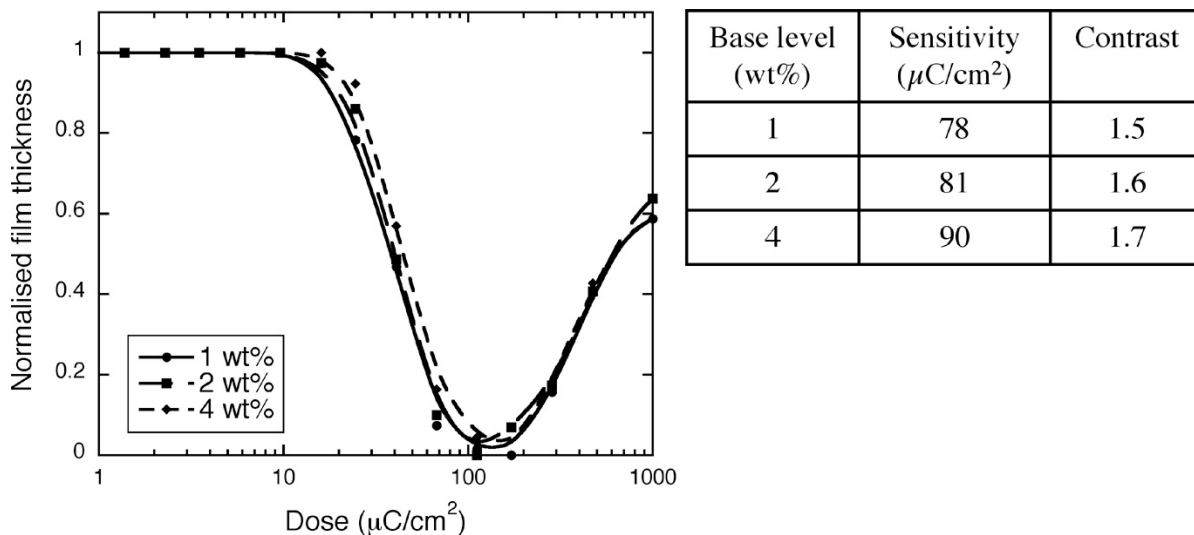


Figure 7.6 Response curves of CA MF-*t*BAC(6):PAG07-01 (50:50 wt%) resist with the addition of BA-3 at 1 wt%, 2 wt% and, 4 wt%.

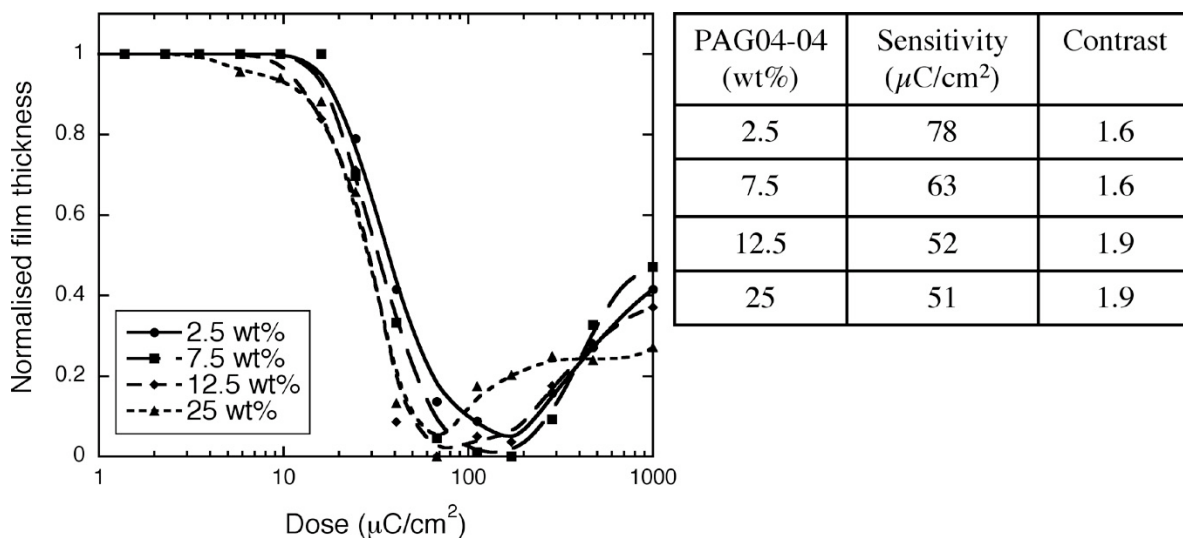


Figure 7.7 Response curves of CA MF-*t*BAC(6):PAG07-01:PAG04-04 containing 50 wt% of PAG; the amount of PAG04-04 was varied from 2.5 wt% to 25 wt%.

7.3.2 Resolution

The high resolution capability of the MF-*t*BAC-based resist system was evaluated using a 30 keV electron beam. The non-chemically amplified fullerene derivative MF-*t*BAC acts as a high resolution

negative tone resist when exposed to electrons at a very high dose. Figure 7.8 shows a semi-dense line space pattern, 30 nm lines at 40 nm half pitch, written in the pure MF-*t*BAC(6) resist with a line dose of 11 nC/cm. The resist was cast with chloroform and developed in MCB:IPA (1:1) for 10 s.

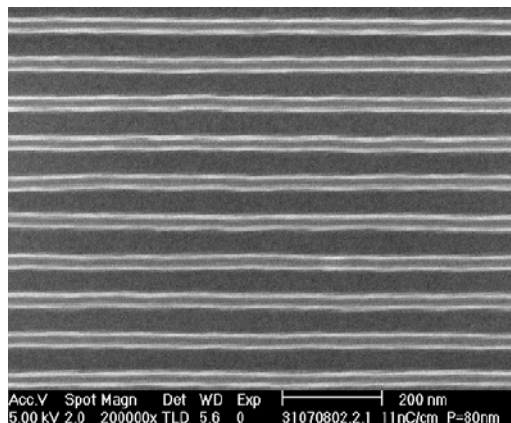


Figure 7.8 The 40 nm half-pitch line space pattern written in the MF-*t*BAC(6) film using a 30 keV electron beam. The PAB and PEB processes were not applied. Development was in MCB:IPA (1:1) for 10 seconds followed by a rinse in IPA.

Chemically amplified MF-*t*BAC resists acted as a positive tone resist at relatively low doses. An evaluation of the resolution was performed for the MF-*t*BAC(2) and MF-*t*BAC(6)-based resist systems as only these resists could be fully clear with aqueous base development. The PEB process caused defects in the resist, as mentioned above. Therefore, all samples in the experiments for the evaluation of resolution were processed without PEB.

7.3.2.1 CA MF-*t*BAC(2) resists

Although a positive image was achievable in the CA MF-*t*BAC(2) resist using 0.26 N TMAH as the developer, this solution was found to be too aggressive for high resolution patterning. Patterns with a sub-micron feature sizes could not be produced successfully when developed in the 0.26 N TMAH solution. A diluted TMAH solution at a 0.026 N concentration was found to be suitable for high resolution patterning in the CA MF-*t*BAC(2) resists. A comparison of the resolution for samples developed in TMAH solution with different base strengths is shown in Figure 7.9. Line-space patterns with 100 nm half pitch were produced in the CA resist MF-*t*BAC(2):PAG07-01 (50:50 wt%)

processed without PAB and PEB. It can be seen that development in 0.26 N TMAH removed sub-micron patterns from the substrate. A well-resolved pattern was achieved with development in rather weak 0.026 N TMAH solution. Development in pure DI water was found to be ineffective. It was found that relatively high doses were required for patterning and the pattern was not resolved with the bridging features when developed in pure DI water.

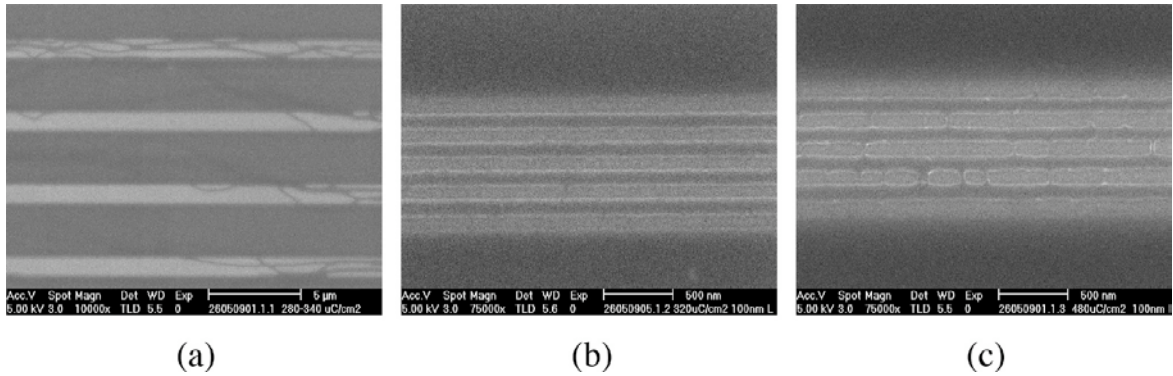


Figure 7.9 The 100 nm line space patterns in the resist MF-*t*BAC(2):PAG07-01 (50:50 wt%) processed without PAB and PEB, developed in (a) 0.26 N, (b) 0.026 N TMAH, and (c) pure DI water. The pattern was exposed with doses of (a) 280 to 340 $\mu\text{C}/\text{cm}^2$, (b) 320 $\mu\text{C}/\text{cm}^2$, and (c) 480 $\mu\text{C}/\text{cm}^2$, respectively.

Figures 7.10 (a) and (b) present the highest resolution dense lines achievable in the CA MF-*t*BAC(2) resist with PAG07-01 levels of 50 wt% and 60 wt%, respectively. The dense pattern of about 30 nm line width and 60 nm half pitch written at a dose of 600 $\mu\text{C}/\text{cm}^2$ in the resist containing 50 wt% PAG was well resolved with variations in line width. A better resolution was achieved in the resist containing 60 wt% PAG, in which a 25 nm line width and a 50 nm half pitch pattern were written at a dose of 340 $\mu\text{C}/\text{cm}^2$. Both samples did not receive PAB and PEB. They were developed in 0.026 N for 10 s and rinsed in DI water.

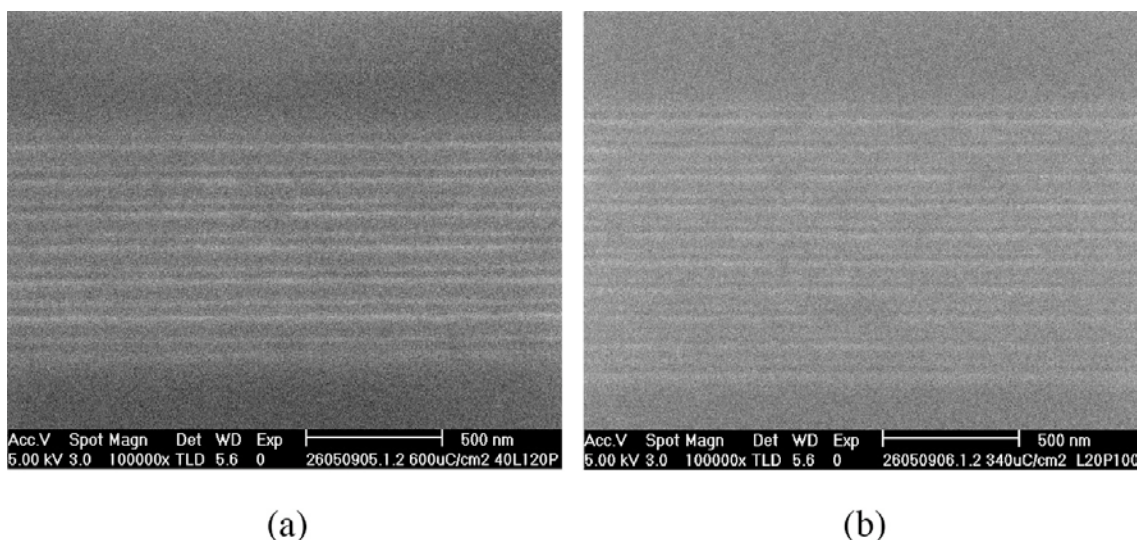


Figure 7.10 (a) The 60 nm half-pitch line patterns written at $600 \mu\text{C}/\text{cm}^2$ in the resist MF-*t*BAC(2):PAG07-01 containing 50 wt% PAG and (b) the 50 nm half-pitch line patterns written at $340 \mu\text{C}/\text{cm}^2$ in the resist MF-*t*BAC(2):PAG07-01 containing 60 wt% PAG. The samples received no PAB and PEB. Development was in 0.026 N TMAH for 10 seconds, followed by a rinse in DI water.

Although the resists formulated with PAG03-01 and PAG03-02 exhibited high sensitivity, they showed poor resolution capability due to excessive acid diffusion. It was not possible to achieve sub-micron patterns in the resist with well-defined dimension. Figures 7.11 (a) and (b) show the results of patterning 100 nm line space patterns in the CA MF-*t*BAC(2) resists containing 20 wt% of PAG03-01 and PAG03-02, respectively. Both resists were processed without PAB and PEB, and they were developed in 0.026 N TMAH for 5 seconds followed by a rinse in DI water. It can be seen that the size of the positive images in the resists was much larger than that of the designed pattern. In addition, the patterns in the resist with PAG03-01 suffered from acid diffusion and showed feature roughness more than those in the resist with PAG03-02. Development in pure DI water did not improve resolution as the resist was found to be under-developed in DI water.

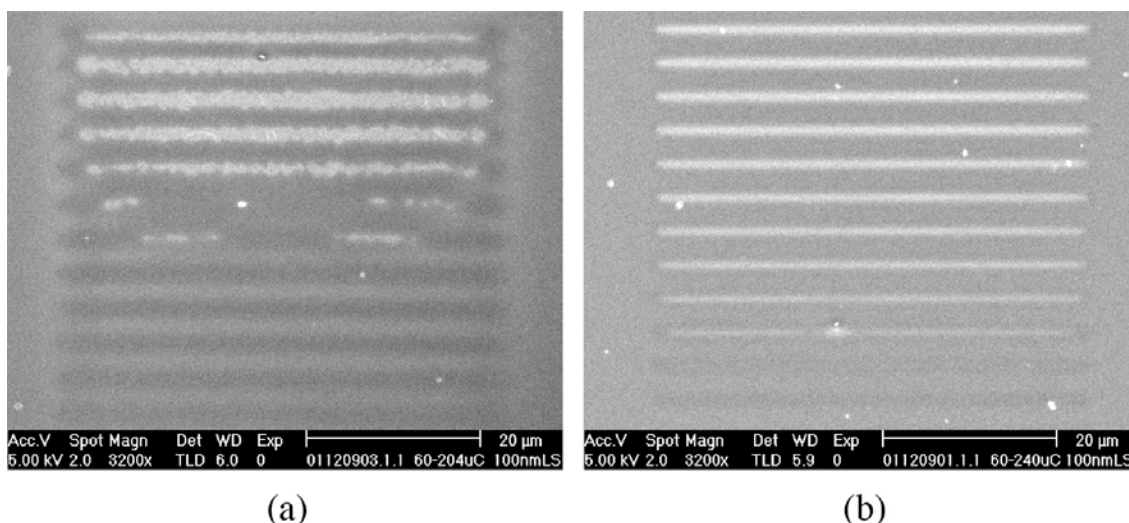


Figure 7.11 Patterning of 100 nm line and space patterns in the CA MF-*t*BAC(2) resist containing 20 wt% of (a) PAG03-01 and (b) PAG03-02 with doses between 60 and 240 $\mu\text{C}/\text{cm}^2$. The resists received no PAB and PEB. Development was in 0.026 N TMAH for 5 seconds followed by a rinse in DI water.

7.3.2.2 CA MF-*t*BAC(6) resists

An aqueous solution of TMAH was also found to be too aggressive for the CA MF-*t*BAC(6) resists. High resolution patterning in the CA MF-*t*BAC(6) resist was successful with development in pure DI water. The highest sparse and dense resolutions achievable in the MF-*t*BAC(6):PAG07-01 (50:50 wt%) resist are shown in Figures 7.12 (a) and (b). Sparse lines with 20 nm width and 400 nm pitch, Figure 7.12 (a), and dense line space pattern with 60 nm half pitch, Figure 7.12 (b), were patterned in a 40 nm thick resist with doses of 1.2 nC/cm and 450 $\mu\text{C}/\text{cm}^2$, respectively. The resists were processed without PAB and PEB. Development was in DI water for 10 s. It was found that PAB provided no significant improvement in the resist resolution. The smallest pitch size of 120 nm was also achievable in the CA MF-*t*BAC(6) resists containing PAG levels between 44 wt% and 55 wt% and processed under the same conditions.

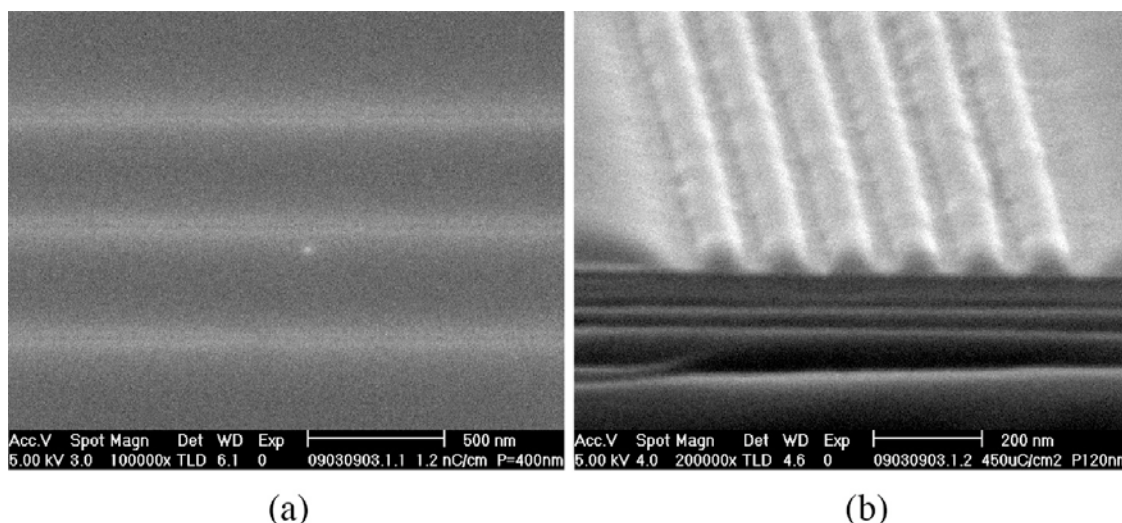


Figure 7.12 (a) The 20 nm sparse lines at 1.2 nC/cm and (b) cross-section of the 60 nm half pitch line space pattern at 450 $\mu\text{C}/\text{cm}^2$ in the resist MF-*t*BAC(6):PAG07-01 (50:50 wt%). The resist received no PAB and PEB. Development was in DI water for 10 seconds.

Incorporation of the additives into the resist formulation, unfortunately, did not improve the resolution capability of the positive tone resist. It was found that the addition of the base quencher BA-3 and the dissolution inhibitor PAG04-04 to the CA MF-*t*BAC(6) resists worsen the resist capability for resolution. Relatively poor contrast features in the high resolution image was observed in the resist with BA-3 added between 1 wt% and 4 wt%. In opposition to the addition of the base quencher, the additional PAG04-04 helped to improve contrast at the edge feature but it left an insoluble residue in the exposed areas, as shown in Figures 7.13 (a) and (b). Line-space patterns with 100 nm half-pitch, Figure 7.13 (a), and dense lines with 50 nm half pitch, Figure 7.13 (b), were written with doses of 200 $\mu\text{C}/\text{cm}^2$ and 480 $\mu\text{C}/\text{cm}^2$, respectively, in the resist MF-*t*BAC(6):PAG07-01:PAG04-04 (50:37.5:12.5 wt%). The resist was processed with a PAB of 100 °C for 30 minutes, no PEB, and development in DI water for 10 seconds. The line space patterns were not resolved with a dose of 480 $\mu\text{C}/\text{cm}^2$. It can be seen that the patterns were not resolved although the edge features were clear.

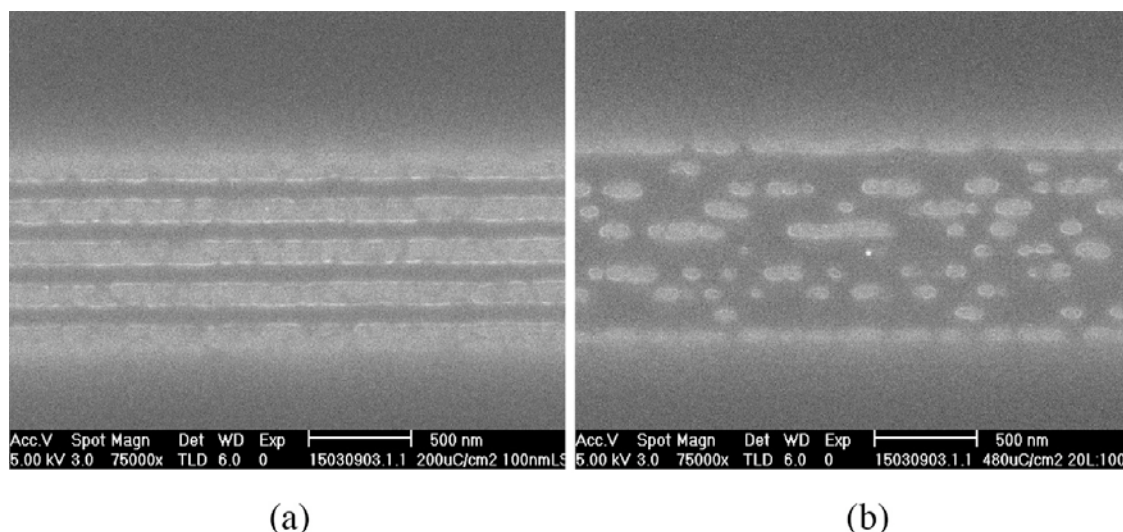


Figure 7.13 (a) The 100 nm 1:1 line:space pattern at 200 $\mu\text{C}/\text{cm}^2$ and (b) 50 nm half pitch lines at 480 $\mu\text{C}/\text{cm}^2$ produced in the resist MF-*t*BAC(6):PAG07-01:PAG04-04 (50:37.5:12.5 wt%). PAB was 100 °C for 30 minutes and development was in DI water for 10 seconds without PEB.

7.3.3 Dissolution characteristics

Dissolution characteristics of the CA MF-*t*BAC resist in an aqueous base developer were studied in order to understand the behaviour of the resists in a developer and to find appropriate development conditions. All resist samples were cast with PGMEA. The resists MF-*t*BAC(1):PAG07-01 (50:50 wt%) and MF-*t*BAC(2):PAG07-01 (50:50 wt% or 40:60 wt%) received no PAB, whilst the resist MF-*t*BAC(6):PAG07-01 (50:50 wt%) received PAB at 100 °C for 30 minutes. The resist samples were exposed to varying doses and repeatedly developed in DI water or in the TMAH solution and remaining film thickness was measured. The dissolution characteristic curves are presented for unexposed and exposed films as discussed below.

7.3.3.1 Unexposed resist films

The dissolution curves of the unexposed resist films in an aqueous solution of TMAH are compared in Figure 7.14 (a). Development in 0.26 N TMAH was followed by a rinse in DI water for 2 seconds, except for the CA MF-*t*BAC(6) resist which was developed without rinsing. It can be clearly seen that the resists dissolved by the TMAH solution at a constant rate even though they were unexposed and that the resist formulated with the fullerene derivative with the lowest number of adducts had a better

resistance to dissolution in the developer, and thus a lower dissolution rate. The CA MF-*t*BAC(1) resist containing 50 wt% PAG07-01 showed the lowest dissolution with a rate of 0.04 nm/s in 0.26 N TMAH. The dissolution rates of the CA MF-*t*BAC(2) resists with 50 wt% and 60 wt% PAG were 0.27 nm/s and 0.14 nm/s, respectively. A dissolution rate as high as 0.44 nm/s was found in the CA MF-*t*BAC(6) with 50 wt% PAG.

DI water was used as a developer for resists which require a less aggressive developer than the TMAH solution. Dissolution curves of the resists in DI water are shown in Figure 7.14 (b). The dissolution rates of the CA MF-*t*BAC(2) resists with 50 wt% and 60 wt% PAG in DI water were 0.18 nm/s and 0.17 nm/s, respectively, comparable to those in 0.26 N TMAH. The CA MF-*t*BAC(6) with 50 wt% PAG shows a slightly higher rate of 0.33 nm/s.

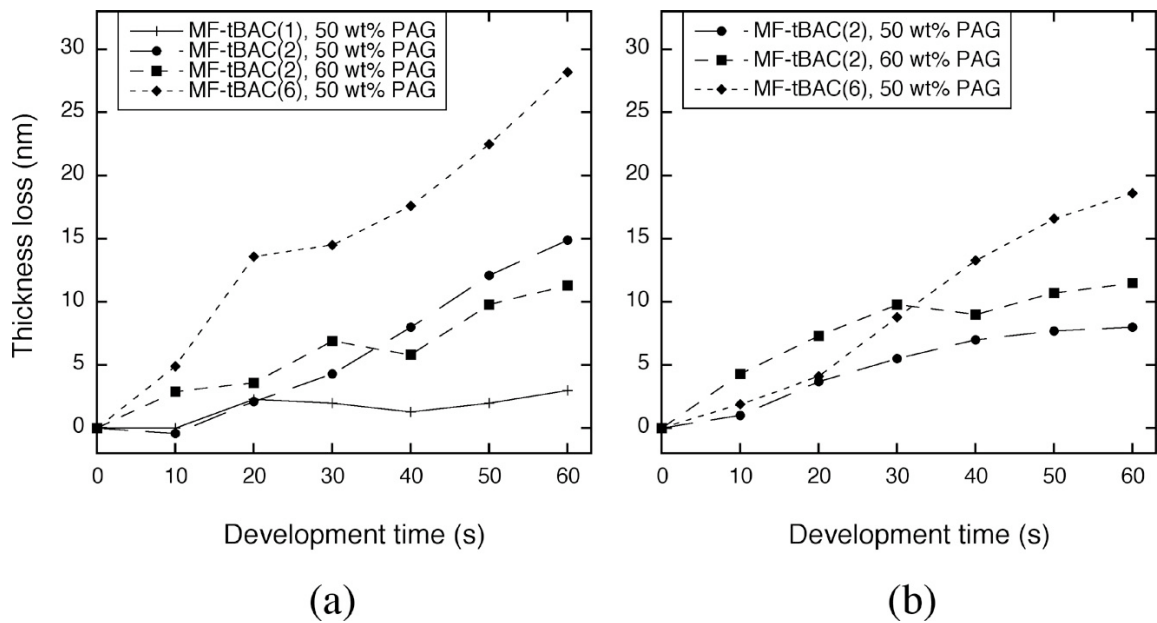


Figure 7.14 Dissolution curves of the unexposed MF-*t*BAC:PAG07-01 resists at PAG level of 50-60 wt%, (a) developed in 0.26 N TMAH solution and (b) in DI water.

7.3.3.2 Exposed resist films

The 40 nm thick MF-*t*BAC(6):PAG07-01 (50:50 wt%) resist was exposed to doses varying between 50 and 200 $\mu\text{C}/\text{cm}^2$. The sample was developed in DI water and the relative thickness loss, the step height between the exposed and unexposed areas developed together, was measured to produce the dissolution curves, as shown in Figure 7.15. An initial thickness loss of up to 15 nm after exposure to

a dose of $200 \mu\text{C}/\text{cm}^2$ was found. This could be due to either film compaction or evaporation of volatile by-products. At a low dose of $50 \mu\text{C}/\text{cm}^2$, the exposed resist was partially removed but the dissolution rate fell to zero after the first few seconds. The minimum clearing dose were $100 \mu\text{C}/\text{cm}^2$ requiring a the development time of about 10 seconds. The dissolution rate at $100 \mu\text{C}/\text{cm}^2$ was 3 nm/s, about 10 times that of the unexposed film. The dissolution rates slightly increased at higher doses to 3.3 nm/s and 4.2 nm/s at $150 \mu\text{C}/\text{cm}^2$ and $200 \mu\text{C}/\text{cm}^2$, respectively.

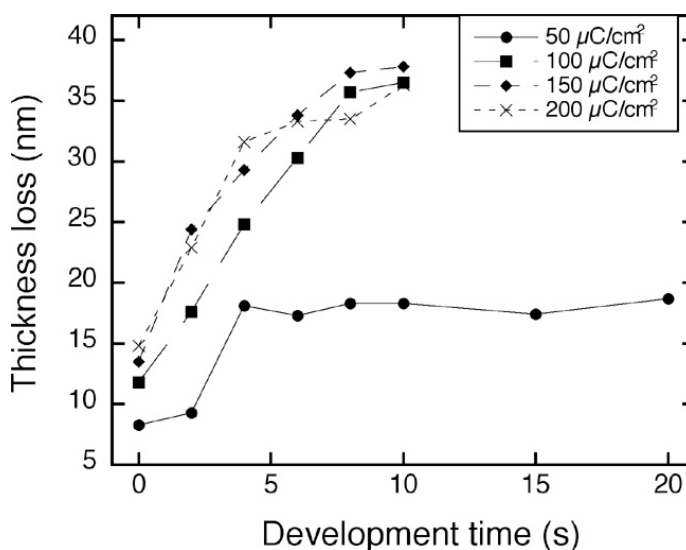


Figure 7.15 Dissolution curves of the MF-*t*BAC(6):PAG07-01 resist at a PAG level of 50 wt% exposed to an electron beam with doses varying between 50 and $200 \mu\text{C}/\text{cm}^2$ and repeatedly developed in DI water.

Samples of the MF-*t*BAC(2):PAG07-01 (50:50 wt%) resist were exposed to different doses and then developed in DI water, 0.026 N TMAH, or 0.26 N TMAH. A comparison of the dissolution curves is shown in Figure 7.16. It can be clearly seen that the resist was under-developed in DI water at the doses examined. At $50 \mu\text{C}/\text{cm}^2$, the resist dissolved faster in stronger TMAH solution than in DI water. The dissolution rates in DI water, 0.026 N TMAH, and 0.26N TMAH were 1 nm/s, 10 nm/s, and 15 nm/s, respectively, before stopping at certain film thicknesses. A clearing dose was achieved at $100 \mu\text{C}/\text{cm}^2$ in TMAH solutions at a 0.026 N strength and above. The dissolution rate of the resist at $100 \mu\text{C}/\text{cm}^2$ was 0.8 nm/s in DI water, only about three times that of the unexposed resist, whilst the

dissolution rate in the TMAH solutions was approximately 27 nm/s, giving a 100 times greater selectivity to the unexposed resist.

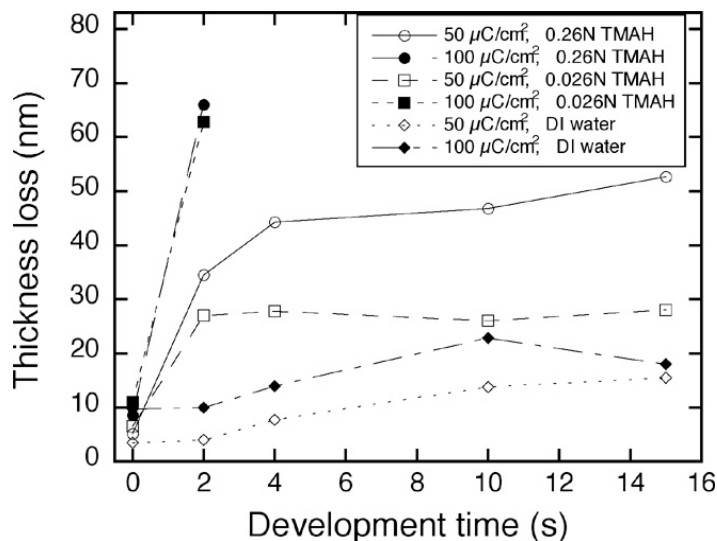


Figure 7.16 Dissolution curves of the MF-*t*BAC(2):PAG07-01 resist at a PAG level of 50 wt%. The resist was exposed to 50 and 200 $\mu\text{C}/\text{cm}^2$ and repeatedly developed in 0.26 N TMAH, 0.026N TMAH, and DI water.

7.3.4 Etch resistance

The resistance of the positive tone fullerene resists to plasma etching was evaluated using the ICP etcher. A silicon substrate protected with a resist pattern was anisotropically etched and the etch selectivity between the silicon and the resist was calculated. The commercial resist SAL601 (Rohm and Haas) was etched simultaneously as a control. The etching process employed a mixture of SF_6 and C_4F_8 at a flow rate of 20 sccm and 30 sccm, respectively. Samples were etched at the RF power of 20 W, the ICP power of 220 W, a pressure of 15 mTorr, and a temperature of 20 °C. The relative etch resistance of various resists to that of silicon are shown in Figure 7.17. Etch resistance of the SAL601 resist was 5.4 times greater than that of silicon. The MF-*t*BAC(6):PAG07-01 resists showed comparable values of etch resistance. They were 3.7, 3.5, and 3.8 times that of silicon at PAG loadings of 44 wt%, 50 wt%, and 60 wt%, respectively. The etch resistance of the MF-*t*BAC(2):PAG07-01 resists was higher than those formulated with the hexa-adduct derivative and were comparable to

SAL601. They were 5.6, 5, and 4.7 times that of silicon, decreasing with increasing concentration of PAG in the resist from 44 wt% to 50 wt%, and 60 wt%, respectively.

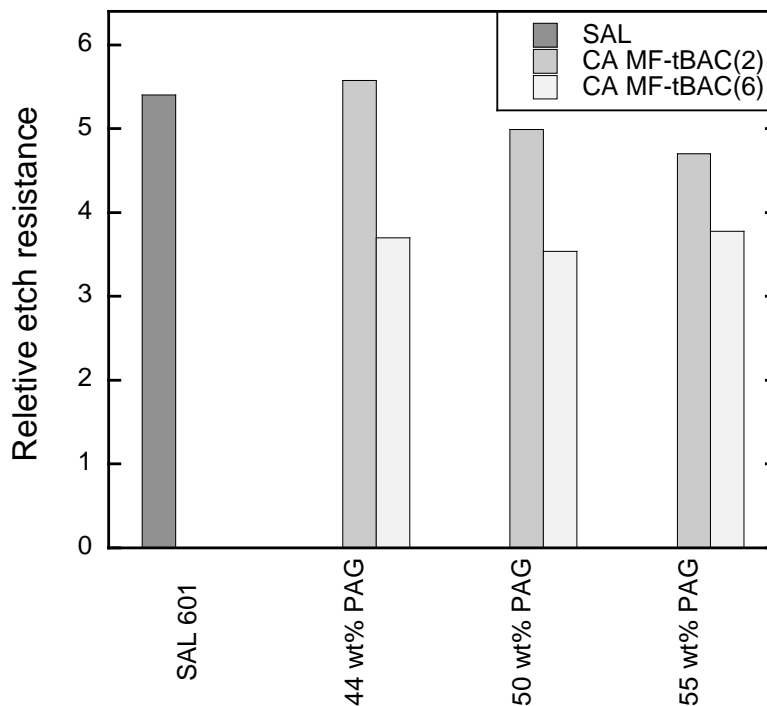


Figure 7.17 Comparison of the etching resistance of the CA fullerene resists and SAL601 relative to that of silicon.

7.4 Conclusions

The MF-THP and four MF-*t*BAC derivatives which differ in the number of adducts were investigated as positive tone chemically amplified fullerene based molecular resists for electron beam lithography. The chemical amplification of the derivatives using an acid-catalysed deprotection scheme was demonstrated by blending the derivatives with several PAGs and optional additives. The unexposed MF-THP film dissolved too fast in aqueous base developer, making it unsuitable for lithography. The CA MF-*t*BAC resist was more promising, with the exception of the tri-adduct MF-*t*BAC(3), which could not form a smooth film using the spin coating technique. It is obvious that the number of addends in a fullerene molecule has a significant impact on resist properties and lithographic properties, as summarised in Table 7.1. Some of the resist films, such as those based on MF-*t*BAC(1)

and MF-*t*BAC(2) could not withstand the baking process and tended to produce a number of pinholes upon the PAB. Unfortunately, PEB was found to be incompatible with most of the CA MF-*t*BAC films. The exposed resist patterns became distorted upon baking. This may have been due to the large acid diffusion. A major disadvantage is that the resist sensitivity could be adjusted only by varying the PAG concentrations. The resists were developable in aqueous solutions of TMAH. Doses to clear were not found for the mono-adduct MF-*t*BAC(1) resists when developed in a TMAH solution up to a 0.26 N concentration. High resolution patterning was successfully achieved using a weak TMAH developer at 0.026N for the MF-*t*BAC(2) resists and pure DI water for the CA MF-*t*BAC(6) resists.

The highest lithographic resolution of 50 nm half pitch has been demonstrated in the resist MF-*t*BAC(2) using the formulation and processing conditions summarised in Table 7.2. Addition of base quencher or dissolution inhibitor did not improve resolution capability of the resist. The introduction of base quencher at 1 to 4 wt% did not appear to significantly limit acid diffusion, although a small decrease in resist sensitivity was seen. Addition of dissolution inhibitor caused the resist to be under-developed, leaving residue in exposed areas. The etch resistance of the fullerene resist system depended on the type and concentration of the derivative in the resist. The CA MF-*t*BAC(2) resists had a comparable etch resistance to that of SAL601 under the same etching conditions.

Table 7.1 A summary of the lithographic properties of the MF-*t*BAC resists with the different numbers of adducts.

	MF- <i>t</i> BAC derivatives			
	Mono	Di	Tri	Hexa
Spin-coating film	✓	✓	✗	✓
PAB compatible	✗	✗	n/a	✓
PEB compatible	✗	✗	n/a	✗
Developable in 0.26 N TMAH solution	✗	✓	n/a	✓
High resolution	n/a	✓	n/a	✓
Etch resistance	n/a	✓	n/a	✓

Table 7.2 Resist formulation and processing conditions for the high-resolution, positive-tone, chemically amplified, fullerene based resist.

Resist formulation	
Fullerene derivative	MF- <i>t</i> BAC(2)
PAG	PAG07-01
Base additive	No
Fullerene weight ratio (parts)	1
PAG weight ratio (parts)	1.5
Casting solvent	PGMEA
Processing conditions	
PAB	No
PEB	No
Developer	0.026 N TMAH
Development time	10 seconds
Rinse	DI water

Chapter 8

Conclusions and Future Outlooks

8.1 Conclusions

The work presented in this thesis describes the development and lithographic evaluation of several chemically amplified fullerene molecular resist systems for NGL. The resist materials in this study were primarily designed for electron beam lithography, a potential candidate of NGL. The fullerene derivative based resist was represented a combination of the concepts of a molecular resist and chemical amplification, in which a low molecular weight material with the potential to provide high resolution with low line width roughness, has its sensitivity enhanced by chemical amplification. Other lithographic properties such as etch durability, stability, and compatibility to manufacturing processes also have to meet requirements.

The experiments began with the development and evaluation of a negative tone molecular resist. The fullerene derivative MF07-01 was chemically amplified to work as a 3-component negative tone e-beam resist by combining the derivative with an onium salt PAG and an epoxy novolac resin. Smooth resist films, with no significant of crystallisation, can be prepared by the spin coat technique. The resist can be prepared and developed in a range of organic solvents, although the best lithographic results were achieved when processed with a halogenated solvent. The CA MF07-01 resists were simultaneously capable of high sensitivity, high resolution, low line width roughness, and high etch durability. Enhancement of the resist sensitivity from about $600 \mu\text{C}/\text{cm}^2$ to below $10 \mu\text{C}/\text{cm}^2$ at 20keV with optimised process conditions was achieved. The resists also had a wide PAB and PEB process latitude and could be processed with a range of baking temperatures and times without a strong change in sensitivity and resolution. The highest sparse resolution demonstrated was 12 nm, whilst dense resolution of 20 nm half-pitch was demonstrated. LWR(3σ) was typically 3 - 4 nm in sparse features

and 5 - 7 nm in 25 nm half-pitch dense features. The reduction of LWR can be achieved by adjusting the resist formulation and process condition. LWR(3σ) as low as 2 nm in sparse feature was achieved in some optimum conditions. It was found that inclusion of an additive compound to the resist formulation could not significantly improve the resist performance. The etch resistance of the resists was comparable to that of SAL601, a high etch durability commercial resist, under the same etching conditions. Fabrication of high aspect ratio and anisotropic silicon structures was demonstrated using a resist pattern as a mask under the mixed SF_6/C_4F_8 plasma etching.

In addition to the work on the negative tone resists, the development and evaluation of a positive tone molecular resist is also presented in this thesis. The positive tone fullerene resist was developed under a chemically amplified deprotection scheme and designed to be processed with an aqueous base developer which is more friendly to manufacturing processes than a strong organic solvent. The resists were formulated with the fullerene derivative and a PAG. The CA resists of the fullerene MF-*t*BAC(2) or MF-*t*BAC(6) were capable of forming a film on a silicon substrate and developable in an aqueous solution of TMAH. They acted as a positive tone resist at a low dose by chemical amplification and turned to a negative tone resist at much higher doses. The positive tone resists could not withstand any baking process. PAB degraded the film of the MF-*t*BAC(2) resist, whilst the PEB process caused defects in exposed area in all cases. The sensitivity of the CA MF-*t*BAC resist was found to be not significantly worse than that of the negative tone resist system. When formulated with PAG07-01, the resist sensitivity ranged between 70 and 150 $\mu C/cm^2$ depending on type of the derivative, the concentration of PAG, and the strength of developer. High resolution capability of the resist was successfully demonstrated. Feature resolution of 20 nm in sparse pattern and 50 nm half-pitch for dense pattern were achieved in the CA MF-*t*BAC resists developed in a weak solution of TMAH or in a pure DI water.

In summary, the fullerene molecular resists show their potential as a candidate material for NGL. In Table 8.1, the lithographic properties of the molecular resists presented in this thesis are compared with the ITRS resist requirements and those of commercially available e-beam resists.

Table 8.1 Comparison for the lithographic performance of the fullerene molecular resists, commercially available e-beam resist, and ITRS requirements.

Resist	Classification	Sensitivity ($\mu\text{C}/\text{cm}^2$)	Resolution* (nm)	LWR(3σ) [†] (nm)	References
ITRS resist requirements for MPU gate by the year 2013	n/a	5-30 (50-100 kV)	28	2.2	[18]
Fullerene MF07-01	Negative, CAR	<10 (20 kV)	12 (30 kV)	2-4	Chapter 3, 5
Fullerene MF- <i>t</i> BAC	Positive, CAR	~100 (20 kV)	20 (30 kV)	n/a	Chapter 7
PMMA (MicroChem)	Commercial, Positive	350 (50 kV)	~5 (80 kV)	3-4	[78,79]
	Commercial, Negative	~100 times that of positive PMMA	12 (300 kV)	n/a	[80]
ZEP (Nippon Zeon)	Commercial, Positive	15-30 (25 kV)	10		[110,111]
HSQ (Dow Corning)	Commercial, Negative	~300 (70 kV)	< 10 (70-100 kV)	< 2	[112-114]
SAL601 (Rohm and Haas)	Commercial, Negative, CAR	7-9 (20-40 kV)	20 (5 kV)	~5	[81,82]

* The minimum width of an isolated line.

[†] The radius of gyration of the resist molecule if the LWR(3σ) value is not available.

8.2 Suggested future work

There are areas that could benefit from a future work. A disadvantage of the negative tone chemically amplified resist is that it is incompatible with aqueous base development which is typically used in the industry. A key to develop an aqueous base developable negative tone resist is to use a water-soluble crosslinker in resist formulation. A water-soluble epoxy resin is one of the interesting crosslinkers to be used without adding a complex modification of the current 3-component negative tone resist system or discarding the good resist performance. Additionally, it is suggested that the resist characteristics and type and the number of a functional group on the C_{60} fullerene are closely related. Further work on the positive tone resist could be done by a design and synthesis of a new fullerene

derivative with a functional group providing high reactivity to an acid and high resistance to processing temperature.

The fullerene molecular resists have a potential to extend their application to other lithographic technologies such as extreme ultraviolet (EUV) lithography and multilayer resist technology. It is expected that EUV lithography will be the first post-optical next generation lithography to be implemented in a high-volume production line in 2013. As a result, research on a resist material for EUV lithography has been increasingly of interest. Due to the fact that many electron beam resists can be used with EUV lithography interchangeably because of the similar exposure mechanisms, the fullerene molecular resist is an interesting EUV candidate.

References

1. Morton Jr., D. L., Gabriel, J., Electronics: the life story of a technology, Westport, CT: Greenwood Press, pp 29-34 (2004).
2. Morton Jr., D. L., Gabriel, J., Electronics: the life story of a technology, Westport, CT: Greenwood Press, pp 74-82 (2004).
3. Kilby, J. S., Miniaturized electronic circuits, U.S. Patent 3,138,743 (1964).
4. Noyce, R. N., Semiconductor device-and-lead structure, U.S. Patent 2,981,877 (1961).
5. Moore, G. E., Cramming more components onto integrated circuits, Electronics 38(8), 114-117 (1965).
6. Intel corporation.
7. Bates, A. K., Rothschild, M., Bloomstein, T. M., Fedynyshyn, T. H., Kunz, R. R., Liberman, V., Switkes, M., Review of technology for 157-nm lithography, IBM J. Res. Dev. 45(5), 605-614 (2001).
8. Brainard, R. L., Barclay, G. G., Anderson, E. H., Ocola, L. E., Resists for next generation lithography, Microelectron. Eng. 61-62, 707-715 (2002).
9. Levinson, H. J., Arnold, W. H., Handbook of microlithography, micromachining, and microfabrication Vol. 1, ed. Rai-Choudhury, P., Bellingham, WA:SPIE Press, p 28 (1997).
10. Levinson, H. J., Arnold, W. H., Handbook of microlithography, micromachining, and microfabrication Vol. 1, ed. Rai-Choudhury, P., Bellingham, WA:SPIE Press, p 57 (1997).
11. Mack, C., Fundamental principles of optical lithography: the science of microfabrication, West Sussex, England: John Wiley & Sons Ltd, p 22 (2007).
12. Mack, C., Fundamental principles of optical lithography: the science of microfabrication, West Sussex, England: John Wiley & Sons Ltd, pp 419-450 (2007).
13. Wei, Y., Back, D., 193 nm immersion lithography: status and challenges, SPIE newsroom: micro/nano lithography & fabrication, doi: 10.1117/2.1200703.0001 (2007).
14. Sanders, D. P., Advances in patterning materials for 193 nm immersion lithography, Chem. Rev. 110, 321-360 (2010).
15. Wei, Y., Back, D., Mastering the resist-leaching and aqueous-contact angle challenges, SPIE newsroom, doi: 10.1117/2.1200705.0758 (2007).
16. Wei, Y., Bouble and antibubble defects in 193i lithography, SPIE newsroom, doi: 10.1117/2.1200802.0974 (2008).

- 17 Wei, Y., Extendability of 193 nm immersion lithography, SPIE newsroom, doi: 10.1117/2.1200802.0974 (2008).
- 18 International Technology Roadmap for Semiconductors, 2009 Edition, <http://www.itrs.net>.
- 19 Hughes, G., Litt, L. C., Wüest, A., Palaiyanur, S., Mask and wafer cost of ownership (COO) from 65 to 22 nm half-pitch nodes, Proc. SPIE 7028, 70281P (2008).
- 20 Dai, H., Bencher, C., Chen, Y., Woo, H., Ngai, C., Xu, X., 45 nm and 32 nm half-pitch with 193 dry lithography and double patterning, Proc. SPIE 6924, 652421 (2008).
- 21 Bencher, C., Chen, Y., Dai, H., Montgomery, W., Huli, L., 22 nm half-pitch patterning by CVD spacer self alignment double patterning (SADP), Proc. SPIE 6924, 65244E (2008).
- 22 Bailey, G. E., Tritchkov, A., Park, J.-W., Hong, L., Wiaux, V., Hendrickx, E., Verhaegen, S., Xie, P., Versluijs, J., Double pattern EDA solution for 32 nm HP and beyond, Proc. SPIE 6521, 65211K (2007).
- 23 Drapeau, M., Wiaux, V., Hendrickx, E. Verhaegen, S., Machida, T., Double patterning design split implementation and validation for the 32 nm node, Proc. SPIE 6521, 652109 (2007)
- 24 Shiu, W., Liu, J. H., Wu, J. S., Tseng, T.-L., Liao, C. T., Liao, C. M., Liu, J., Wang, T., Advanced self-aligned double patterning development for sub-30-nm DRAM manufacturing, Proc. SPIE 7274, 72740E (2009).
- 25 Carlson, A., King Liu, T.-J., Negative and iterated spacer lithography processes for low variability and ultra-dense integration, Proc. SPIE 6924, 69240B (2008).
- 26 Meiling, H., Buzing, N., Cummings, K., Harned, N., Hultermans, B., de Jonge, R., Kessels, B., Kürz, P., Lok, S., Lowisch, M., Mallman, J., Pierson, B., Wagner, C., van Dijk, A., van Setten, E., Zimmerman, J., EUVL system: moving towards production, Proc. SPIE 7271, 727102 (2009).
- 27 Wurm, S., Lithography perspective for the 22nm half-pitch, Solid State Technology 53(2), 16-18 (2010).
- 28 Wurm, S., EUV lithography development and research challenges for the 22 nm half-pitch, J. Photopolym. Sci. Technol. 22(1), 31-42 (2009).
- 29 Wu, B., Kumar, J., Extreme ultraviolet lithography: a review, J. Vac. Sci. Technol. B 25(6), 1743-1761 (2007).
- 30 Chou, Y., Krauss, P. R., Renstrom, P. J., Imprint of sub-25 nm vias and trenches in polymers, Appl. Phys Lett. 67(21), 3114-3317 (1995)
- 31 Haisma, J., Verheijen, M., van den Heuvel, K., van den Berg, J., Mold-assisted nanolithography: a process for reliable pattern replication, J. Vac. Sci. Technol. B 14(6), 4124-4128 (1996).
- 32 Schift, H., Nanoimprint lithography: An old story in modern times? A review, J. Vac. Sci. Technol. B 26(2), 458-480 (2008).

- 33 McCord, M. A., Rooks, M. J., Handbook of microlithography, micromachining, and microfabrication Vol. 1, ed. Rai-Choudhury, P., Bellingham, WA:SPIE Press, p 144 (1997).
- 34 McCord, M. A., Rooks, M. J., Handbook of microlithography, micromachining, and microfabrication Vol. 1, ed. Rai-Choudhury, P., Bellingham, WA:SPIE Press, p 156 (1997).
- 35 Pain, L., Icard, B., Tedesco, S., Kampherbeek, B., Gross, G., Klein, C., Loeschner, H., Platzgummer, E., Morgan, R., Manakli, S., Kretz, J., Holhe, C., Choi, K.-H., Thrum, F., Kassel, E., Pilz, W., Keil, K., Butschke, J., Irmscher, M., Letzkus, F., Hudek, P., Paraskevopoulos, A., Ramm, P., Weber, J., MAGIC: a European program to push the insertion of maskless lithography, Proc. SPIE 6921, 69211S (2008).
- 36 Wieland, M. J., de Boer G., ten Berge, G. F., Jager, R., van de Peut, T., Peijster, J. J. M., Slot, E., Steenbrink, S. W. H. K., Teepen, T. F., van Veen, A. H. V., Kampherbeek, B. J., MAPPER: high throughput maskless lithography, Proc. SPIE 7271, 72710O (2009).
- 37 Steenbrink, S. W. H. K., Kampherbeek, B. J., Wielanda, M. J., Chenb, J. H., Changb, S. M., Pasc, M., Kretzd J., Hohled, C., van Steenwinckele, D., Manaklif, S., Le-Denmatf, J., Paing, L., High throughput maskless lithography: low voltage versus high voltage, Proc. SPIE 6921, 69211T (2008).
- 38 Slot, E., Wieland, M. J., de Boer, G., Kruit, P., ten Berge, G. F., Houkes, A. M. C., Jager, R., van de Peut, T., Peijster, J. J. M., Steenbrink, S. W. H. K., Teepen, T. F., van Veen, A. H. V., Kampherbeek, B. J., MAPPER: high throughput maskless lithography, Proc. SPIE 6921, 69211P (2008).
- 39 Klein, C., Platzgummer, E., Klikovits, J., Piller, W., Loeschner, H., Bejdak, T., Dolezel P., Kolarik, V., Klingler, W., Letzkus, F., Butschke, J., Irmscher, M., Witt, M., Pilz, W., Jaschinsky, P., Thrum, F., Hohle, C., Kretz, J., Nogatch, J.T., Zepka, A., PML2: The maskless multibeam solution for the 22nm node and beyond, Proc. SPIE 7271, 72710N (2009).
- 40 Kleina, C., Platzgummera, E., Loeschnera, H., Grossa, G., Dolezelb, P., Tmej, M., Kolarikb, V., Klinglerc, W., Letzkusc, F., Butschkec, J., Irmscherc, M., Wittd, M., Pilzd, W., Projection maskless lithography (PML2): proof-of-concept setup and first experimental results, Proc. SPIE 6921, 69211O (2008).
- 41 McCord, M. A., Rooks, M. J., Handbook of microlithography, micromachining, and microfabrication Vol. 1, ed. Rai-Choudhury, P., Bellingham, WA:SPIE Press, p 202 (1997).
- 42 McCord, M. A., Rooks, M. J., Handbook of microlithography, micromachining, and microfabrication Vol. 1, ed. Rai-Choudhury, P., Bellingham, WA:SPIE Press, p 203 (1997).
- 43 Constantoudis, v., Patsis, G. P., Gogolides, E., Photoresist line-edge roughness analysis using scaling concepts, Proc. SPIE 5038, 901 (2003).
- 44 Scheckler, E. W., Ogawa, T., Yamanashi, H., Soga, T., Ito, M., Resist pattern fluctuation limits in extreme-ultraviolet lithography, J. Vac. Sci. Technol. B 12, 2361-2371 (1994).
- 45 Chandhok, M., Datta, S., Lionberger, D., Vesecky, S., Impact of line-width roughness on Intel's 65-nm process devices, Proc. SPIE 6519, 65191A (2007).

- 46 Ban, Y., Sundareswaran, S., Panda, R., Pan, D. Z., Electrical impact of line-edge roughness on sub-45nm node standard cell, Proc. of SPIE 7275, 727518 (2009).
- 47 Yamaguchi, T., Yamazaki, K., Namatsu, H., Influence of molecular weight of resist polymers on surface roughness and line-edge roughness, J. Vac. Sci. Technol. B 22(6), 2604-2610 (2004).
- 48 Leunissen, L. H. A., Ercken, M., Patsis, G. P., Determining the impact of statistical fluctuations on resist line edge roughness, Microelectron. Eng. 78-79, 2-10 (2005).
- 49 Patsis, G. P., Constantoudis, V., Gogolides, E., Effects of photoreist polymer molecular weight on line-edge roughness and its metrology probed with Monte Carlo simulations, Microelectron. Eng. 75, 207-308 (2004).
- 50 Patsis, G. P., Gogolides, E., Van Werden, K., Effects of photoreist polymer molecular weight and acid diffusion on line-edge roughness, Jpn. J. Appl. Phys. 44(8), 6341-6348 (2005).
- 51 Yoshimura, T., Shiraishi, H., Yamamoto, J., Okazaki, S., Nano edge roughness in polymer resist patterns, Appl. Phys. Lett. 63, 764-766 (1993).
- 52 Fedynyshyn, T. H., Pottebaum, I., Astolfi, D. K., Cabral, A., Roberts, J., Meagley, R., Contribution of photoacid generator to material roughness, J. Vac. Sci. Technol. B 24(6), 3031-3039 (2006).
- 53 Fedynyshyn, T. H., Astolfi, D. K., Goodman, R. B., Cann, S., Roberts, J., Contribution of resist polymer to material roughness, J. Vac. Sci. Technol. B 26(6), 2281-2289 (2008).
- 54 Hirayama, T., Shiono, D., Matsumaru, S., Ogata, T., Hada, H., Onodera, J., Arai, T., Sakamizu, T., Yamaguchi, A., Shiraishi, H., Fukuda H., Ueda, M., Depth profile and line-edge roughness of low-molecular-weight amorphous electron beam resists, Jpn. J. Appl. Phys. 44(7B), 5484-5488 (2005).
- 55 Kozawa, T., Oizumi, H., Itani, T., Tagawa, S., Evaluation of chemical gradient enhancement methods for chemically amplified extreme ultraviolet resists, Jpn. J. Appl. Phys. 48, 126004 (2009).
- 56 Reynolds, G. W., Taylor, J. W., Factors contributing to sidewall roughness in a positive-tone, chemically amplified resist exposed by x-ray lithography, J. Vac. Sci. Technol. B 17(2), 334-344 (1999).
- 57 Shin, J., Han, G., Ma, Y., Moloni, K., Cerrina, F. J., Resist line edge roughness and aerial image contrast, Vac. Sci. Technol. B 19(6), 2890-2895 (2001).
- 58 Shin, J., Ma, Y., Cerrina F., Depth dependence of resist line-edge roughness: relation to photoacid diffusion length, J. Vac. Sci. Technol. B 20(6), 2927-2931 (2002).
- 59 Rau N., Stratton, F., Fields, C., Ogawa, T., Neureuther, A., Kubena, R., Willson G., Shot-noise and edge roughness effects in resists patterned at 10 nm exposure, J. Vac. Sci. Technol. B 16, 3784-3788 (1998).
- 60 Kruit, P., Steenbrink, S., Jager, R., Wieland, M., Optimum dose for shot noise limit CD uniformity, J. Vac. Sci. Technol. B 22, 2948-2955 (2004).

- 61 Yasin, S., Khalid, M. N., Hasko, D. G., Ahmed, H., Influence of polymer phase separation on roughness of resist features in UVIII, *Microelectron. Eng.* 73-74, 259-264 (2004).
- 62 Yasin, S., Hasko, D. G., Khalid, M. N., Weaver, D. J., Ahmed, H., Influence of polymer phase separation on roughness of resist features, *J. Vac. Sci. Technol. B* 22(2), 574-578 (2004).
- 63 Flanagan, L. W., Singh, V. K., Willson, C. G., Surface roughness development during photoresist dissolution, *J. Vac. Sci. Technol. B* 17(4), 1371-1379 (1999).
- 64 Yoshizawa, M., Moriya, S., Study of the acid-diffusion effect on line edge roughness using the edge roughness evaluation method, *J. Vac. Sci. Technol. B* 20, 1342-1347 (2002).
- 65 Ito, H., Willson, C. G., Chemical amplification in the design of dry developing resist materials, *Polym. Eng. Sci.* 23(18), 1012-1018 (1983).
- 66 Ito, H., Willson, C. G., Frechet, J. M. J., Positive- and negative-working resist compositions with acid generating photoinitiator and polymer with acid labile groups pendant from polymer backbone, U. S. Patent 4,491,628 (1985).
- 67 Ito, H., Chemical amplification resists for microlithography, *Adv. Polym. Sci.* 172, 37-245 (2005).
- 68 Ito, H., Chemical amplification resists: history and development within IBM, *IBM J. Res. Dev.* 44(1), 119-130 (1997).
- 69 McKean, D. R., Schaedeli, U., MacDonald, S. A., Acid photogeneration from sulfonium salts in solid polymer matrices, *J. Polym. Sci., Part A: Polym. Chem.* 27, 3927-3935 (1989).
- 70 Dektar, J. L., Hacker, N. P., Photochemistry of triarylsulfonium salts, *J. Am. Chem. Soc.* 112, 6004-6015 (1990)
- 71 Crivello, J. V., The discovery and development of onium salt cationic photoinitiators, *J. Polym. Sci. Part A: Polym. Chem.* 37, 4241-4254 (1999).
- 72 Bilenberg, B., Jacobsen, S., Schmidt, M. S., Skjolding, L.H.D., Shi, P., Boggild, P., Tegenfeldt, J. O., Kristensen, A., High resolution 100 kV electron beam lithography in SU-8, *Microelectron. Eng.* 83, 1609-1612 (2006).
- 73 Glezos, N., Argitis, P., Velessiotis, D., Raptis, I., Hatzakis, M., Hudek, P., Kostic, I., Aqueous base development and acid diffusion length optimization in negative epoxy resist for electron beam lithography, *J. Vac. Sci. Technol. B* 18, 3431-3434 (2000).
- 74 Argitis, P., Glezos, N., Vasilopoulou, M., Raptis, I., Hatzakis, M., Everett, J., Meneghini, G., Palumbo, A., Ardito, M., Hudek, P., Kostic, I., Aqueous base developable epoxy resist for high sensitivity electron beam lithography, *Microelectron. Eng.* 53(1-4), 453-456 (2000).
- 75 Brainard, R. L., Trefonas, P., Lammers, J. H., Cutler, C. A., Mackevich, J. F., Trefonas, A., Robertson, S. A., Shot noise, LER, and quantum efficiency of EUV photoresists, *Proc. SPIE* 5374, 74-85 (2004).

- 76 Gallatin, G. M., Resist blur and line edge roughness, Proc. SPIE 5754, 38-52 (2004).
- 77 Gallatin G. M., Naulleau P, Brainard R., Fundamental limits to EUV photoresist, Proc. SPIE 6519, 651911 (2007).
- 78 McCord, M. A., Rooks, M. J., Handbook of microlithography, micromachining, and microfabrication Vol. 1, ed. Rai-Choudhury, P., Bellingham, WA:SPIE Press, p 205 (1997).
- 79 Yasin, S., Hasko, D. G., Ahmed, H., Fabrication of < 5 nm width lines in poly(methylmethacrylate) resist using a water:isopropyl alcohol developer and ultrasonically-assisted development, Appl. Phys. Lett. 78, 2760-2762 (2001).
- 80 Hoole, A. C. F., Welland, M. E., Broers, A. N., Negative PMME as a high-resolution resist-the limits and possibilities, Semicond. Sci. Technol. 12 1166-1170 (1997).
- 81 Yoshimura, T., Nakayama, Y., Okazaki, S., Acid-diffusion effect on nanofabrication in chemical amplified resist, J. Vac Sci. Technol. B 10(6), 2615-2619 (1992).
- 82 McCord, M. A., Rooks, M. J., Handbook of microlithography, micromachining, and microfabrication Vol. 1, ed. Rai-Choudhury, P., Bellingham, WA:SPIE Press, pp 211-212 (1997).
- 83 Fujita, J., Ochiai, Y., Nomura, E., Matsui, S., Ultrahigh resolution of calixarene negative tone resist in electron beam lithography, Appl. Phys. Lett. 68(9), 1297-1299 (1995).
- 84 Fujita, J., Ochiai, Y., Nomura, E., Matsui, S., Nanometer-scale resolution of calixarene negative resist in electron beam lithography, J. Vac Sci. Technol. B 14, 4272-4276 (1996).
- 85 Ishida, M., Fujita, J., Ogura, T., Ochiai, Y., Ohshima, E., Momoda, J., Sub-10-nm-scale lithography using p-chloromethyl-methoxy-calix[4]arene resist, Jpn. J. Appl. Phys. 42, 3913-3916 (2003).
- 86 Sailer, H., Ruderisch, A., Henschel, W., Schurig, V., Kern, D. P., High resolution electron beam lithography using a chemically amplified calix[4]arene based resist, J. Vac. Sci. Technol. B 22 (6), 3485-3488 (2004).
- 87 Robinson, A. P. G., Palmer, R. E., Tada, T., Kanayama, T., Allen, M. T., Preece, J. A., Harris, K. D. M., 10 nm scale electron beam lithography using a triphenylene derivative as a negative/positive tone resist, J. Phys. D: Appl. Phys. 32, L75-L78 (1999).
- 88 Robinson, A. P. G., Palmer, R. E., Tada, T., Kanayama, T., Allen, M. T., Preece, J. A., Harris, K. D. M., Polysubstituted derivatives of triphenylene as high resolution electron beam resists for nanolithography, J. Vac. Sci. Technol. B 18(6), 2730-2736 (2000).
- 89 Tada, T., Kanayama, T., Robinson, A. P. G., Palmer, R. E., Allen, M. T., Preece, J. A., Harris, K. D. M., A triphenylene derivative as a novel negative/positive tone resist for 10 nanometer resolution, Microelectron. Eng. 53, 425-428 (2000).
- 90 Robinson, A.P.G., Zaid, H.M., Gibbons, F. P., Palmer R.E., Manickam, M., Preece, J.A., Brainard, R., Zampini, T., O'Connell, K., Chemically amplified molecular resists for electron beam lithography, Microelectron. Eng. 83(4-9), 1115-1118 (2006).

- 91 Zaid, H. M., Robinson, A.P.G., Palmer, R.E., Manickam, M., Preece J.A., Chemical amplification of a triphenylene molecular electron beam resist, *Adv. Funct. Mater.* 17(14), 2522-2527 (2007).
- 92 Robinson, A.P.G., Zaid, H.M., Manickam, M., Preece, J.A., Palmer R.E., Anomalous acid diffusion in a triphenylene molecular resist with melamine crosslinker, *Microelectron. Eng.* 85(7) 1540-1544 (2008).
- 93 Kroto, H. W., Heath, J. R., O'Brien, S. C., Curl, R. F., Smalley, R. E., C60: Buckminsterfullerene, *Nature* 318, 162-163 (1985).
- 94 Tada T., Kanayama T., Nanolithography using fullerene films as an electron beam resist, *Jpn. J. Appl. Phys.* 35, L63-L65 (1996).
- 95 Hunt, M. R. C., Schmidt, J., Palmer, R. E., Electron-beam damage of C60 films on hydrogen-passivated Si(100), *Appl. Phys. Lett.* 72(3), 323-325 (1998).
- 96 Robinson, A. P. G., Palmer, R. E., Tada, T., Kanayama, T., Preece J. A., A fullerene derivative as an electron beam resist for nanolithography, *Appl. Phys. Lett.* 72, 1302-1304 (1998).
- 97 Robinson, A. P. G., Palmer, R. E., Tada, T., Kanayama, T., Shelley, E. J., Philp D., Preece, J. A., Electron beam induced fragmentation of fullerene derivatives, *Chem. Phys. Lett.* 289, 586-590 (1998).
- 98 Robinson, A. P. G., Palmer, R. E., Tada, T., Kanayama, T., Shelley, E. J., Philp D., Preece, J. A., Exposure mechanism of fullerene derivative electron beam resists, *Chem. Phys. Lett.* 312, 469-474 (1999).
- 99 Gibbons, F.P., Robinson, A.P.G., Palmer, R.E., Manickam, M., Preece J.A., Ultrathin fullerene films as high-resolution molecular resists for low-voltage electron-beam lithography, *Small* 2(8-9), 1003-1006 (2006).
- 100 Gibbons, F.P., Zaid, H. M., Manickam, M., Preece J.A., Palmer, R. E., Robinson, A.P.G., A chemically amplified fullerene derivative molecular electron beam resist, *Small* 3(12), 2076-2080 (2007).
- 101 Gibbons, F.P., Robinson, A.P.G., Palmer, R.E., Diegoli, S., Manickam, M., Preece J.A., Fullerene resist materials for the 32nm node and beyond, *Adv. Funct. Mater.* 18(13), 1977-1982 (2008).
- 102 Meuris, M., Arnauts, S., Cornelissen, I., Kenis, K., Lux, M., Degendt, S., Mertens, P. J., Teerlinck, R., Leowensteine, L., Heyns, M. M., Wolke, K., Implementation of the IMEC-Clean in advanced CMOS manufacturing, *IEEE Semi. Manu.* 157-160 (1999).
- 103 Patsis, G. P., Constantoudis, V., Tserepi, A., Gogolides, E., Grozev, G., Quantification of line-edge roughness of photoresists. I. A comparison between off-line and on-line analysis of top-down scanning electron microscopy images, *J. Vac. Sci. Technol B* 21(3), 1008-1018 (2003).
- 104 Constantoudis, V., Patsis, G. P., Tserepi, A., Gogolides, E., Quantification of line-edge roughness of photoresists. II. Scalling and fractal analysis and the best roughness descriptors, *J. Vac. Sci. Technol B* 21(3), 1019-1026 (2003).

- 105 Contantoudis, V., Patsis, G. P., Leunissen, L. H. A., Gogolides, E., Line edge roughness and critical dimension variation: fractal characterization and comparison using model functions, *J. Vac. Sci. Technol. B* 22, 1974-1981 (2004).
- 106 Manyam, J., Gibbons, F. P., Diegoli, S., Manickam, M., Preece, J. A., Palmer, R. E., Robinson, A. P. G., Chemically amplified fullerene resists for e-beam lithography, *Proc. SPIE*, 6923, 69230M (2008).
- 107 Powloski, A. R., Nealey, C. F., Nealey, P. F., The multifunctional role of base quenchers in chemically amplified photoresists, *Chem. Mater.* 14, 4192-4201 (2002).
- 108 Private communication with Henderson, C. L., School of Chemical and Biomolecular Engineering, Georgia Institute of Technology, GA, USA.
- 109 Gibbons, F. P., Molecular resist materials for electron beam lithography, in *School of Physics and Astronomy, University of Birmingham*, p.134 (2007).
- 110 McCord, M. A., Rooks, M. J., *Handbook of microlithography, micromachining, and microfabrication* Vol. 1, ed. Rai-Choudhury, P., Bellingham, WA:SPIE Press, p 208 (1997).
- 111 Wang, H., Laws, G. M., Minicic, S., Boland, P., Handugan, A., Pratt, M., Eschrich, T., Myhajlenko, S., Allgair, J. A., Bunday, B., Low temperature ZEP-520A development process for enhanced critical dimension realization in reactive ion etched polysilicon, *J. Vac. Sci. Technol. B* 25(1), 102-105 (2007).
- 112 Namatsu, H., Yamaguchi, T., Nagase, M., Yamazaki, K., Kurihara, K., Nano-patterning of a hydrogen silsesquioxane resist with reduced linewidth fluctuations, *Microelectron. Eng.* 41/42, 331-334 (1998).
- 113 Grigorescu, A. E., van der Krogt, M. C., Hagen, C. W., Kruit, P., 10 nm lines and spaces written in HSQ, using electron beam lithography, *Microelectron. Eng.* 84, 822-824 (2007).
- 114 Cord, B., Yang, J., Duan, H., Joy, D. C., Klingfus, J., Berggren, K. K., Limiting factor in sub-10 nm scanning-electron-beam lithography, *J. Vac. Sci. Technol. B* 27(6), 2616-2621 (2009).